

Title	Development of Nonlinear Analysis Method to Simulate Nonlinear Behavior of RC Walls in RC Wall-Frame Buildings Suffering Damage from Earthquake and Subsequent Tsunami
Author(s)	LATCHAROTE, Panon
Citation	高知工科大学, 博士論文.
Date of issue	2015-03
URL	<a href="http://hdl.handle.net/10173/1280">http://hdl.handle.net/10173/1280</a>
Rights	
Text version	ETD



Kochi, JAPAN

<http://kutarr.lib.kochi-tech.ac.jp/dspace/>

Development of Nonlinear Analysis Method to Simulate  
Nonlinear Behavior of RC Walls in RC Wall-Frame  
Buildings Suffering Damage from Earthquake and  
Subsequent Tsunami

Panon Latcharote

A dissertation submitted to Kochi University of Technology in partial fulfillment of the  
requirements for the degree of Doctor of Engineering

Graduate School of Engineering  
Kochi University of Technology  
Kochi, Japan  
March 2015

© Copyright by Panon Latcharote 2015  
All rights reserved

Development of Nonlinear Analysis Method to Simulate Nonlinear  
Behavior of RC Walls in RC Wall-Frame Buildings Suffering  
Damage from Earthquake and Subsequent Tsunami

Panon Latcharote

B.S. Civil Engineering (Chulalongkorn University, Bangkok, Thailand) 2009

M.S. Structural Engineering (Chulalongkorn University, Bangkok, Thailand) 2011

A dissertation submitted to Kochi University of Technology in partial fulfillment of the  
requirements for the degree of Doctor of Engineering

Advisor:	Prof. Yoshiro Kai
Co-advisor:	Prof. Hiroshi Shima Prof. Seigo Nasu
Committee:	Prof. Masataka Takagi Prof. Shinichi Yamagiwa

## ABSTRACT

After the 2011 Great East Japan earthquake and tsunami, overestimated and unexpected damage, such as overturned buildings in Onagawa town, was a result of earthquake and subsequent tsunami. In the future, more severe and different unexpected damage by earthquake and subsequent tsunami may occur in the Tokai, Tonankai, and Nankai region. The occurrence of building overturning in Onagawa town encouraged the author to focus on structural damage of RC wall-frame buildings from earthquake and subsequent tsunami. Previously, macro plate model had been proposed to simulate earthquake response of a wall member in RC walls. In this research, macro plate model was proposed to simulate tsunami response as same as nonlinear analysis in earthquake response. Since macro plate model had been developed based on nodal displacement, distributed force from tsunami was converted to nodal force in order to evaluate out-of-plane strain using average curvature. Then, nonlinear analysis of out-of-plane behavior was performed using hysteresis rules. For verification of macro plate model, the analytical results of a six-story RC wall-frame building were compared with the test results at E-Defense. For in-plane behavior of macro plate model, the verification results show a good correlation with the test results without considering post-peak behavior. For out-plane behavior, the analysis results of macro plate model were compared with observed damage of a three-story RC wall-frame building from transverse tsunami load in the 2011 Great East Japan earthquake and tsunami. The verification results seem to comply with observed damage. The main objective of this research is to understand failure mechanism of sequential behavior in RC wall-frame buildings suffering damage from earthquake and subsequent tsunami. In order to perform nonlinear structural analysis, a nonlinear analytical model of the six-story RC wall-frame building was carried out to investigate structural damage of beam, column, and wall. For simulating sequential behavior of earthquake and tsunami response, nonlinear structural analysis was performed by means of the same hysteresis models for a series of earthquake, striking wave, and receding wave of tsunami. In this analysis, input tsunami load was modified to induce out-of-plane bending failure of transverse wall at 1<sup>st</sup> floor in order to investigate sequential behavior of other structural

components, such as beam, column, and shear wall. From analysis results, it was found that more damage from sequential tsunami response could occur with most of structural members except for bending failure mode of shear wall. Due to out-of-plane bending failure of wing wall at 1<sup>st</sup> floor, it was found that shear force was redistributed to concentrate on shear wall at 2<sup>nd</sup> wall. Comparing column at 1<sup>st</sup> floor with other floors, more serious damage from sequential tsunami response could occur significantly as same as the case of earthquake response. This study shows that how it is important to consider sequential behavior of RC wall-frame buildings from earthquake and subsequent tsunami. Lastly, this research aimed to apply this proposed analytical model for damage prediction of all RC buildings in a target area. In this research, sequential earthquake and tsunami simulation was developed to predict structural damage from earthquake and subsequent tsunami by means of the application in Integrated Earthquake Simulation (IES). Since IES can simulate only earthquake scenarios with beam-column frame models, IES was modified for input tsunami load acting on a proposed wall-frame model in order to simulate tsunami scenarios using predicted data of tsunami inundation depth. A target area in Kochi city was selected to simulate an earthquake and tsunami scenario because this area has many public buildings and is important for economic activities. A double-layer platform of high performance computing was proposed to simulate this earthquake and tsunami scenario with parallel processing on CPUs and GPUs. The results of sequential earthquake and tsunami simulation show that three-story RC buildings had a significant risk that maximum drift ratio could occur during sequential tsunami response. However, maximum drift ratio from sequential tsunami response was still less than 0.3% in which structural damage didn't occur obviously. For the worst case scenario that tsunami inundation depth was double, structural damage from sequential tsunami response was much more serious than that of the normal-case scenario in which maximum drift ratio was less than 5% for a four-story RC building. In addition, it was found that low-rise buildings (three-story to seven-story) had a significant risk that maximum drift ratio was higher than 1% during sequential tsunami response. The results of sequential earthquake and tsunami simulation can be used to construct further prevention measures.

# CONTENTS

	<b>Pages</b>
<b>Abstract</b>	i
<b>Contents</b>	iii
<b>List of Figures</b>	vi
<b>List of Tables</b>	ix
<b>Chapter I: Introduction</b>	
1.1 General overview	1
1.2 Research Objective	1
1.2.1 Originality	1
1.2.2 Procedure	2
1.2.3 Contribution	2
1.3 Background	2
1.3.1 The 2011 Great East Japan earthquake and tsunami	2
1.3.2 Unexpected occurrence of overturned buildings in Onagawa town	7
1.3.3 Development of a nonlinear analytical model for RC walls	8
1.3.4 Nonlinear structural analysis of RC wall-frame buildings subject to earthquake	11
1.3.5 Structural analysis of RC wall-frame buildings subject to tsunami	13
1.3.6 Integrated Earthquake Simulation (IES)	15
1.4 Outline of dissertation	17
<b>Chapter II: Earthquake and Subsequent Tsunami</b>	
2.1 Abstract	18
2.2 Introduction	19
2.3 Nonlinear analytical model	20
2.3.1 One-component model	20
2.3.2 Macro plate model	22
2.4 A six-story RC wall-frame building	26
2.4.1 Outline of building	26
2.4.2 Analytical model	27
2.4.3 Input ground motion	28

2.4.4	Verification results	30
2.5	A three-story RC wall-frame building	32
2.5.1	Outline of building	32
2.5.2	Analytical model	32
2.5.3	Input tsunami load	33
2.5.4	Verification results	34
2.6	Sequential analysis from earthquake and tsunami	41
2.6.1	Input ground motion and tsunami load	41
2.6.2	Analysis results	42
2.7	Conclusions	52

### **Chapter III: Damage Prediction in a Target Area**

3.1	Abstract	54
3.2	Introduction	55
3.3	Damage prediction from earthquake and subsequent tsunami	57
3.3.1	Evaluation of tsunami load	57
3.3.2	Proposed building modeling	59
3.4	Sequential analysis from earthquake and tsunami	61
3.5	Double-layer platform of high performance computing	62
3.6	Earthquake and tsunami scenario in Kochi city	63
3.6.1	GIS data for building modeling	64
3.6.2	Wave data of strong ground motion	65
3.6.3	Predicted data of tsunami inundation depth	67
3.7	Results of sequential earthquake and tsunami simulation	69
3.8	The worst-case scenario	75
3.9	Single and sequential tsunami response	80
3.10	Conclusions	83
3.11	Appendix	84

### **Chapter IV: Recommendations and Future Research**

4.1	Recommendations	102
4.1.1	Sequential analysis from earthquake and tsunami for individual RC building	102
4.1.2	Damage prediction of all RC building in a target area	103
4.2	Future research	103

4.2.1	Macro plate model	103
4.2.2	Sequential analysis from earthquake and tsunami for individual RC building	104
4.2.3	Damage prediction of all RC building in a target area	104

## **References**

## **List of Publication**

## LIST OF FIGURES

	<b>Pages</b>
<b>Figure 1.1</b> Overall damage from earthquake and tsunami	4
<b>Figure 1.2</b> Individual damage of steel-frame building and wooden house	5
<b>Figure 1.3</b> Failure type of RC buildings from earthquake and tsunami	5
<b>Figure 1.4</b> Importance of RC building during earthquake and tsunami	6
<b>Figure 1.5</b> Six overturned buildings in Onagawa town	7
<b>Figure 1.6</b> The three-vertical-line element model (TVLEM)	9
<b>Figure 1.7</b> The multi-vertical-line element model (MVLEM)	9
<b>Figure 1.8</b> The 2D nonlinear plane element model	9
<b>Figure 1.9</b> The iso-parametric element model (IPEM)	10
<b>Figure 1.10</b> Macro plate model (MPM)	10
<b>Figure 1.11</b> In-plane and out-of-plane displacement of MPM	11
<b>Figure 1.12</b> Pseudo-dynamic earthquake response test of a full-scale seven-story RC wall-frame structure	12
<b>Figure 1.13</b> A full-scale six-story RC wall-frame building tested at E-Defense	12
<b>Figure 1.14</b> Three-story RC wall-frame building damaged by tsunami	13
<b>Figure 1.15</b> A three-story steel-frame building damaged by tsunami	14
<b>Figure 1.16</b> FEM analysis of a large fish market building damaged by tsunami	14
<b>Figure 1.17</b> FEM analysis of a large single panel with hydrodynamic pressure	14
<b>Figure 1.18</b> Ocean-facing RC wall damaged by direct strike from tsunami bore	15
<b>Figure 1.19</b> FEM analysis of damaged RC wall with various pressure distribution	15
<b>Figure 1.20</b> Integrated Earthquake Simulation	16
<b>Figure 1.21</b> Common Modeling Data	16
<b>Figure 2.1</b> One-component model	21
<b>Figure 2.2</b> Takeda model	21
<b>Figure 2.3</b> Axial-stiffness model	22
<b>Figure 2.4</b> Back-bone curve	22
<b>Figure 2.5</b> Macro plate model	23
<b>Figure 2.6</b> Peak-oriented model	24
<b>Figure 2.7</b> Distributed force	25
<b>Figure 2.8</b> Average moment	26
<b>Figure 2.9</b> Plan of a six-story RC wall-frame building	27
<b>Figure 2.10</b> Analytical model of a six-story RC wall-frame building	28

<b>Figure 2.11</b> Input ground motion (JMA Kobe)	29
<b>Figure 2.12</b> Analytical results of TVLEM and experimental results at E-Defense	30
<b>Figure 2.13</b> Verification results of macro plate model (MPM)	31
<b>Figure 2.14</b> Damage of a three-story RC wall-frame building	32
<b>Figure 2.15</b> Analytical model of a three-story RC wall-frame building	33
<b>Figure 2.16</b> Distributed tsunami load acting on macro plate model	34
<b>Figure 2.17</b> Location of beam, column, and wall	35
<b>Figure 2.18</b> Description of CASE-I and CASE-II	35
<b>Figure 2.19</b> Analysis results of transverse wall for CASE-I	37
<b>Figure 2.20</b> Analysis results of transverse beam and column for CASE-I	38
<b>Figure 2.21</b> Analysis results of transverse wall and column for CASE-II	40
<b>Figure 2.22</b> Input tsunami load	42
<b>Figure 2.23</b> The results of relative displacement at each story	43
<b>Figure 2.24</b> The results of wing wall at 1st floor	44
<b>Figure 2.25</b> The results of wing wall at 2nd and 3rd floor	44
<b>Figure 2.26</b> The results of shear wall at 1st floor	45
<b>Figure 2.27</b> The results of shear wall at 2nd floor	46
<b>Figure 2.28</b> The results of shear wall at 3rd floor	46
<b>Figure 2.29</b> The results of columns at 1st floor	47
<b>Figure 2.30</b> The results of columns at 2nd floor	48
<b>Figure 2.31</b> The results of columns at 3rd floor	49
<b>Figure 2.32</b> The results of beams at 2nd floor	50
<b>Figure 2.33</b> The results of beams at 3rd floor	51
<b>Figure 3.1</b> Integrated Earthquake Simulation	56
<b>Figure 3.2</b> Common Modeling Data (CMD)	56
<b>Figure 3.3</b> Triangle distribution of hydrostatic pressure	57
<b>Figure 3.4</b> Location of RC buildings and wooden houses in a target area	58
<b>Figure 3.5</b> The direction of tsunami load acting on each RC building in a target area	59
<b>Figure 3.6</b> Proposed building modeling	60
<b>Figure 3.7</b> Common Modeling Data for wall elements	60
<b>Figure 3.8</b> Sequential analysis of earthquake and tsunami	61
<b>Figure 3.9</b> Hysteretic loop for earthquake and subsequent tsunami	62
<b>Figure 3.10</b> A proposed double layer of parallel processing on CPUs and GPUs	63
<b>Figure 3.11</b> A selected target area in Kochi city	64
<b>Figure 3.12</b> GIS data of this target area	64

<b>Figure 3.13</b>	Building shapes from GIS data	65
<b>Figure 3.14</b>	Seismic hazard map for Nankai earthquake	65
<b>Figure 3.15</b>	Two separated zone for two source data of earthquake model	66
<b>Figure 3.16</b>	The wave data of strong ground motion	67
<b>Figure 3.17</b>	Tsunami hazard map for Nankai earthquake	67
<b>Figure 3.18</b>	Seven divided area for each station of tsunami inundation data	68
<b>Figure 3.19</b>	Predicted inundation depth at each station	69
<b>Figure 3.20</b>	Visualization of damage prediction	70
<b>Figure 3.21</b>	Story displacement at 1 <sup>st</sup> floor	70
<b>Figure 3.22</b>	Maximum story drift ratio for zone N1	71
<b>Figure 3.23</b>	Maximum story drift ratio for zone N2	72
<b>Figure 3.24</b>	Maximum story drift ratio for zone N3	72
<b>Figure 3.25</b>	Maximum story drift ratio for zone S1	73
<b>Figure 3.26</b>	Maximum story drift ratio for zone S2	73
<b>Figure 3.27</b>	Maximum story drift ratio for zone S3	74
<b>Figure 3.28</b>	Maximum story drift ratio for zone S4	74
<b>Figure 3.29</b>	The worst-case scenario by increasing double of tsunami inundation depth	75
<b>Figure 3.30</b>	Maximum story drift ratio for zone N1 (worst case)	76
<b>Figure 3.31</b>	Maximum story drift ratio for zone N2 (worst case)	76
<b>Figure 3.32</b>	Maximum story drift ratio for zone N3 (worst case)	77
<b>Figure 3.33</b>	Maximum story drift ratio for zone S1 (worst case)	77
<b>Figure 3.34</b>	Maximum story drift ratio for zone S2 (worst case)	78
<b>Figure 3.35</b>	Maximum story drift ratio for zone S3 (worst case)	78
<b>Figure 3.36</b>	Maximum story drift ratio for zone S4 (worst case)	79
<b>Figure 3.37</b>	Comparison between single and sequential tsunami response for north zone	80
<b>Figure 3.38</b>	Comparison between single and sequential tsunami response for north zone	82

## LIST OF TABLES

	<b>Page</b>
<b>Table 1.1</b> Description of damage level for building damage	3
<b>Table 1.2</b> Number of damaged buildings from all affected area	4
<b>Table 2.1</b> Hysteresis model for in-plane and out-of-plane behaviour of a wall member	23
<b>Table 2.2</b> Input ground motion of Kobe earthquake	29
<b>Table 2.3</b> Failure mode of each structural member	52
<b>Table 3.1</b> The $a$ factor based on damage observation	59
<b>Table 3.2</b> Number of RC buildings for maximum story drift ratio	75
<b>Table 3.3</b> Number of RC buildings for maximum story drift ratio (worst case)	79

# **CHAPTER I**

## **INTRODUCTION**

### **1.1 GENERAL OVERVIEW**

After the 2011 Great East Japan earthquake and tsunami, overestimated and unexpected damage, such as overturned buildings in Onagawa town, was a result of earthquake and subsequent tsunami. In the future, more severe and different unexpected damage by earthquake and subsequent tsunami may occur in the Tokai, Tonankai, and Nankai region. Therefore, it is interesting to consider structural damage from earthquake and subsequent tsunami. After earthquake, structural properties of RC buildings can be changed to resist against the coming tsunami which may be stronger or weaker. The main objective in a research field of earthquake engineering is to reduce the loss of human life during earthquake and tsunami. Based on this objective, it is necessary to prevent building collapse from earthquake and subsequent tsunami.

### **1.2 RESEARCH OBJECTIVE**

#### **1.2.1 Originality**

Development of sequential earthquake and tsunami simulation was aimed to predict structural damage of all RC buildings in a city area from earthquake and subsequent tsunami. This simulation tool was developed originally from IES (earthquake simulation tool proposed by Prof. Hori) and macro plate model in OBASAN (structural analysis program proposed by Prof. Kai).

## **1.2.2 Procedure**

1. To propose macro plate model for simulating in-plane and out-of-plane behavior of RC walls in nonlinear structural analysis of RC wall-frame buildings from earthquake and subsequent tsunami.
2. To verify macro plate model with test results and observed damage.
3. To investigate structural damage and show that how it is important to consider sequential behavior of RC wall-frame buildings suffering damage from earthquake and subsequent tsunami.
4. To develop a simulation tool for damage prediction of all RC buildings in a target area from earthquake and tsunami scenarios.

## **1.2.3 Contribution**

The results of sequential earthquake and tsunami simulation were damage prediction of all RC buildings in a city area from earthquake and tsunami scenarios. These results can be used to construct further prevention measures.

## **1.3 BACKGROUND**

### **1.3.1 The 2011 Great East Japan earthquake and tsunami**

On 11<sup>th</sup> March 2011, the Great East Japan earthquake and tsunami occurred in the Tohoku region. It was the largest earthquake (M9.0) in the history of Japan which caused a wide range of devastating damages and a devastating tsunami with the maximum height of 40 m. The tsunami caused about 19,000 casualties and more than 676,000 damaged buildings [9]. Due to the awareness of disaster evacuation, people's experience with past earthquake and tsunami can reduce the fatality ratio in coastal areas [9]. Therefore, disaster recognition of people is a key point to reduce damage from earthquake and tsunami. During the 2011 Great East Japan earthquake and tsunami, many buildings were damaged by the

combination of following items; earthquake ground motion, liquefaction, tsunami hydrodynamic force, and floating debris. All damaged buildings can be classified into different levels of building damage, such as minor damage (level 1), moderate damage (level 2), major damage (level 3), complete damage (level 4), collapse (level 5), and wash away (level 6) recommended by the Ministry of Land, Infrastructure and Transportation of Japan (MLIT) as shown in Table 1.1. The MLIT website also provide damage inspection of 252,268 buildings, which are classified to RC building, steel building, and wooden building for each damage level as shown in Table 1.2.

Table 1.1 Description of damage level for building damage in the 2011 Great East Japan earthquake and tsunami recommended by MLIT

Damage level	Classification	Description	Condition
1	Minor damage	There is no significant structural or nonstructural damage, possibly only minor flooding	Possible to be used immediately after cleaning up minor floor and wall
2	Moderate damage	Slight damage to nonstructural components	Possible to be used after moderate repair
3	Major damage	Heavy damage to some walls but no damage to columns	Possible to be used after major repair
4	Complete damage	Heavy damage to many walls and some columns	Possible to be used after complete repair and retrofitting
5	Collapse	Destructive damage to many walls (more than half of wall density) and many column (bended or destroyed)	Loss of functionality (Structural system collapse), Irreparable or great cost for retrofitting
6	Wash away	Wash away, only foundation remains, completely overturning	Irreparable, reconstruction

Table 1.2 Number of damaged buildings from all affected area in the 2011 Great East Japan earthquake and tsunami investigated by MLIT

Damage level	RC building	Steel building	Wooden building
1	555	895	16,952
2	1,176	2,221	30,808
3	1,158	2,099	27,357
4	1,215	1,904	5,005
5	793	2,222	25,092
6	407	1,375	63,396

Fig. 1.1 shows overall damage in Onagawa town from the 2011 Great East Japan earthquake and tsunami. Some buildings were collapsed and some were survived. As can be seen in Fig. 1.1, steel-frame buildings were damaged from earthquake and tsunami. Some RC buildings were overturned and some were damaged. Moreover, Fig. 1.1(a) shows wooden house washed away by tsunami and became floating debris as shown in Fig. 1.1(b). Fig. 1.2 shows an example of individual damage from earthquake and tsunami consist of a damaged steel-frame building in Fig. 1.2(a) and a collapsed wooden house in Fig. 1.2(b).



Fig. 1.1 Overall damage from earthquake and tsunami



(a)



(b)

Fig. 1.2 Individual damage of steel-frame building and wooden house



(a)



(b)



(c)



(d)

Fig. 1.3 Failure type of RC buildings from earthquake and tsunami

Fig. 1.3 shows a failure type of RC buildings in the 2011 Great East Japan earthquake and tsunami. As can be seen in Fig. 1.3(a), this building was collapsed by strong ground motion due to column failure at the first floor. Fig. 1.3(b) shows RC walls damaged by tsunami in out-of plane direction. As can be seen in Fig. 1.3(c), this RC frame building was damaged by earthquake and tsunami. Fig. 1.3(d) shows an overturned RC building from earthquake and tsunami in Onagawa town.



Fig. 1.4 Importance of RC building during earthquake and tsunami

Fig. 1.4 shows public buildings such as school, hospital, apartment, and hotel. As can be seen in Fig. 1.4, these buildings were survived from the 2011 Great East Japan earthquake and tsunami. During earthquake and tsunami, these public buildings are very important because these must be temporary evacuation building for people in surrounding area.

### 1.3.2 Unexpected occurrence of overturned buildings in Onagawa town

After the 2011 Great East Japan earthquake and tsunami, overestimated and unexpected damage was a result of earthquake and subsequent tsunami. Six buildings (five RC buildings and one steel-frame building) in Fig. 1.5 were founded unexpectedly overturned in Onagawa town. A field survey revealed that one of these six overturned buildings in Onagawa town was on a shallow foundation and the others had pile foundations; one of those was overturned and moved 70 m from its original position. In Onagawa town, maximum inundation depth exceeded the height of all overturned buildings. Therefore, it was assumed that all of those buildings were overturned during overtopping tsunami flow.



Fig. 1.5 Six overturned buildings in Onagawa town

Previously, overturning failure of buildings had not been observed in past earthquake and tsunami which was not considered in foundation design. However, overturning failure is now considered in the design guideline of building foundations [1] especially in tsunami evacuation buildings. In recent seismic performance design of pile

foundation, rocking of pile caps and negative friction of piles are considered to resist uplift of buildings. Due to tsunami flow, overturning failure can occur as a result of lateral force (hydrodynamic force) and uplift force (buoyancy force), where buoyancy force also depends on the dimensions from top of window opening to ceiling in buildings. Based on the survey data, most piles were probably broken by ground shaking and soil liquefaction, which easily caused piles to be pulled out of the ground and then fail in tension.

From analysis results of all overturned buildings [6], it was found that a shallow foundation was not effective protection against building overturning. For some cases, it was found that piles could fail during earthquake or tsunami. This could result in a decrease in resisting moment and then cause building overturning during tsunami. For some cases, it was found that soil liquefaction had a significant effect on building overturning. Based on lessons learned from the 2011 Great East Japan earthquake and tsunami, the loss of human life and property might occur due to unexpected damage caused by earthquake and subsequent tsunami. Therefore, it is necessary to predict possible future damage from earthquake and subsequent tsunami.

### **1.3.3 Development of a nonlinear analytical model for RC walls**

In RC buildings, RC walls are widely used to increase resistance against lateral loads imposed by earthquake, wind, and tsunami. For such buildings, RC walls and beam-column frames are combined in nonlinear structural analysis, so a proper modeling of RC walls is very important for structural engineering applications. Many analytical models have been proposed for nonlinear analysis of RC walls. These analytical models are classified as microscopic and macroscopic models, representing local and overall behavior of RC walls respectively. For microscopic models, finite element model (FEM) is conducted to predict local behavior of RC walls using a constitutive model of materials. On the other hand, various macroscopic models have been proposed for RC walls verified with experimental results and these macroscopic models can be used practically for wall-frame structural analysis. These macroscopic models, such as the three-vertical-line element

model (TVLEM) [14] in Fig. 1.6, the multi-vertical-line element model (MVLEM) [38] in Fig. 1.7, the 2-D nonlinear plane element model [22] in Fig. 1.8, and the iso-parametric element model (IPEM) [12] in Fig. 1.9, have been proposed for modeling RC walls. Due to state-of-the-art constitutive models and less computation time, macroscopic models are more practical and efficient than microscopic models for structural engineering applications.

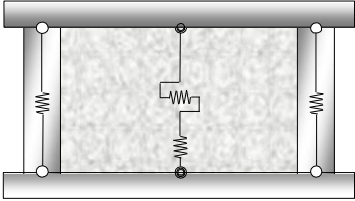


Fig. 1.6 The three-vertical-line element model (TVLEM) [14]

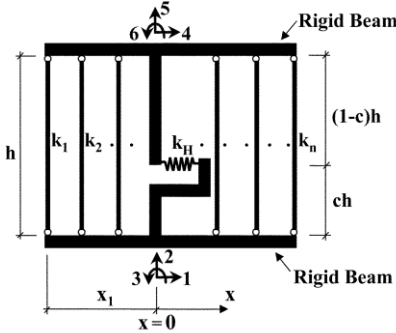


Fig. 1.7 The multi-vertical-line element model (MVLEM) [17]

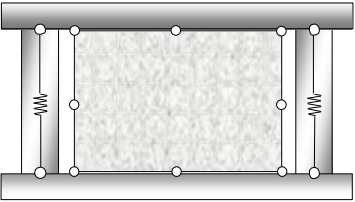


Fig. 1.8 The 2D nonlinear plane element model

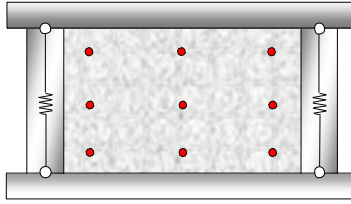


Fig. 1.9 The iso-parametric element model (IPEM) [29]

For earthquake response analysis, macro plate model developed by Prof. Kai [14] has been proposed to represent a wall member in RC walls shown in Fig. 1.10. As can be seen in Fig. 1.10(a), macro plate model is a four-node element model which has been developed originally from the theory of elasticity [37] for in-plane behavior and the theory of plate bending [43] for out-of-plane behavior. Since macro plate model has been developed from elastic theory of plate element, stress-strain relationships in macro plate model has been derived to simulate inelastic response of RC walls using hysteretic stress-strain relationships in hysteretic rules.

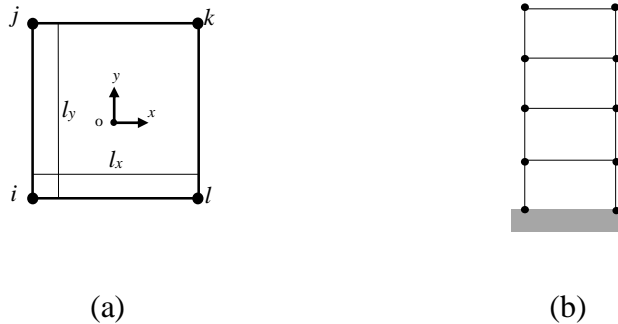


Fig. 1.10 Macro plate model (MPM) [14]

For simulating in-plane and out-of-plane behavior, in-plane and out-of plane displacement of node  $i$ ,  $j$ ,  $k$ , and  $l$  are defined as shown in Fig. 1.11(a) and Fig. 1.11(b) respectively.

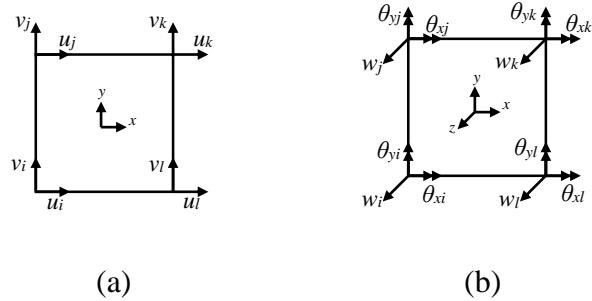


Fig. 1.11 In-plane and out-of-plane displacement of MPM

For nonlinear analysis of RC walls represented by MVLEM and IPFM, hysteretic behavior of a wall member have been described using hysteretic constitutive models of steel and concrete. For macro plate model, hysteretic behavior of a wall member can be simulated as same as TVLEM which can be described using conventional hysteretic rules, such as Takeda model, peak-oriented model, origin-oriented model, axial-stiffness model [13] and other hysteretic models from experimental results in order to track inelastic responses. Therefore, numerical derivation of stress and strain in macro plate model is necessary for application of hysteretic models, in which the cracking, yielding, and ultimate strength of back-bone curves are determined using empirical equations recommended by building design standards.

### 1.3.4 Nonlinear structural analysis of RC wall-frame buildings subject to earthquake

The main objective in a research field of earthquake engineering is to reduce the loss of human life during earthquake and tsunami. Based on this objective, it is very important to prevent building collapse from earthquake and tsunami. For RC wall-frame buildings, experimental and analytical studies have been carried out to understand building collapse from earthquake. Nonlinear structural analysis of RC wall-frame buildings focusing on earthquake response has been proposed in many previous research studies. In 1982, pseudo-dynamic earthquake response test of a full-scale seven-story RC wall-frame

structure was conducted as a part of U.S.-Japan Cooperative Research Program [14] at the Large Size Structures Laboratory of Building Research Institute (BRI). In addition, analytical studies of the full-scale seven-story RC wall-frame structure in Fig. 1.12 were proposed to compare with test results [14].

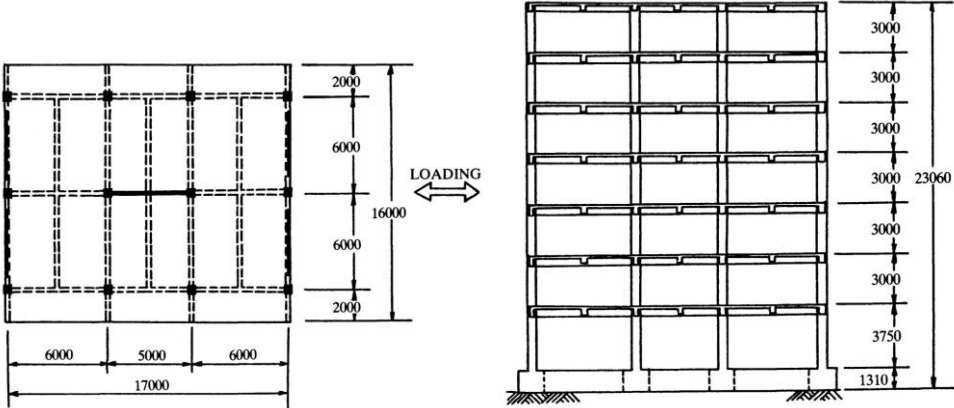


Fig. 1.12 Pseudo-dynamic earthquake response test of a full-scale seven-story RC wall-frame structure [14]

In 2006, a full-scale six-story RC wall-frame building was tested at E-Defense [17]-[21] by National research Institute for Earth science and Disaster (NIED) as shown in Fig. 1.13. In addition, analytical studies of the six-story RC wall-frame building were proposed before the full-scale test at E-Defense [13], [16], [25] and after the full-scale test [17]-[21].



Fig. 1.13 A full-scale six-story RC wall-frame building tested at E-Defense [17]

### 1.3.5 Structural analysis of RC wall-frame buildings subject to tsunami

During the 2011 Great East Japan earthquake and tsunami, many buildings were damaged and collapsed by tsunami wave [5], [9]. The equivalent tsunami load on a three-story RC wall-frame building in Fig. 1.14 was estimated from observe damage in relation with tsunami inundation depth [57]. This study aimed to propose appropriate tsunami load for structural design of tsunami evacuation buildings.



Fig. 1.14 Three-story RC wall-frame building damaged by tsunami [57]

Empirical equations for various conditions of fluid loading were validated through failure analysis for several damaged buildings, using finite element modeling [56]. These analysis studies were applied to full-scale buildings with clearly identified failure mechanisms to validate methodologies to be included in a new chapter on “Tsunami Loads and Effects” in the ASCE 7-2016 Standard, Minimum Design Loads for Buildings and Other Structures. In Fig. 1.15, a three-story steel-frame building was submerged in flow velocity 7.5 m/s. Fig. 1.16 shows RC walls of a building damaged by tsunami load in out-of-plane direction. In Fig. 1.17, this case study of a large single panel was used to verify hydrodynamic pressure by FEM analysis. Fig. 1.18 shows the ocean facing wall of a building that failed through out-of-plane flexure due to large hydrodynamic force and FEM analysis was conducted to RC wall with various pressure distribution as shown in Fig. 1.19.



Fig. 1.15 A three-story steel-frame building damaged by tsunami [56]



Fig. 1.16 FEM analysis of a large fish market building damaged by tsunami [56]



Fig. 1.17 FEM analysis of a large single panel with hydrodynamic pressure [56]



Fig. 1.18 Ocean-facing RC wall damaged by direct strike from tsunami bore [56]

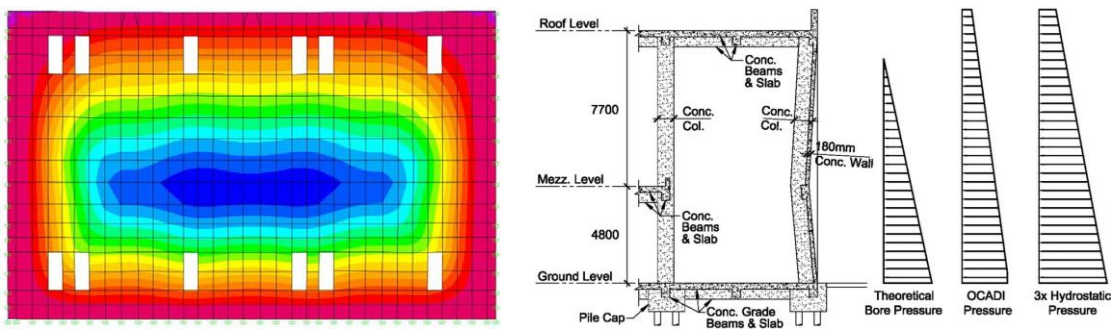


Fig. 1.19 FEM analysis of damaged RC wall with various pressure distribution [56]

### 1.3.6 Integrated Earthquake Simulation (IES)

In order to reduce the loss of human life in future earthquake and tsunami, damage prediction is a key role for constructing prevention measure and raising awareness of people. For damage prediction in a target area, computer technology has been applied to simulate earthquake scenarios, such as Integrated Earthquake Simulation (IES) [59]-[65]. Integrated Earthquake Simulation (IES) is an earthquake simulation tool for predicting and illustrating structural damage of all buildings in a target area simultaneously in selected earthquake scenarios. Based on Geographic Information System (GIS) data in Fig. 1.20(a), thousands of buildings in a target area are modeled to polygon shapes in Fig. 1.20(b) from

building shape and height. Based on building design code, Common Modeling Data (CMD) is a modeling approach to convert a polygon shape in Fig. 1.21(a) as a structural model in Fig. 1.21(b), consisting of beam and column element including section and material properties of each element. In Fig. 1.20(c), nonlinear structural analysis of all buildings in a target area is performed to predict structural damage and then illustrate structural damage of all buildings simultaneously as shown in Fig. 1.20(d).

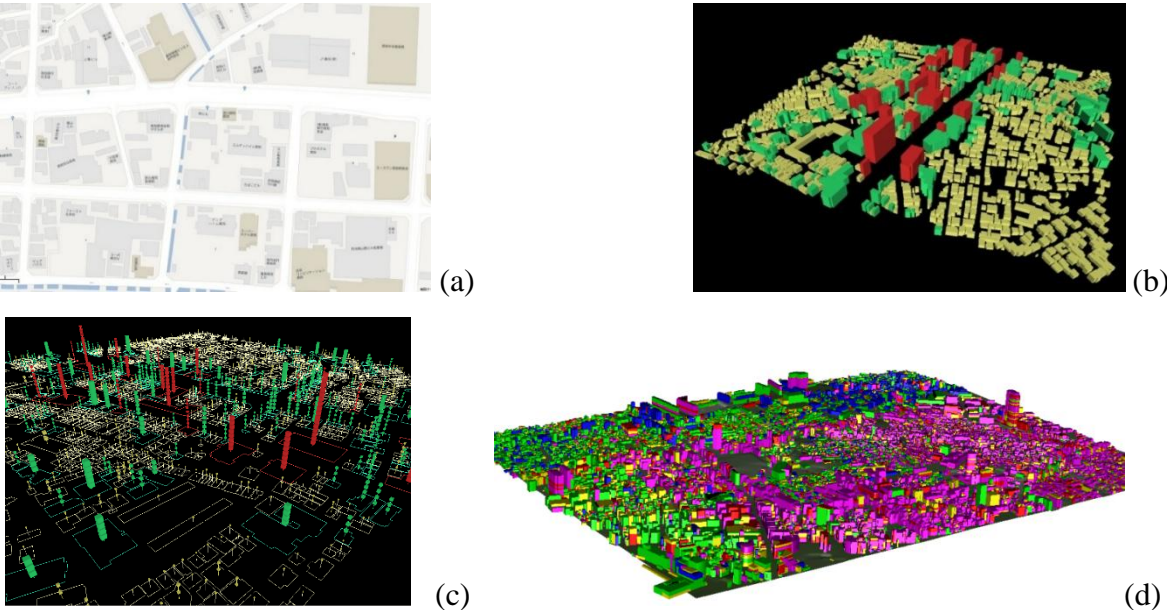


Fig. 1.20 Integrated Earthquake Simulation [62]

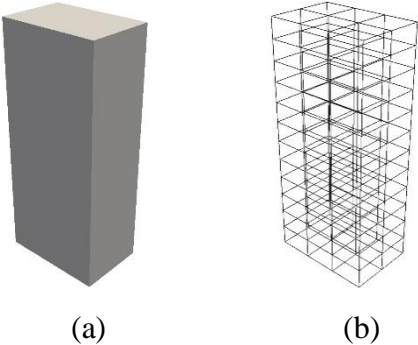


Fig. 1.21 Common Modeling Data (CMD) [68]

For thousands of buildings in a target area, IES can visualize structural damage to raise awareness of disaster prevention among people in that area. Since high performance computing (HPC) is a key role to carry out a large number of buildings in a target area, OpenMPI application has been applied to IES in order to enable parallel processing on the Central Processing Units (CPUs).

#### **1.4 OUTLINE OF DISSERTATION**

This dissertation presents four chapters, providing details on the sequence of finding, development, investigation, and application. The rest of dissertation is organized as follows:

Chapter 2 presents application of macro plate model for tsunami load, verification of macro plate model, and sequential analysis of a RC wall-frame building from earthquake and subsequent tsunami.

Chapter 3 presents development of a simulation tool for damage prediction of all RC buildings in a target area from earthquake and tsunami scenarios.

Chapter 4 presents recommendations and future research.

# **CHAPTER II**

## **EARTHQUAKE AND SUBSEQUENT TSUNAMI**

### **2.1 ABSTRACT**

Nonlinear structural analysis of RC wall-frame buildings focusing on earthquake response has been proposed in many previous research studies. In this chapter, analytical studies were carried out to propose nonlinear structural analysis of RC wall-frame buildings subjected to earthquake and subsequent tsunami. For a nonlinear analytical model of RC wall-frame buildings, macro frame model was used to represent a beam and column member, whereas macro plate model was used to represent a wall member. In order to consider out-of-plane strength of RC walls resisting against tsunami load, macro plate model was proposed to simulate out-of-plane behavior of shear and bending. For the case of earthquake, a proposed nonlinear analytical model was verified with a six-story RC wall-frame building tested at E-Defense. For the case of tsunami, a proposed analytical model was verified with a three-story RC wall-frame building damaged by tsunami in the 2011 Great East Japan earthquake and tsunami. For simulating sequential behavior of earthquake and tsunami response, the proposed nonlinear analytical model of the six-story RC wall-frame building was performed by means of the same hysteresis models. After out-of-plane bending failure of wing wall, analysis results show failure mode of each structural member from earthquake response and sequential tsunami response in which more damage from sequential tsunami response could occur with most of structural members except for bending failure mode of shear wall.

## 2.2 INTRODUCTION

The main objective in a research field of earthquake engineering is to reduce the loss of human life during earthquake and tsunami. Based on this objective, it is very important to prevent building collapse from earthquake and subsequent tsunami. For RC wall-frame buildings, experimental and analytical studies have been carried out to understand building collapse from earthquake. Nonlinear structural analysis of RC wall-frame buildings focusing on earthquake response has been proposed in many previous research studies. For experimental studies, a full-scale six-story RC wall-frame building was tested at E-Defense [17]-[21]. In addition, analytical studies of the six-story RC wall-frame building were proposed before the full-scale test at E-Defense [13], [16], [21] and after the full-scale test [17]-[21]. In this chapter, a proposed nonlinear analytical model, in which hysteretic behavior of beam, column, and wall is simulated to predict inelastic response on member level, is verified with the results of these previous experimental and analytical studies.

During the 2011 Great East Japan earthquake and tsunami, many RC buildings were damaged and collapsed by earthquake and tsunami [5], [9]. A three-story RC wall-frame building [57] damaged by only tsunami load was selected to verify with a proposed analytical model. From survey data of affected areas, observed damage of some RC buildings cannot be distinguished between earthquake and tsunami. Therefore, based on lesson learn in the 2011 Great East Japan earthquake and tsunami, this chapter proposes nonlinear structural analysis of RC wall-frame buildings suffering damage from earthquake and subsequent tsunami.

In order to study on sequential behavior of earthquake and tsunami response, the proposed nonlinear analytical model of the six-story RC wall-frame building is carried out to perform nonlinear structural analysis. For the nonlinear analytical model using macroscopic models of structural elements, the one-component (OC) model proposed by Prof. Kabeyasawa [21], [49] is used to represent a beam and column member. In addition,

macro plate model proposed by Prof. Kai [14] is used to simulate in-plane and out-of-plane behavior of a wall member in this chapter.

The purpose of this study is to simulate failure process of a RC wall-frame building appropriately subjected to earthquake and subsequent tsunami. This analytical study focuses on predicting more serious damage in structural members, such as beam, column, and wall, caused by earthquake and subsequent tsunami. For the proposed nonlinear analytical model, constitutive and hysteresis models on member level are applied to simulate inelastic response of structural members. Using state-of-the art constitutive and hysteresis models, the analytical model can predict reliable response of structural members in order to investigate failure mode, such as axial, flexural and shear failure, of beam, column, and wall.

## **2.3 NONLINEAR ANALYTICAL MODEL**

In order to carry out analytical studies, macroscopic models were used to construct a nonlinear analytical model of RC wall-frame buildings. Macroscopic models are a structural member model to represent beam, column, and wall in RC buildings in order to simulate overall behavior of a structural member. For a nonlinear analytical model of RC wall-frame buildings in this study, macro plate model was used to represent a wall member and one-component model was used to represent a beam and column member.

### **2.3.1 One-component model**

The one-component model proposed by Prof. Kabeyasawa, a line element model, is a two-node element with nonlinear axial and rotational spring shown in Fig. 2.1. For a column member, flexural behavior is idealized by implementing two nonlinear rotational springs at the end of a structural member and axial behavior is idealized by implementing one nonlinear axial spring [21], [49]. Whereas, shear behavior is assumed to be proportional with flexural behavior, instead of incorporating nonlinear shear spring. For a beam member, flexural and shear behavior are the same as those of a column member but

axial behavior is not considered. For hysteresis models of beam and column in this study, Takeda model in Fig. 2.2 was applied to nonlinear rotational spring in order to simulate hysteretic flexural behavior and axial-stiffness model in Fig. 2.3 was applied to nonlinear axial spring in order to simulate hysteretic axial behavior in which the cracking, yielding, and ultimate strength of back-bone curves in Fig. 2.4 were determined using empirical equations recommended by Architecture Institute of Japan (AIJ) standards [71].



Fig. 2.1 One-component model [16]

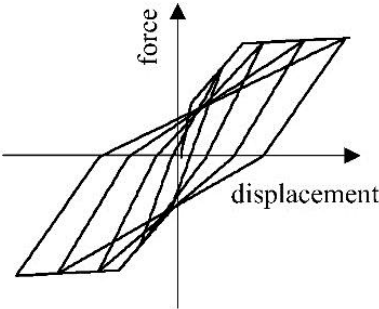


Fig. 2.2 Takeda model [16]

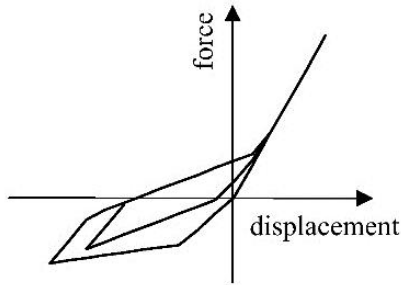


Fig. 2.3 Axial-stiffness model [16]

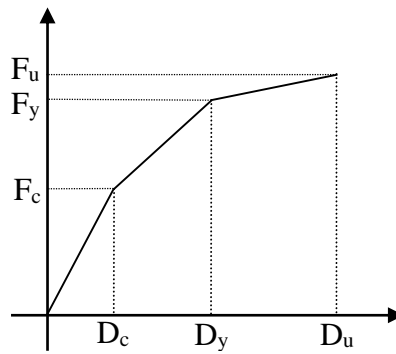


Fig. 2.4 Back-bone curve

### 2.3.2 Macro plate model

Macro plate model proposed by Prof. Kai, a plate element model for a wall member, is a four-node element with rectangular shape in the  $x$ - $y$  plane, consisting of nodes  $i$ ,  $j$ ,  $k$ , and  $l$  shown in Fig. 2.5(a). Macro plate model has been developed originally from the theory of elasticity [37] for in-plane behavior and the theory of plate bending [43] for out-of-plane behavior. For each node of macro plate model, a total of five degrees of freedoms were considered: three translational components along the  $x$ -,  $y$ -, and  $z$ -axes and two rotational components about the  $x$ - and  $y$ -axes. Axial, bending, and shear deformation are considered for in-plane behavior, whereas bending and torsional deformation are

considered for out-of-plane behavior. As can be seen in Fig. 2.5(b), macro plate model has been formulated to describe a one-story wall member of RC walls.

For nonlinear structural analysis, hysteretic behavior can be simulated directly using hysteresis models on the level of a wall member in order to predict inelastic response as same as a beam and column member. In this study, hysteresis models of a wall member were applied to each component in Table 2.1: axial-stiffness model was applied to simulate axial behavior: Takeda model was applied to simulate in-plane flexural and shear behavior and out-of-plane flexural behavior: peak-oriented model in Fig. 2.6 was applied to simulate out-of-plane shear behavior. The back-bone curves of a wall member were determined using empirical equations recommended by AIJ standards [71] and Prof. Kai [15] for in-plane and out-of-plane behavior respectively..

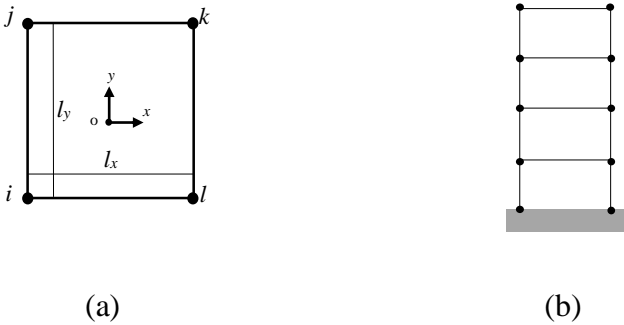


Fig. 2.5 Macro plate model

Table 2.1 Hysteresis models for in-plane and out-of-plane behavior of a wall member

Component	Hysteresis model
Axial behavior	Axial-stiffness model
In-plane flexural behavior	Takeda model
In-plane shear behavior	Takeda model
Out-of-plane flexural behavior	Takeda model
Out-of-plane shear behavior	Peak-oriented model

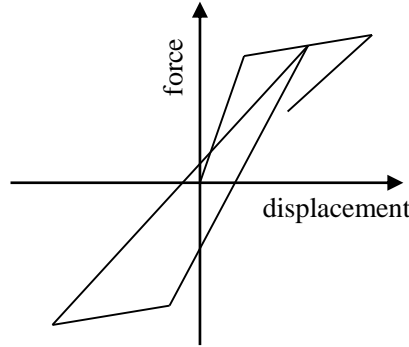


Fig. 2.6 Peak-oriented model

In order to consider out-of-plane strength of RC walls resisting against tsunami load, macro plate model was proposed to simulate out-of-plane behavior of shear and bending. The stress-strain relationship of macro plate model has been derived to simulate out-of-plane behavior in nonlinear analysis using hysteresis rules. Since out-of-plane behavior has been derived starting from the nodal force-displacement relationship and the deformation-displacement relationship, it is necessary to convert distributed force in case of tsunami load to nodal force for nonlinear analysis.

The shape function ( $N$ ) for each node is expressed in terms of normalized coordinates ( $\xi$  and  $\eta$ ) as Eq. (2.1) [43].

$$N_a = \frac{1}{4}(1 + \xi_a \xi)(1 + \eta_a \eta) \quad a = i, j, k, l \quad (2.1)$$

For normalized coordinates:  $(\xi_i, \eta_i) = (-1, -1)$   $(\xi_j, \eta_j) = (-1, 1)$   $(\xi_k, \eta_k) = (1, 1)$   $(\xi_l, \eta_l) = (1, -1)$

The general form of distributed force ( $q$ ) at nodes  $i$ ,  $j$ ,  $k$ , and  $l$  with linear distribution is shown in Fig. 2.7.

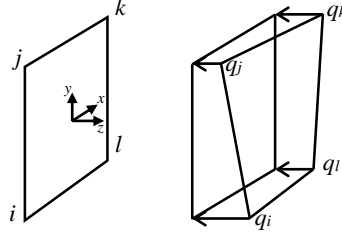


Fig. 2.7 Distributed force

From the shape function in Eq. (2.1), nodal forces acting on each node of macro plate model can be computed from Eq. (2.2).

$$\begin{bmatrix} F_{w_a} \\ F_{\theta_{xa}} \\ F_{\theta_{ya}} \end{bmatrix} = \frac{l_x l_y}{4} \sum_{b=i}^l \int_{-1}^1 \int_{-1}^1 \begin{bmatrix} N_a N_b q_b \\ \frac{l_y}{4} N_a N_b q_b (\eta_a - \eta) \\ \frac{l_x}{4} N_a N_b q_b (\xi_a - \xi) \end{bmatrix} d\xi d\eta \quad (2.2)$$

From solving Eq. (2.2), distributed force can be converted to nodal forces at nodes i, j, k, and l shown in Eq. (2.3).

$$\begin{bmatrix} F_{w_i} \\ F_{\theta_{xi}} \\ F_{\theta_{yi}} \end{bmatrix} = \frac{l_x l_y}{36} \begin{bmatrix} 4q_i + 2q_j + q_k + 2q_l \\ \frac{l_y}{4} (2q_i + 2q_j + q_k + q_l) \\ -\frac{l_x}{4} (2q_i + q_j + q_k + 2q_l) \end{bmatrix} \quad \begin{bmatrix} F_{w_j} \\ F_{\theta_{xj}} \\ F_{\theta_{yj}} \end{bmatrix} = \frac{l_x l_y}{36} \begin{bmatrix} 2q_i + 4q_j + 2q_k + q_l \\ -\frac{l_y}{4} (2q_i + 2q_j + q_k + q_l) \\ -\frac{l_x}{4} (q_i + 2q_j + 2q_k + q_l) \end{bmatrix} \quad (2.3)$$

$$\begin{bmatrix} F_{w_k} \\ F_{\theta_{xk}} \\ F_{\theta_{yk}} \end{bmatrix} = \frac{l_x l_y}{36} \begin{bmatrix} q_i + 2q_j + 4q_k + 2q_l \\ -\frac{l_y}{4} (q_i + q_j + 2q_k + 2q_l) \\ \frac{l_x}{4} (q_i + 2q_j + 2q_k + q_l) \end{bmatrix} \quad \begin{bmatrix} F_{w_l} \\ F_{\theta_{xl}} \\ F_{\theta_{yl}} \end{bmatrix} = \frac{l_x l_y}{36} \begin{bmatrix} 2q_i + q_j + 2q_k + 4q_l \\ \frac{l_y}{4} (q_i + q_j + 2q_k + 2q_l) \\ \frac{l_x}{4} (2q_i + q_j + q_k + 2q_l) \end{bmatrix}$$

For tsunami load, the general form of distributed force in Fig. 2.7 was adequate to represent hydrostatic pressure, which is linearly distributed on building surface. In case of tsunami load acting on transverse wall, out-of-plane curvature occurring in a wall member is varied depending on location. From analysis results in next section, it was found that out-of-plane bending moments at the end of member were distributed as shown in Fig. 2.8, so that the member-end moments were averaged to determine out-of-plane curvature shown in

Fig. 2.8. Average bending moment and shear force can be estimated from member-end moments shown in Eq. (2.4).

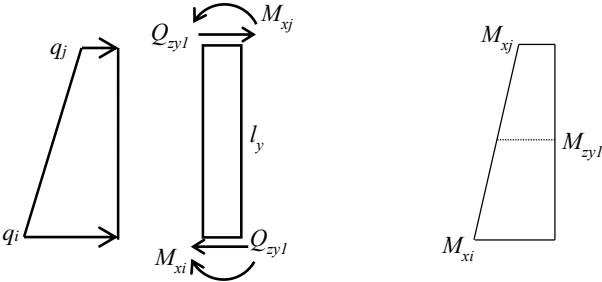


Fig. 2.8 Average moment

$$\begin{bmatrix} M_{zy1} \\ Q_{zy1} \\ M_{zy2} \\ Q_{zy2} \end{bmatrix} = \begin{bmatrix} -1/2 & 1/2 & 0 & 0 \\ 1/l_y & 1/l_y & 0 & 0 \\ 0 & 0 & 1/2 & -1/2 \\ 0 & 0 & 1/l_y & 1/l_y \end{bmatrix} \begin{bmatrix} M_{xi} \\ M_{xj} \\ M_{xk} \\ M_{xl} \end{bmatrix} \tag{2.4}$$

**2.4 A SIX-STORY RC WALL-FRAME BUILDING**

**2.4.1 Outline of building**

A full-scale shaking table test on the six-story RC wall-frame building was carried out at E-Defense of National research Institute for Earth science and Disaster (NIED) [13], [25], [16]-[21]. This building is six-story high with two spans in X-direction and three spans in Y-direction as shown in Fig. 2.9. The height of each story is 2.5 m and the dimension of each span is 5 m, which result in 15 m in total height and 10x15 m in plan [17]. As can be seen in Fig. 2.9, This building in Y-direction consisted of two different kinds of frame, such as open frame (X1 and X3) and shear wall frame (X2) [19]. For this study, spandrel beams were neglected in X1 frame because torsional behavior was not considered. In addition, this building in X-direction with symmetric plan consisted of two open frames (Y2 and Y3) and two wing-wall frames (Y1 and Y4) [19].

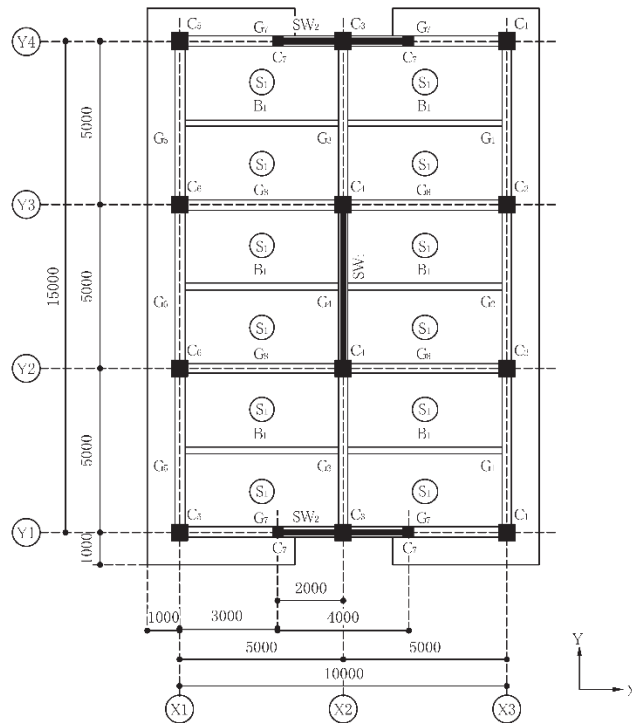


Fig. 2.9 Plan of a six-story RC wall-frame building [46]

#### 2.4.2 Analytical model

For analytical model in Fig. 2.10, each node had six degrees of freedom, which was three translational and three rotational components. For proposed analytical model, macro plate model was assigned for a wall member and the one-component model was assigned for a beam and column member. Each floor was assumed as a rigid diaphragm for translation in X and Y-axis and rotation about Z-axis in which weight  $120 \times 10^3$  kg per floor was divided by tributary area and lumped to each node [17]. In analysis, compressive strength of concrete was assumed to be 21 MPa; yield strength of steel bar D19 (for beam and column) was assumed to be 380 MPa; yield strength of steel bar D10 (for wall) was assumed to be 354 MPa. Column section was 0.5 x 0.5 m with 8-D19; beam section was 0.3 x 0.5 m with 4-D19; wall thickness was 0.15 m with double D10@300 [17]. The Newmark- $\beta$  method ( $\beta=0.25$ ) was used to solve the equation of ground motion in time-history analysis with time-step 0.002 second. The damping matrix was assumed to be the

instant matrix with damping ratio 3%.

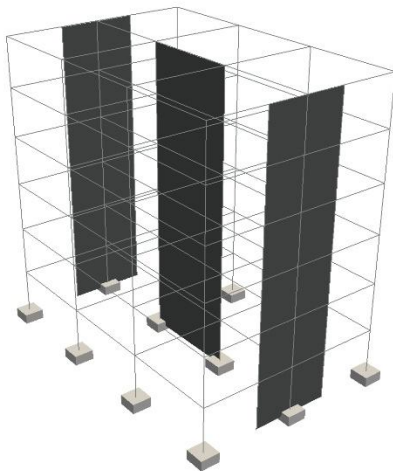


Fig. 2.10 Analytical model of a six-story RC wall-frame building

### 2.4.3 Input ground motion

Three ground motion components in the east-west, north-south, and up-down direction (EW, NS, and UD respectively) of Kobe earthquake recorded by Japan Meteorological Agency (JMA 1995) in Fig. 2.11 were used as input ground motion as same as the test at E-Defense. The NS and EW ground motion component were applied to a nonlinear analytical model at angles of 45 degree and 135 degree from X-axis respectively. The UD ground motion component was also applied in vertical direction. Maximum acceleration of input ground motion in X-, Y-, and Z-axis is shown in Table 2.2. INPUT-I, INPUT-II, and INPUT-III was 25%, 50%, and 100% respectively of input ground motion modified from Kobe earthquake record.

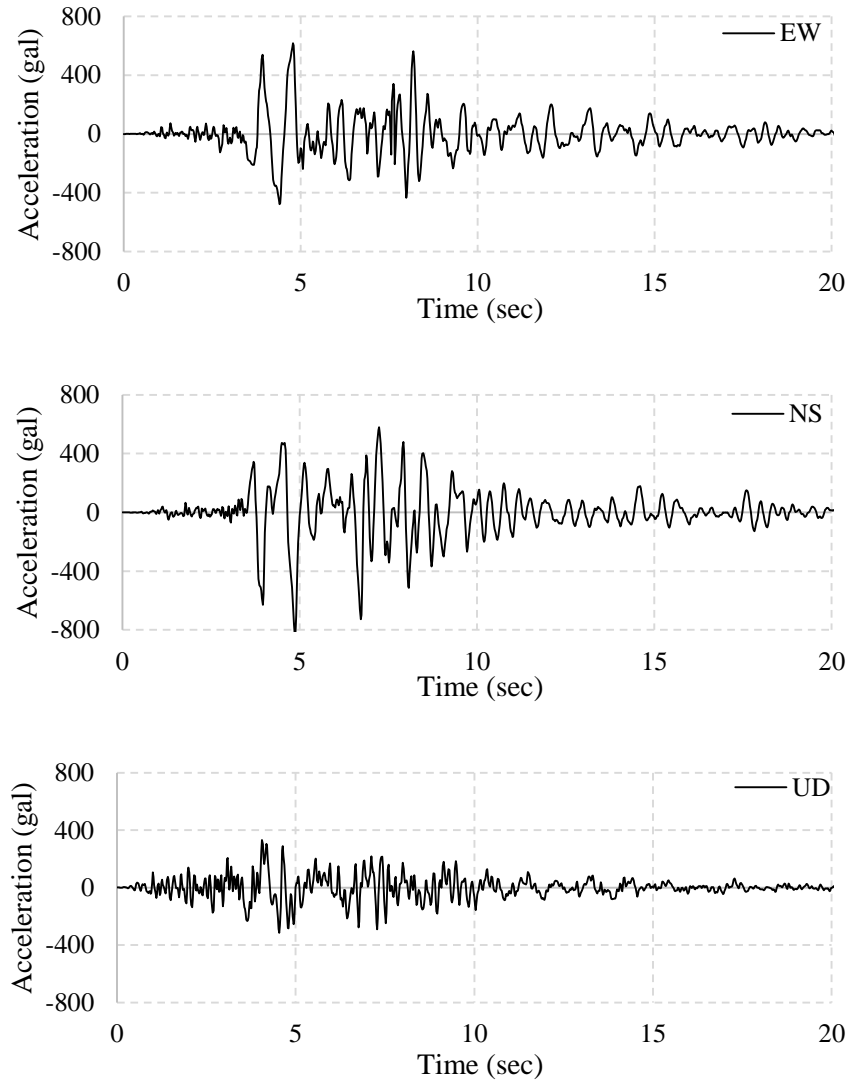


Fig. 2.11 Input ground motion (JMA Kobe)

Table 2.2 Input ground motion of Kobe earthquake (JMA 1995)

Input data	Scale factor	Maximum acceleration (gal)		
		X	Y	Z
INPUT-I	25%	138.88	211.19	83.06
INPUT-II	50%	277.76	422.38	166.12
INPUT-III	100%	555.53	844.76	332.24

### 2.4.4 Verification results

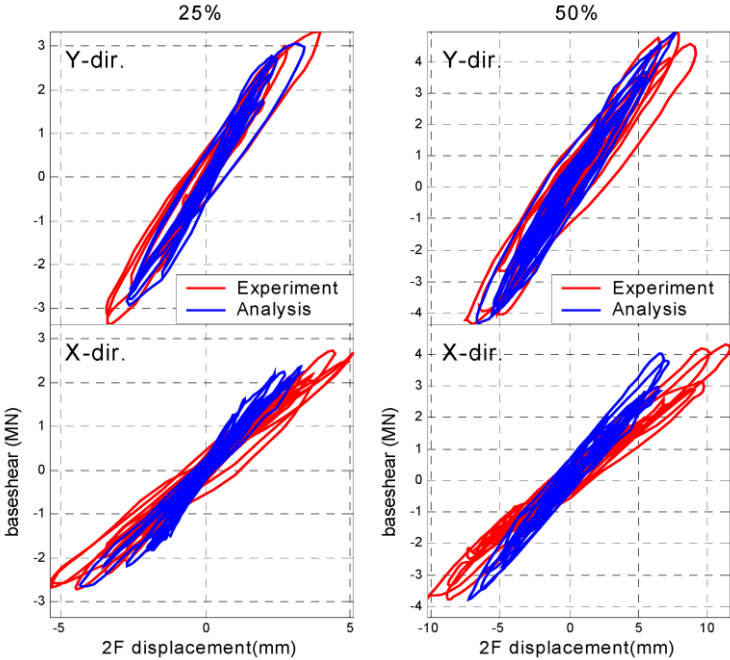


Fig. 2.12 Analytical results of TVLEM and experimental results at E-Defense

In this section, the proposed analytical model of a six-story RC wall-frame building assembled by the one-component model (OCM) and macro plate model (MPM) was verified with the analytical and experimental results at E-Defense [19] shown in Fig 2.12. Since the one-component model and macro plate model are still not capable of simulating strength degradation in post-peak response, only stiffness degradation was considered in the nonlinear analytical model. INPUT-I and INPUT-II in Table 2.2, which was scaled by 25% and 50% respectively of input ground motion, were applied to verify the proposed analytical model with the analytical and experimental results at E-Defense. The relationship between base shear and relative displacement at 2<sup>nd</sup> floor was considered for verification in this study.

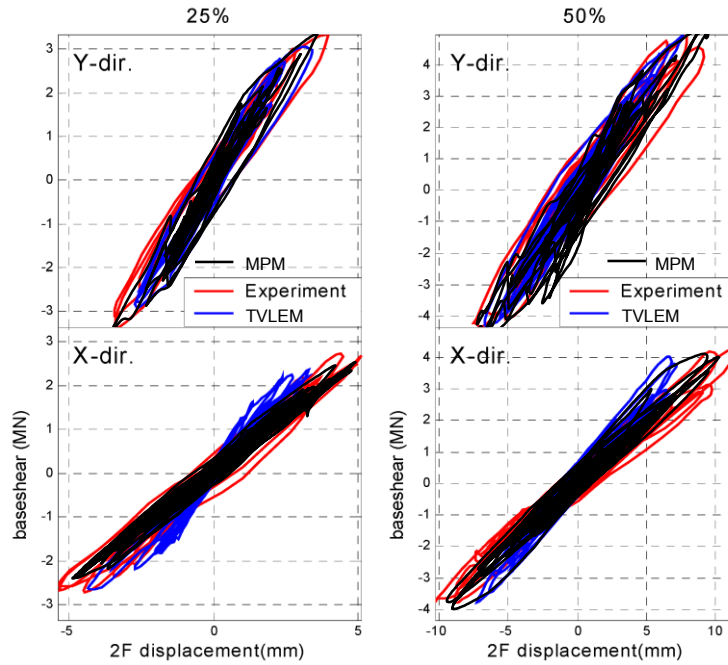


Fig. 2.13 Verification results of macro plate model (MPM)

The analysis results of this proposed analytical model for INPUT-I and INPUT-II was compared with the experimental results at E-Defense as shown in Fig. 2.13. For INPUT-I, the analysis results in X-direction show that the maximum base shear  $2.51 \times 10^6$  N was slightly underestimated and the maximum relative displacement at 2<sup>nd</sup> floor  $4.94 \times 10^{-3}$  m was slightly underestimated: the analysis results in Y-direction show that the maximum base shear  $3.31 \times 10^6$  N was slightly overestimated and the maximum relative displacement  $3.52 \times 10^{-3}$  m was slightly underestimated. For INPUT-II, the analysis results in X-direction show that the maximum base shear  $4.18 \times 10^6$  N was slightly underestimated and the maximum relative displacement  $10.26 \times 10^{-3}$  m was underestimated: the analysis results in Y-direction show that the maximum base shear  $5.19 \times 10^6$  N was slightly overestimated and the maximum relative displacement  $7.98 \times 10^{-3}$  m was overestimated. The verification results show a good correlation between the proposed analytical model and the test at E-Defense for 25% and 50% of input ground motion. Although the input data of ground motion was slightly different from those of shaking table at E-Defense, the proposed analytical model

was agree with experimental results. Therefore, this proposed analytical model can be used in further analysis without considering post-peak response.

## **2.5 A THREE-STORY RC WALL-FRAME BUILDING**

### **2.5.1 Outline of building**



Fig. 2.14 Damage of a three-story RC wall-frame building [57]

A three-story RC wall-frame building located in Sendai city was damaged by tsunami in the 2011 Great East Japan earthquake and tsunami as shown in Fig. 2.14. As can be seen in Fig. 2.14, the out-of-plane deformation was occurred in outer frame by tsunami load [57]. The outer frame consisted of column, transverse beam, and transverse wall. The damaged transverse wall covered two-story and four-span section without floor slabs on second and third floor. The height of first, second, and third floor is 4.5 m, 3.6 m, and 3.6 m respectively and the span length is 5 m. The maximum inundation depth was 10.5 m in front which caused the yielding of reinforcement in beam, column, and wall [57].

### **2.5.2 Analytical model**

For analytical model in Fig. 2.15, each node had six degrees of freedom, which was three translational and three rotational components. Macro plate model was assigned for a wall member in order to consider out-of-plane behavior of transverse wall, which was emphasized in this section. In analysis, compressive strength of concrete was assumed to be  $18 \times 10^6$  Pa; yield strength of steel bar D25 (for beam and column) was assumed to be 345

MPa; yield strength of steel bar D10 (for wall) was assumed to be 295 MPa. Column section was 0.7x0.9 m with 10-D25; beam section was 0.4x0.8 m with 10-D25; wall thickness was 0.3 m with triple D10@250 for vertical and horizontal reinforcement [57]. The static method was used to solve the static pushover analysis with load steps, according to increasing in tsunami inundation depth 0.01 m.

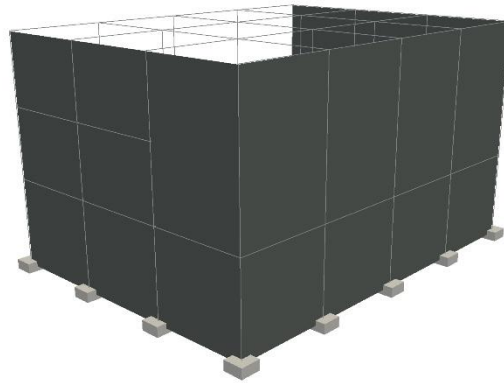


Fig. 2.15 Analytical model of a three-story RC wall-frame building

### 2.5.3 Input tsunami load

Hydrostatic pressure was assumed to be input tsunami load for this analytical model. As shown in Fig. 2.16, fully distributed load in triangular shape was assigned to the outer frame of this analytical model in which hydrostatic pressure was varied by tsunami inundation depth from 0.0 m to 10.5 m. As can be seen in Fig. 2.16, maximum hydrostatic pressure was 116.19 kPa at maximum tsunami inundation depth 10.5 m. This fully distributed load was converted to nodal load acting on each node of this analysis model by means of shape function as mentioned in section 2.3.2. The treatment of tsunami load in section 2.3.2 was adequate for this hydrostatic pressure, which is linearly distributed on building surface. The static pushover analysis was applied to this analytical model with increasing in tsunami inundation depth 0.01 m.

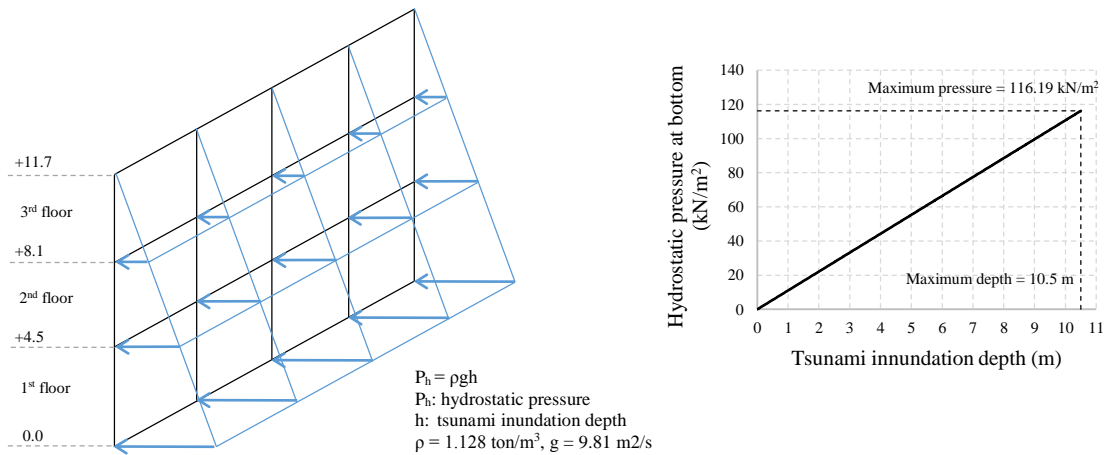


Fig. 2.16 Distributed tsunami load acting on macro plate model

#### 2.5.4 Verification results

In this section, the analytical model of a three-story RC wall-frame building focusing on out-of-plane strength of transverse wall was verified with observed damage from tsunami in the 2011 Great East Japan earthquake and tsunami [57]. For the proposed analytical model, macro plate model was used to represent transverse wall in order to investigate out-of-plane behavior. Since the outer frame of this analytical model was symmetric, the location of transverse beam, column, and transverse wall shown in Fig. 2.17(a) was focused in analysis results. For the analysis results of transverse wall, the definition of wall position is shown in Fig. 2.17(b). Varying with tsunami inundation depth, bending moment and shear force were considered for the failure behavior of transverse beam and column: out-of-plane bending moment and shear force were considered for the failure behavior of transverse wall. Since the reinforcement ratio of transverse wall was small, out-of-plane yield strength was less than out-of-plane crack strength. In order to compare the analysis results with observe damage, two analysis cases were investigated in this study. For CASE-I, out-of-plane crack strength was considered as a failure point, so that transverse wall was assumed to be failed after this point. For CASE-II, strength degradation was considered for out-of-plane strength, so that out-of-plane force was

decreased after the cracking point. For out-of-plane bending and shear behavior, description of CASE-I and CASE-II is shown Fig. 2.18 in which yield bending and shear strength were less than crack bending and shear strength.

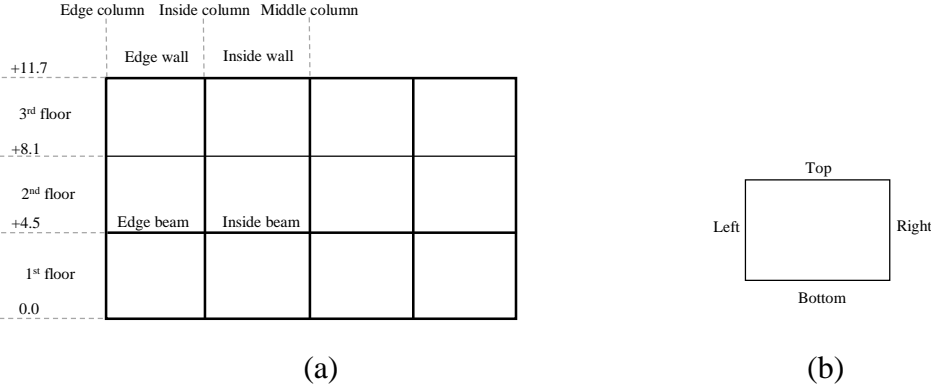


Fig. 2.17 Location of beam, column, and wall

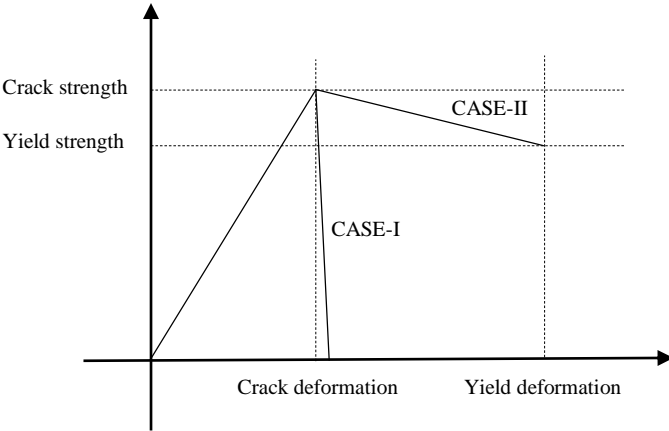
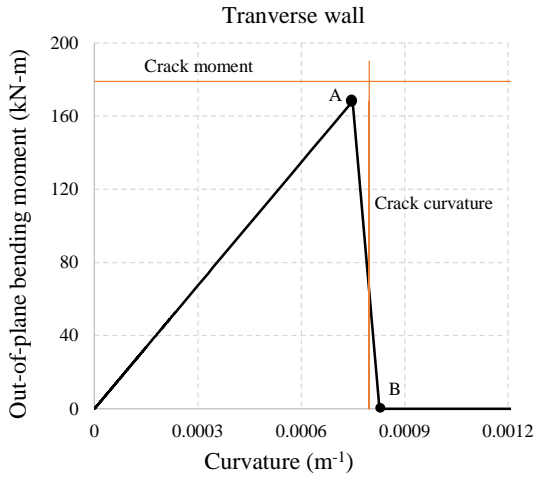


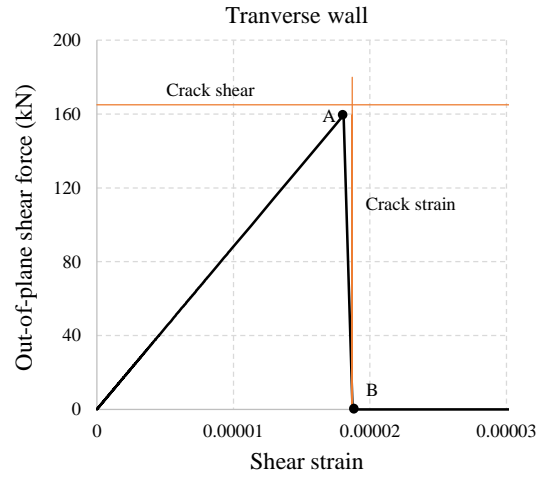
Fig. 2.18 Description of CASE-I and CASE-II

The outer frame of this three-story RC wall-frame building consisted of column, transverse beam, and transverse wall. For the failure mechanism of this outer frame shown in Fig. 2.14, transverse wall was failed by tsunami load. Then transverse beam and column were yield in transverse direction which was the main frame structure of a whole building. The static push-over analysis was performed by varying tsunami inundation depth from 0.0 m to 10.5 m. The analysis results of transverse wall, column, and transverse beam for CASE-I are shown in Fig. 2.19 and Fig. 2.20. The analysis results of transverse wall, column, and transverse beam for CASE-II are shown in Fig. 2.21. For CASE-I in Fig. 2.19(a) considering out-of-plane bending behavior, the edge and inside transverse wall at 1<sup>st</sup> and 2<sup>nd</sup> floor were failed when tsunami inundation depth was more than 7.72 m approximately and the inside transverse wall at 3<sup>rd</sup> floor was failed when tsunami inundation depth was more than 10.42 m approximately. For CASE-I in Fig. 2.19(b) considering out-of-plane shear behavior in vertical direction, the edge transverse wall at 1<sup>st</sup> and 2<sup>nd</sup> floor were failed when tsunami inundation depth was more than 7.70 m approximately and the inside transverse wall at 1<sup>st</sup> and 2<sup>nd</sup> floor were failed when tsunami inundation depth was more than 10.35 m approximately. For CASE-I in Fig. 2.19(c) considering out-of-plane shear behavior in horizontal direction, the left and right position of edge transverse wall at 1<sup>st</sup> floor were failed when tsunami inundation depth was more than 9.81 m and 7.56 m respectively and the right position of inside transverse wall at 1<sup>st</sup> floor were failed when tsunami inundation depth was more than 6.47 m. For CASE-I in Fig. 2.19(d) considering out-of-plane shear behavior in horizontal direction, the left and right position of edge transverse wall at 3<sup>rd</sup> floor were failed when tsunami inundation depth was more than 8.60 m and 7.64 m respectively and the right position of inside transverse wall at 3<sup>rd</sup> floor was failed when tsunami inundation depth was more than 7.62 m. Therefore, it was found that transverse wall at 1<sup>st</sup>, 2<sup>nd</sup>, and 3<sup>rd</sup> floor could be failed for out-of-plane shear and bending behavior within maximum inundation depth 10.50 m. The analysis results of CASE-I for transverse wall seem to comply with observed damage, in which the reinforcement of transverse wall was yielded [57].



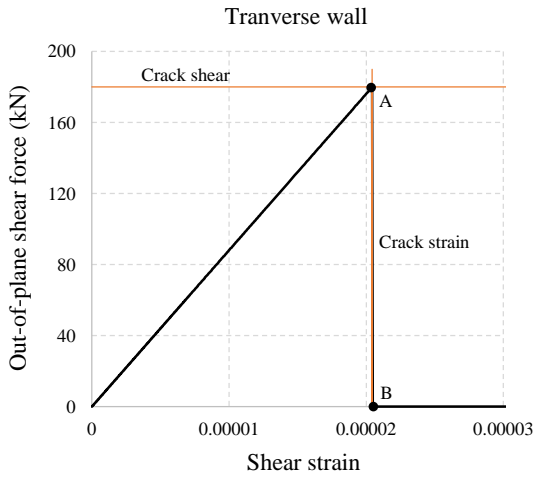
Floor	Loc.	Left		Right	
		A	B	A	B
1 <sup>st</sup>	Edge	7.71 m	7.72 m	7.70 m	7.71 m
	Inside	7.63 m	7.64 m	7.62 m	7.63 m
2 <sup>nd</sup>	Edge	7.69 m	7.70 m	7.64 m	7.65 m
	Inside	7.56 m	7.57 m	7.29 m	7.30 m
3 <sup>rd</sup>	Inside	10.41 m	10.42 m	10.37 m	10.38 m

(a)



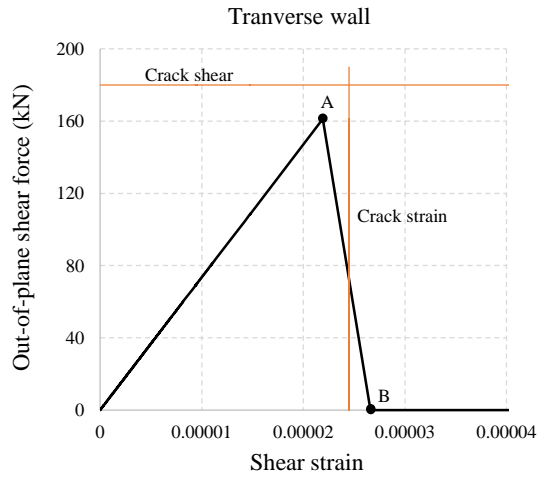
Floor	Loc.	Top		Bottom	
		A	B	A	B
1 <sup>st</sup>	Edge	7.69 m	7.70 m	-	-
	Inside	10.34 m	10.35 m	-	-
2 <sup>nd</sup>	Edge	-	-	7.66 m	7.67 m
	Inside	-	-	10.30 m	10.31 m

(b)



Floor	Loc.	Left		Right	
		A	B	A	B
1 <sup>st</sup>	Edge	9.80 m	9.81 m	7.55 m	7.56 m
	Inside	-	-	6.46 m	6.47 m

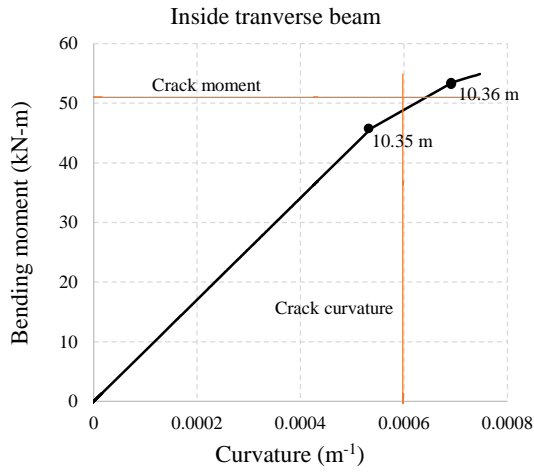
(c)



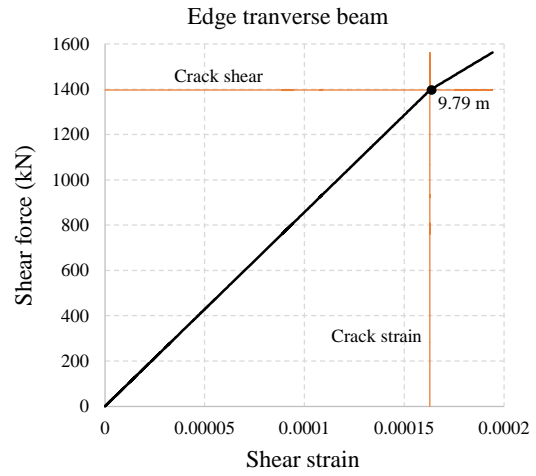
Floor	Loc.	Left		Right	
		A	B	A	B
3 <sup>rd</sup>	Edge	8.59 m	8.60 m	7.63 m	7.64 m
	Inside	-	-	7.61 m	7.62 m

(d)

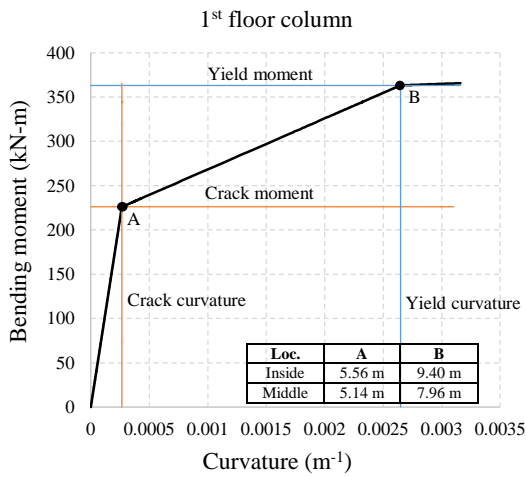
Fig. 2.19 Analysis results of transverse wall for CASE-I



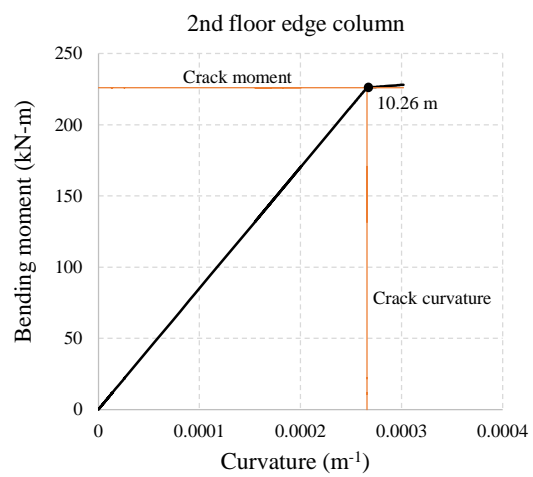
(a)



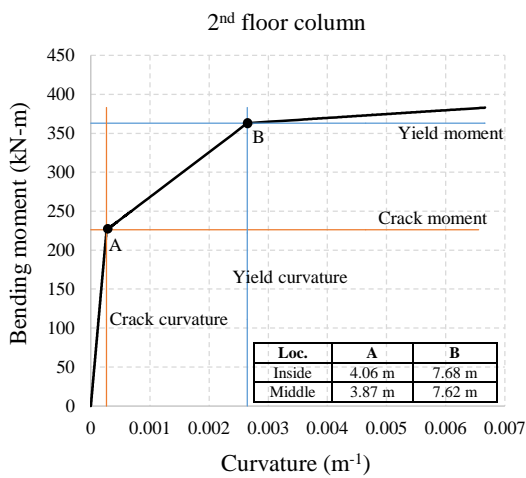
(b)



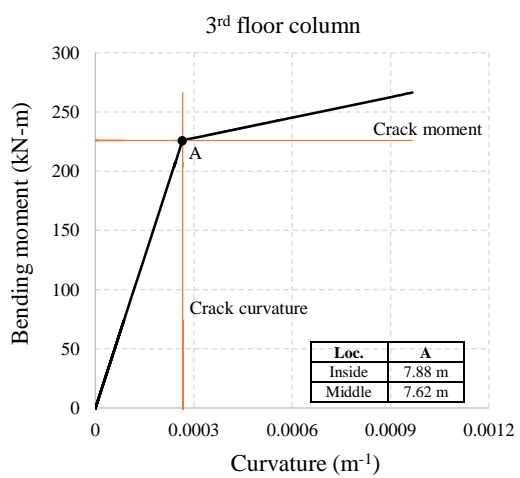
(c)



(d)



(e)



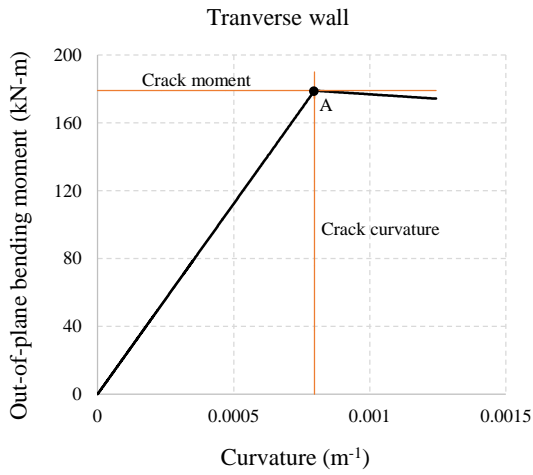
(f)

Fig. 2.20 Analysis results of transverse beam and column for CASE-I

For CASE-I in Fig. 2.20(a) and Fig. 2.20(b) considering bending and shear behavior, the inside transverse beam was cracked when tsunami inundation depth was more than 10.36 m and the edge transverse beam was cracked when tsunami inundation depth was more than 9.79 m. For CASE-I in Fig. 2.20(c) considering bending behavior, the inside and middle column at 1<sup>st</sup> floor were yielded when tsunami inundation depth was more than 9.40 m and 7.96 m respectively. For CASE-I in Fig. 2.20(d) considering bending behavior, the edge column at 2<sup>nd</sup> floor was cracked when tsunami inundation depth was more than 10.26 m. For CASE-I in Fig. 2.20(e) considering bending behavior, the inside and middle column at 2<sup>nd</sup> floor were yielded when tsunami inundation depth was more than 7.68 m and 7.62 m respectively. For CASE-I in Fig. 2.20(f) considering bending behavior, the inside and middle column at 3<sup>rd</sup> floor were cracked when tsunami inundation depth was more than 7.88 m and 7.62 m respectively. The analysis results of CASE-I for column at 1<sup>st</sup> and 2<sup>nd</sup> floor seem to comply with observed damage, in which the reinforcement of column was yielded [57]. However, the analysis results of CASE-I for transverse beam seem to underestimate comparing with observed damage, in which the reinforcement of beam was yielded [57].

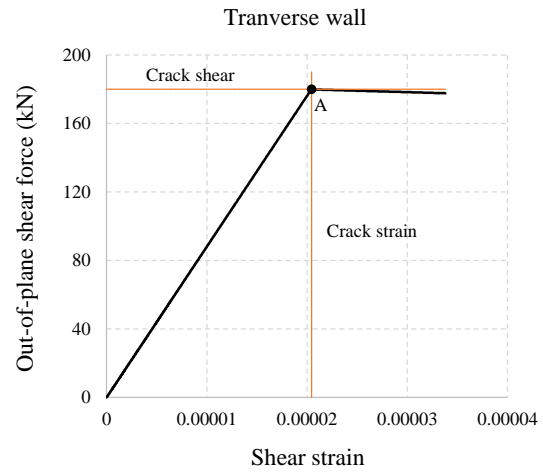
For CASE-II in Fig. 2.21(a) considering out-of-plane bending behavior, the inside transverse wall at 2<sup>nd</sup> floor were cracked when tsunami inundation depth was more than 9.68 m approximately. For CASE-II in Fig. 2.21(b) considering out-of-plane shear behavior in horizontal direction, the edge transverse wall at 1<sup>st</sup> and 3<sup>rd</sup> floor were cracked when tsunami inundation depth was more than 8.38 m and 10.02 m respectively and the inside transverse wall at 1<sup>st</sup> and 3<sup>rd</sup> floor were cracked when tsunami inundation depth was more than 6.62 m and 8.75 m respectively. For CASE-II in Fig. 2.21(c) considering bending behavior, the inside and middle column at 1<sup>st</sup> floor were cracked when tsunami inundation depth was more than 5.56 m and 5.14 m respectively. For CASE-II in Fig. 2.21(d), the inside and middle column at 2<sup>nd</sup> floor were cracked when tsunami inundation depth was more than 4.06 m and 3.87 m respectively. The analysis results of CASE-II seem to underestimate comparing with observed damage. However, tsunami load might be larger than hydrostatic pressure shown in Fig. 2.16 due to the effect of impact load. Focusing on

the effect of strength degradation in CASE-II, it was found that macro plate model can simulate well out-of plane behavior of transverse wall.



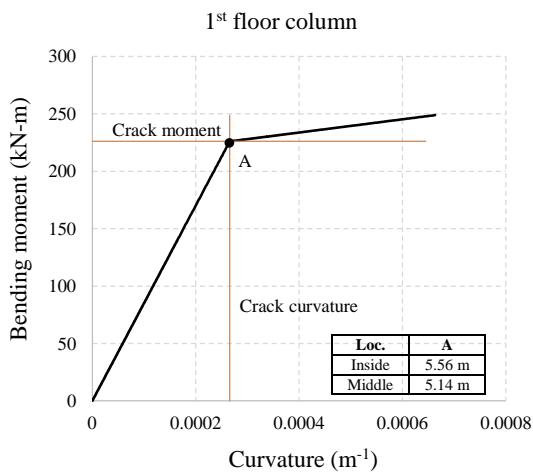
Floor	Loc.	Left	Right
		A	
2 <sup>nd</sup>	Inside	9.68 m	9.43 m

(a)



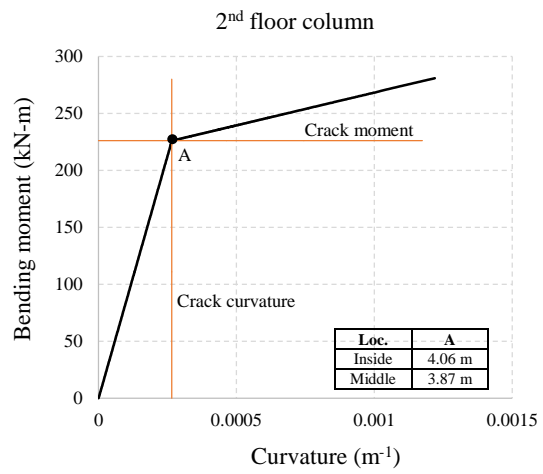
Floor	Loc.	Left	Right
		A	
1 <sup>st</sup>	Edge	-	8.38 m
	Inside	6.62 m	6.46 m
3 <sup>rd</sup>	Edge	-	10.02 m
	Inside	8.75 m	8.70 m

(b)



Loc.	A
Inside	5.56 m
Middle	5.14 m

(c)



Loc.	A
Inside	4.06 m
Middle	3.87 m

(d)

Fig. 2.21 Analysis results of transverse wall and column for CASE-II

## **2.6 SEQUENTIAL ANALYSIS FROM EARTHQUAKE AND TSUNAMI**

In order to study on nonlinear structural analysis of a RC building suffering damage from earthquake and subsequent tsunami, a nonlinear analytical model of the six-story RC wall-frame building in Fig. 2.10 was carried out to investigate structural damage of beam, column, and wall. In analysis, an earthquake and tsunami scenario was simulated to occur with this six-story RC wall-frame building. In the case of earthquake, dynamic structural response analysis was performed to investigate structural damage of this building subject to strong ground motion. Sequentially, static pushover analysis was performed to investigate more structural damage to this building subject to hydrodynamic force from tsunami. For simulating sequential behavior of earthquake and tsunami response, nonlinear structural analysis was performed by means of the same hysteresis models. The initial assumption was that more serious damage from sequential tsunami response might be able to occur with beam, column, and wall.

### **2.6.1 Input ground motion and tsunami load**

For input ground motion, the INPUT-II in Table 2.2 was applied to the nonlinear analytical model in order to perform dynamic structural response analysis from earthquake. For input tsunami load in Fig. 2.22, hydrodynamic force was estimated from tsunami inundation depth and flow velocity, which obtained from tsunami inundation simulation [2]. As shown in Fig. 2.22, input tsunami load was divided to striking wave (1<sup>st</sup> wave) and receding wave (2<sup>nd</sup> wave) in y-direction. According to FEMA 2011 [56], hydrodynamic pressure in Fig. 2.22 was applied uniformly to the nonlinear analytical model along building height according to the maximum inundation depth 15 m in order to perform static pushover analysis from tsunami. Therefore, the nonlinear analytical model was proposed to investigate structural damage of the six-story RC wall-frame building subject to a series of earthquake, striking wave, and receding wave of tsunami.

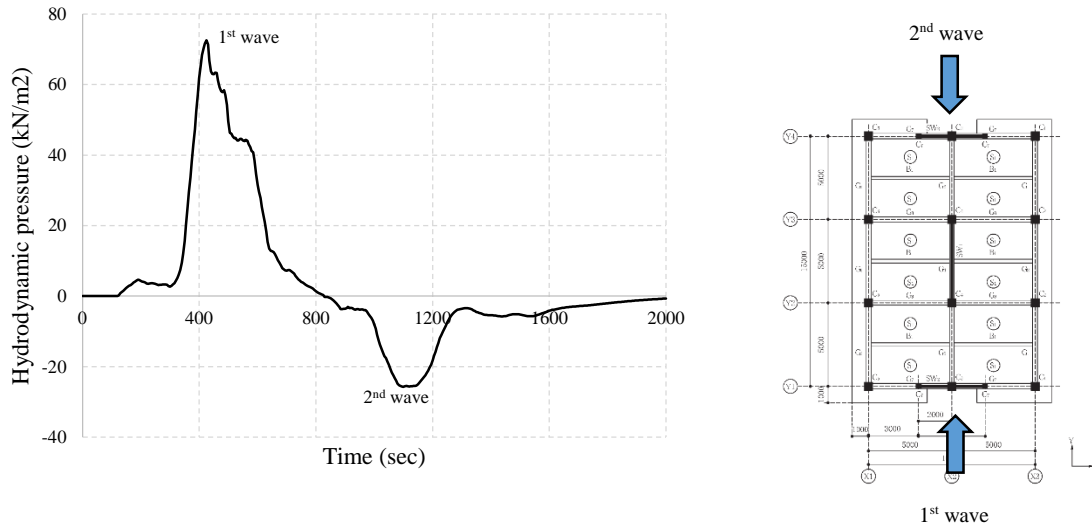


Fig. 2.22 Input tsunami load

## 2.6.2 Analysis results

Due to a symmetric plan of the six-story RC wall-frame building, the focused structural components in analysis results were columns located at X1-Y1, X2-Y1, X1-Y2, and X2-Y2: beams located between Y1-Y2 and Y2-Y3 of X1 frame and Y1-Y2 of X2 frame: shear wall located at X2 frame: wing wall located between X1-X2 of Y1 frame. Since input tsunami load was applied in y-direction, only analysis results in y-direction were discussed for bending moment of columns and beams: axial force, in-plane bending moment, and shear force of shear wall: out-of-plane bending moment and shear force of wing wall. Initially, the structural components of the first three floors were investigated for sequential behavior. Input tsunami load in Fig. 2.22 was modified until the maximum pressure can reach out-of-plane bending failure of wing wall at 1<sup>st</sup> floor as shown in Fig. 2.24(a). The results of relative displacement at each story are shown in Fig. 2.23. As shown in Fig. 2.23, the results can be divided into four parts of analysis, such as strong ground motion during 0 sec to 20 sec, free vibration during 20 sec to 25 sec, striking wave during 25 sec to 41.5 sec, and receding wave during 41.5 sec to 65 sec in which duration time of tsunami load was modified from input tsunami load in Fig. 2.22. The maximum relative

displacement at roof was 0.0433 m from earthquake response and 0.0544 m from tsunami response.

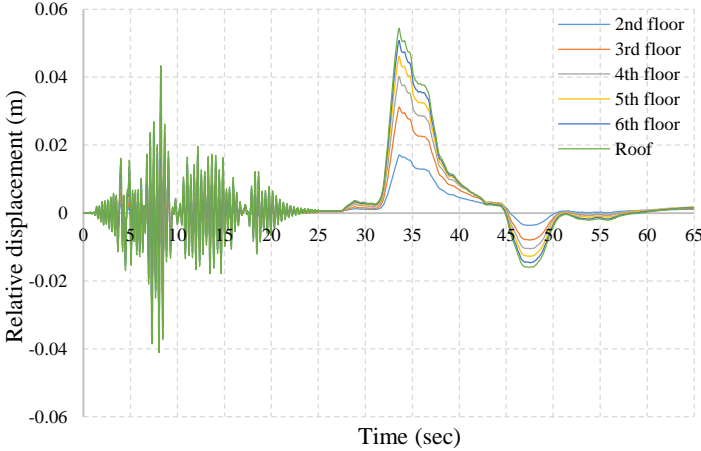


Fig. 2.23 The results of relative displacement at each story

As mentioned above, input tsunami load was modified to induce out-of-plane bending failure of wing wall at 1<sup>st</sup> floor shown in Fig. 2.24(a) in order investigate sequential behavior of each structural component, such as beam, column, and shear wall. As shown in Fig. 2.24(a), out-of-plane bending behavior of wing wall was in linear range during earthquake response (red line) and then the out-of-plane bending failure occurred during sequential tsunami response (blue line) at the maximum hydrodynamic pressure. For out-of-plane bending strength of wing wall, a crack point was considered as a failure point because the reinforcement ratio of wing wall was small, so that ultimate curvature was  $0.001756 \text{ m}^{-1}$ . Therefore, out-of-plane bending moment was drop to zero after this failure during sequential tsunami response shown in Fig. 2.24(a). The result of out-of-plane shear behavior is shown in Fig. 2.24(b). It was found that out-of-plane shear behavior of wing wall was in nonlinear range during earthquake response and then out-of-plane shear strain increased during sequential tsunami response. It means that more structural damage of wing wall at 1<sup>st</sup> floor occurred from sequential tsunami response. As well as wing walls at 2<sup>nd</sup> and 3<sup>rd</sup> floor in Fig. 2.25(a) and Fig. 2.25(b) respectively, more structural damage in out-of-plane shear behavior occurred from sequential tsunami response. For out-of-plane shear

strength of all wing walls, crack strain was 0.000020751 and ultimate strain was 0.0003152. Therefore, out-of-plane shear strain of wing wall at 1<sup>st</sup> and 3<sup>rd</sup> floor in Fig. 2.24(b) and Fig. 2.25(b) was still less than ultimate strain. However, out-of-plane shear strain of wing wall at 2<sup>nd</sup> floor in Fig. 2.25(a) was approaching to ultimate strain due to out-of-plane bending failure of wing wall at 1<sup>st</sup> floor.

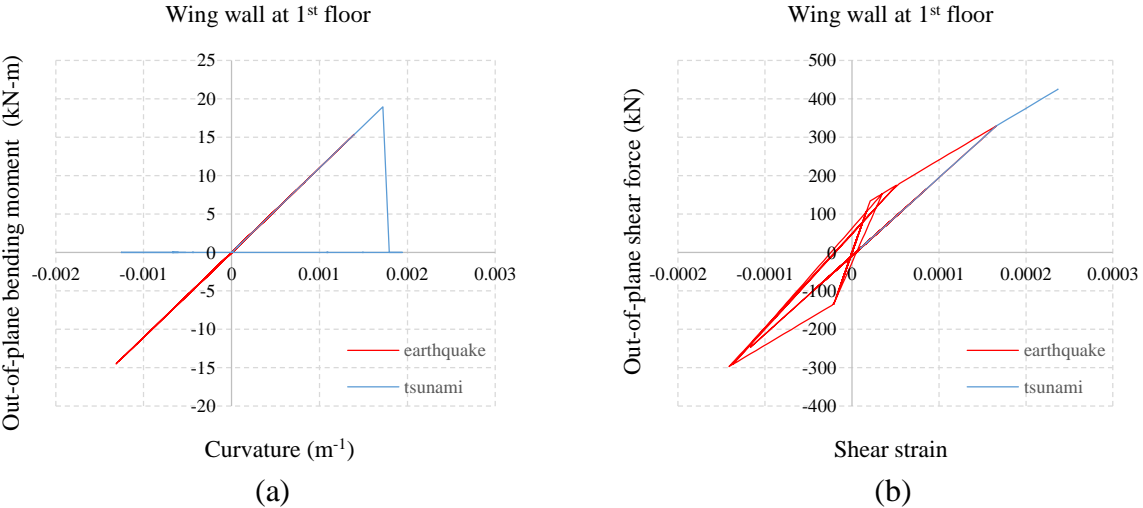


Fig. 2.24 The results of wing wall at 1<sup>st</sup> floor

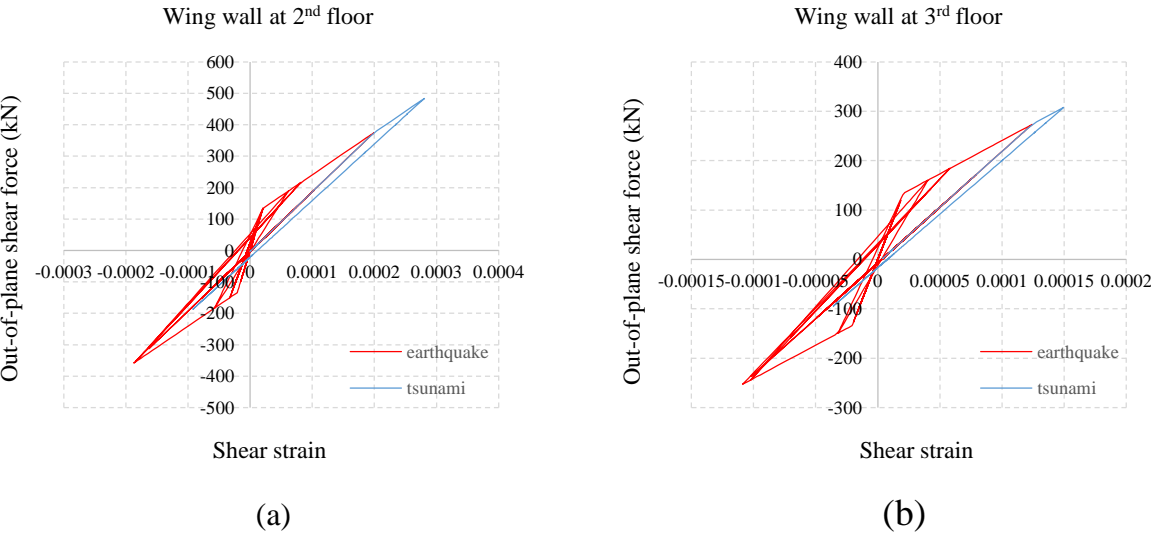


Fig. 2.25 The results of wing wall at 2<sup>nd</sup> and 3<sup>rd</sup> floor

The results of shear wall at 1<sup>st</sup> floor are shown in Fig. 2.26. As shown in Fig. 2.26(a), axial behavior of shear wall was in nonlinear range during earthquake response and then axial strain increased during sequential tsunami response. It means that more structural damage of shear wall occurred from sequential tsunami response. As well as in-plane bending and shear behavior of shear wall at 1<sup>st</sup> floor in Fig. 2.26(b) and Fig. 2.26(c) respectively, more structural damage occurred from sequential tsunami response.

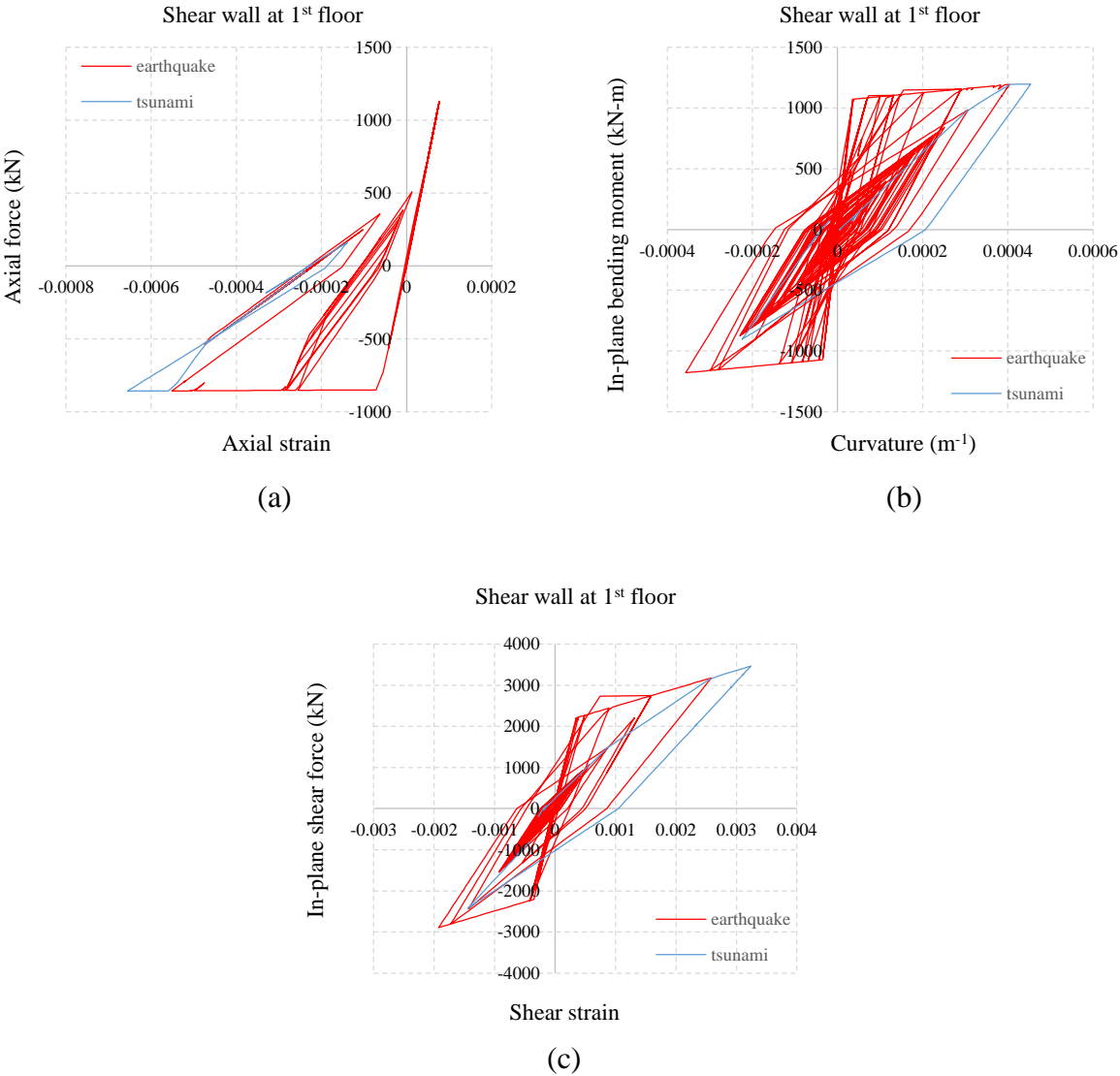


Fig. 2.26 The results of shear wall at 1<sup>st</sup> floor

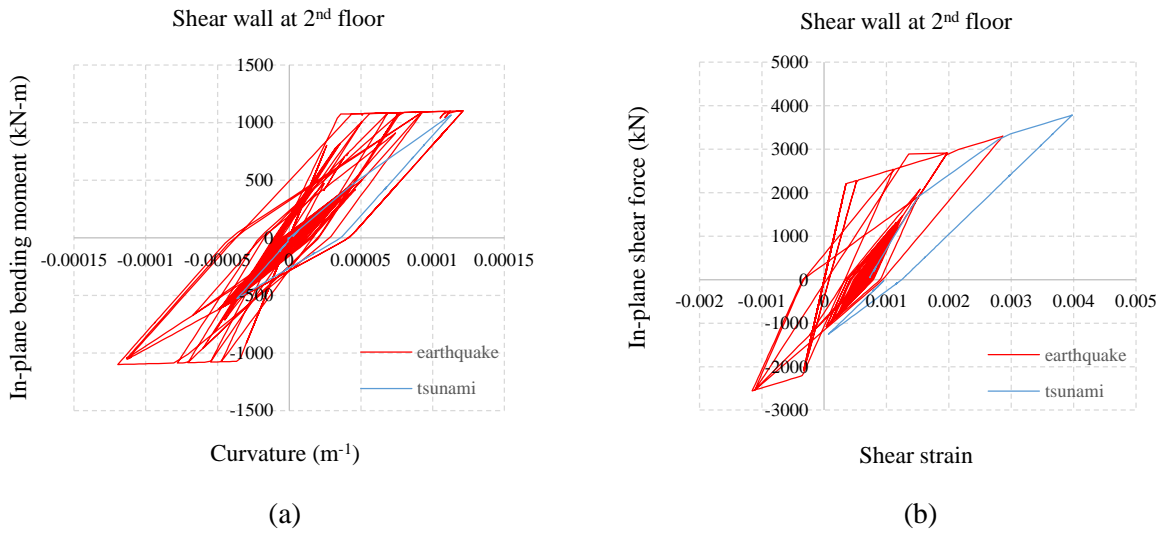


Fig. 2.27 The results of shear wall at 2<sup>nd</sup> floor

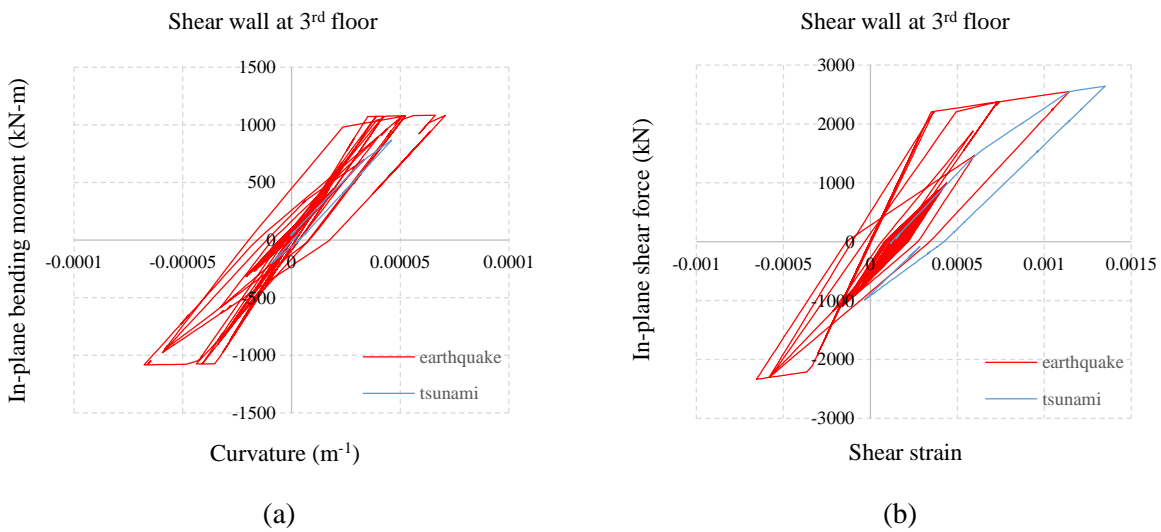


Fig. 2.28 The results of shear wall at 3<sup>rd</sup> floor

The results of shear walls at 2<sup>nd</sup> and 3<sup>rd</sup> floor are shown in Fig. 2.27 and Fig. 2.28 respectively. For both shear walls at 2<sup>nd</sup> and 3<sup>rd</sup> floor, in-plane curvature didn't increase shown in Fig. 2.27(a) and Fig. 2.28(a) respectively, so that no more structural damage in in-plane bending behavior occurred from sequential tsunami response. On the other hand, in-plane shear strain increased for both shear walls at 2<sup>nd</sup> and 3<sup>rd</sup> floor shown in Fig. 2.27(b) and Fig. 2.28(b) respectively, so that more structural damage in in-plane shear behavior

occurred from sequential tsunami response. For in-plane bending strength of all shear walls, crack curvature was  $0.000035 \text{ m}^{-1}$ , yield curvature was  $0.000406 \text{ m}^{-1}$ , and ultimate curvature was  $0.008115 \text{ m}^{-1}$ , so that in-plane curvature of shear wall at 1<sup>st</sup> floor in Fig. 2.26(b) was a little larger than yield curvature. For in-plane shear strength of those, crack strain was 0.00035 and ultimate strain was 0.004, so that in-plane shear strain of shear walls in Fig. 2.26 - Fig. 2.28 were still less than ultimate strain. However, in-plane shear strain of shear wall at 2<sup>nd</sup> floor was approaching to ultimate strain due to out-of-plane bending failure of wing wall at 1<sup>st</sup> floor.

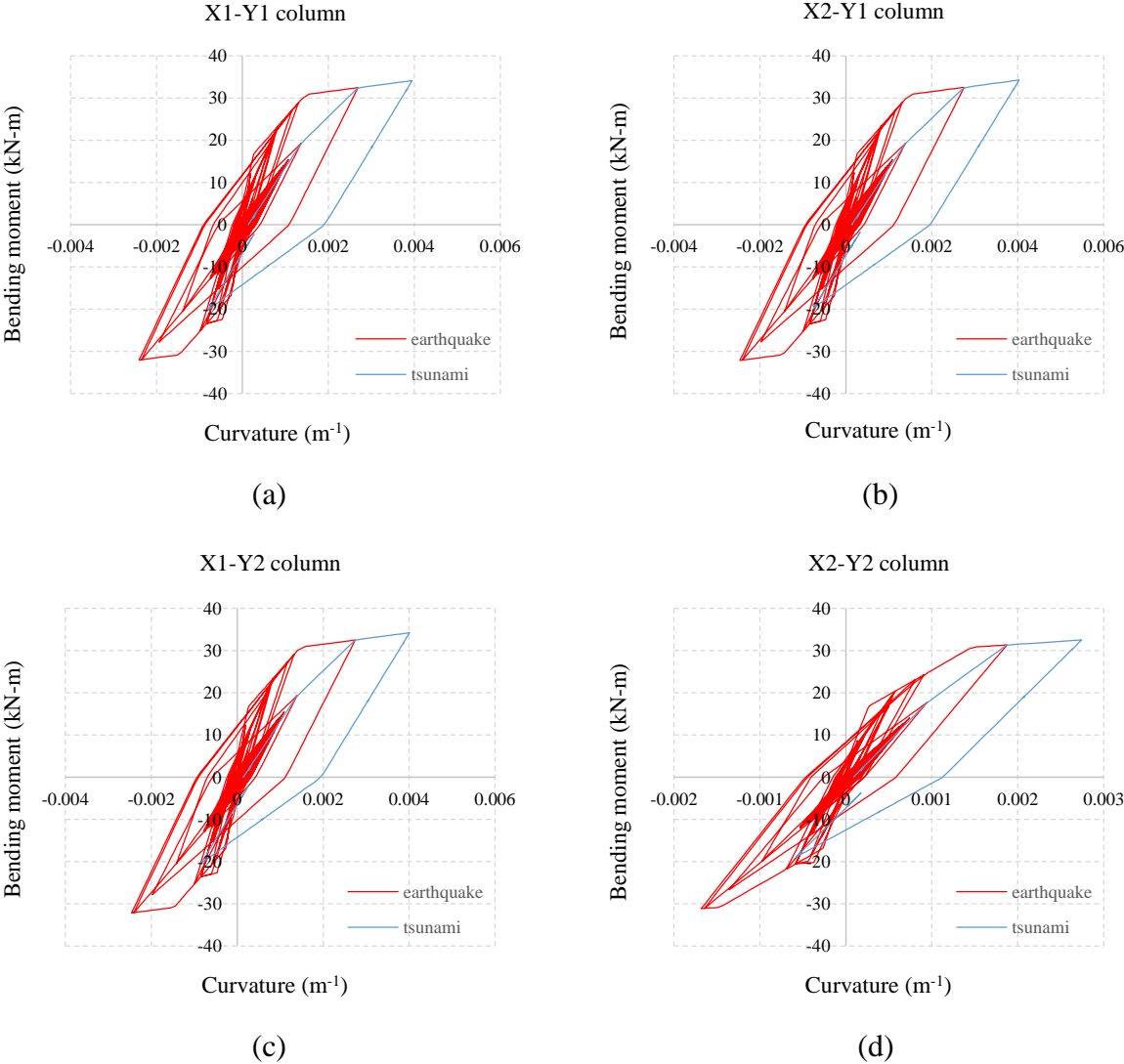


Fig. 2.29 The results of columns at 1<sup>st</sup> floor

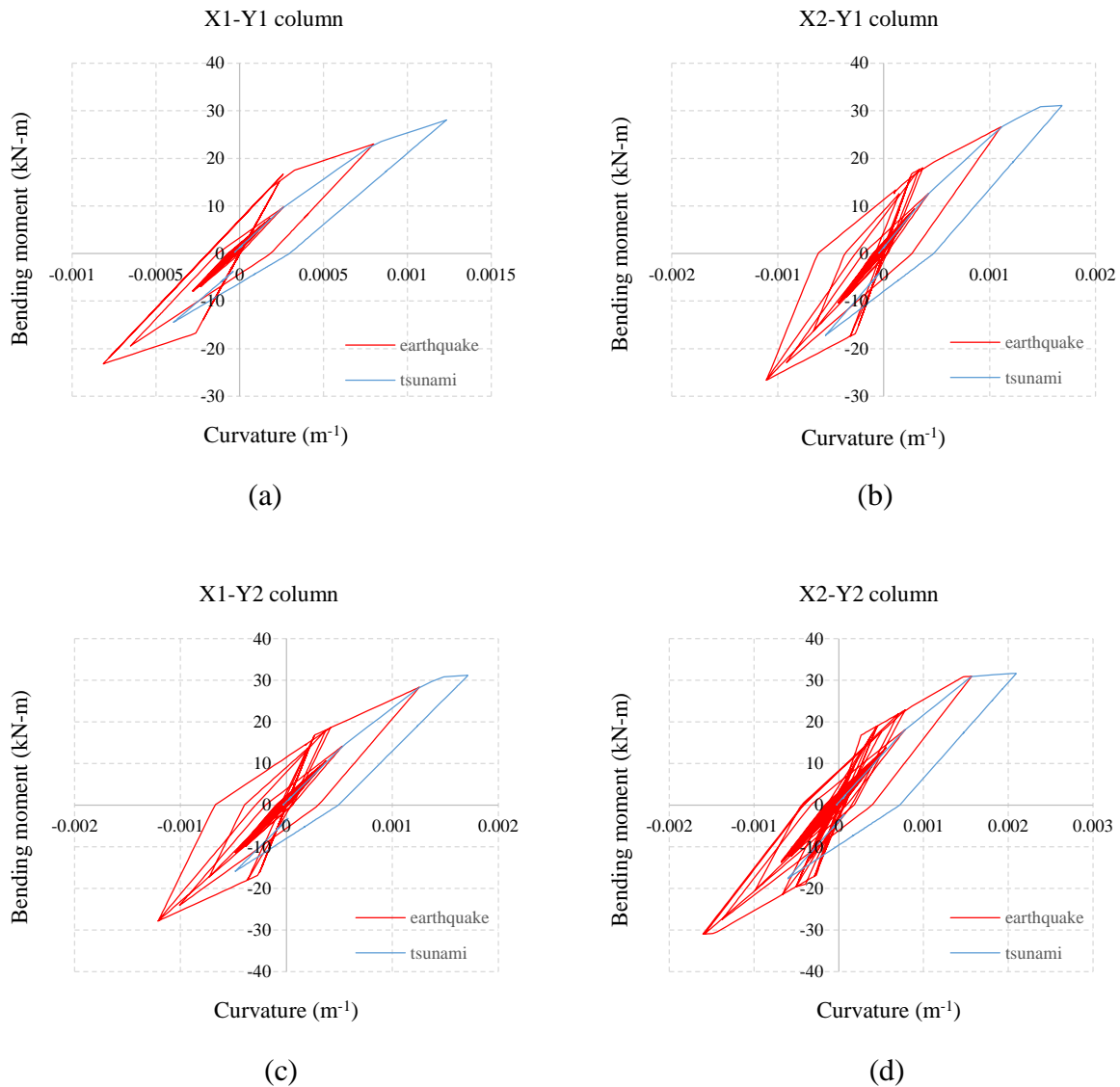


Fig. 2.30 The results of columns at 2<sup>nd</sup> floor

The results of columns at 1<sup>st</sup>, 2<sup>nd</sup>, and 3<sup>rd</sup> floor are shown in Fig. 2.29 - Fig. 2.31 respectively. For all columns shown in Fig. 2.29 - Fig. 2.31, bending behavior was in nonlinear range during earthquake response and then curvature increased during sequential tsunami response, in which it means that more structural damage in bending behavior occurred from sequential tsunami response. For bending strength of columns in Fig. 2.29 - Fig. 2.31, crack curvature was 0.000263 m<sup>-1</sup>, yield curvature was 0.00147 m<sup>-1</sup>, and ultimate curvature was 0.0115 m<sup>-1</sup>. Since curvature of all columns at 1<sup>st</sup> floor in Fig. 2.29 was less

than 0.004, these columns were still yielding. As shown in Fig. 2.30, all columns except for X1-Y1 column in Fig. 2.30(a) were cracked from earthquake response and then yielding from sequential tsunami response. As shown in Fig. 2.31, all columns were cracked except for X2-Y2 column in Fig. 2.31(d), which was yielding from sequential tsunami response.

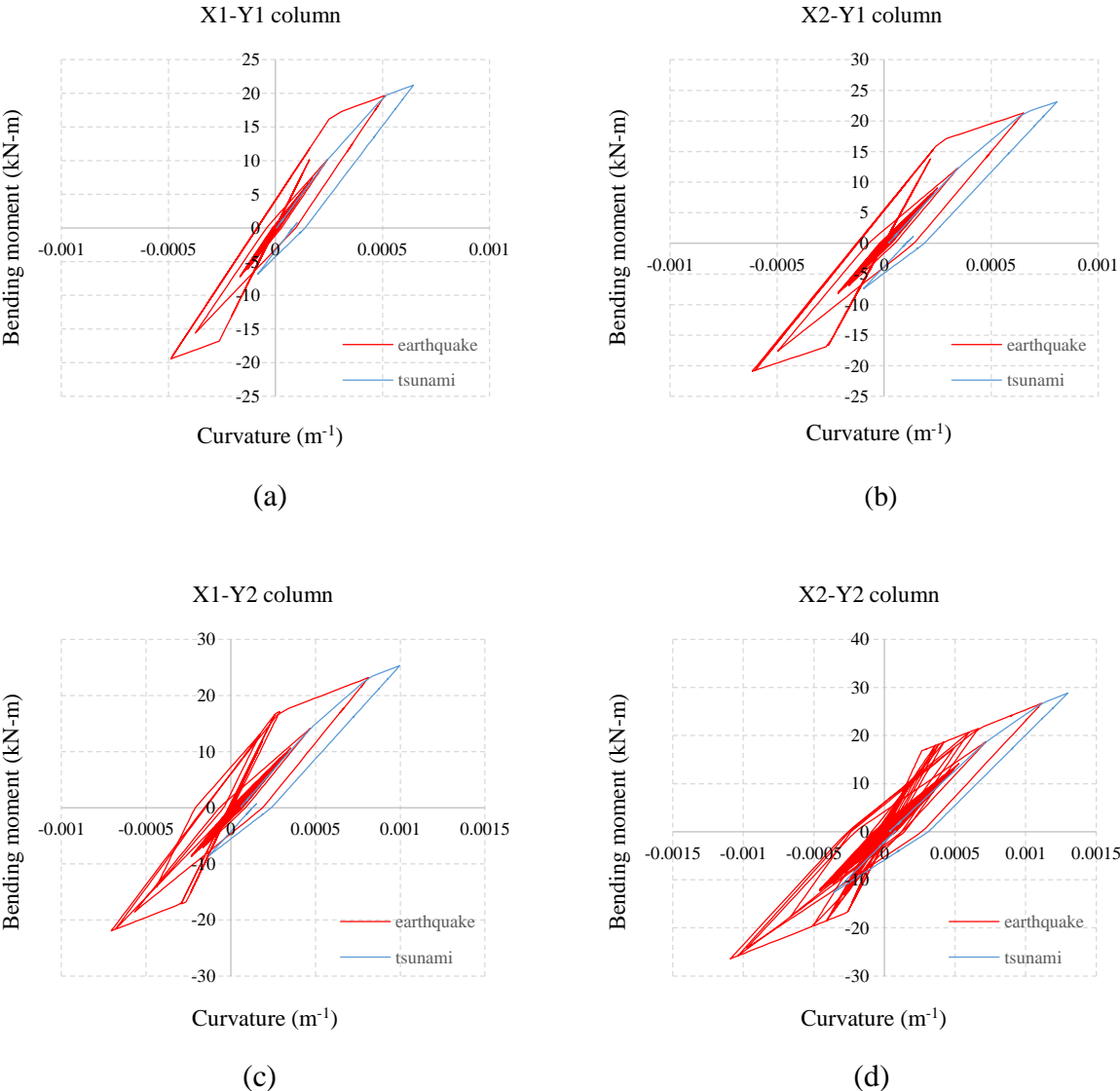


Fig. 2.31 The results of columns at 3<sup>rd</sup> floor

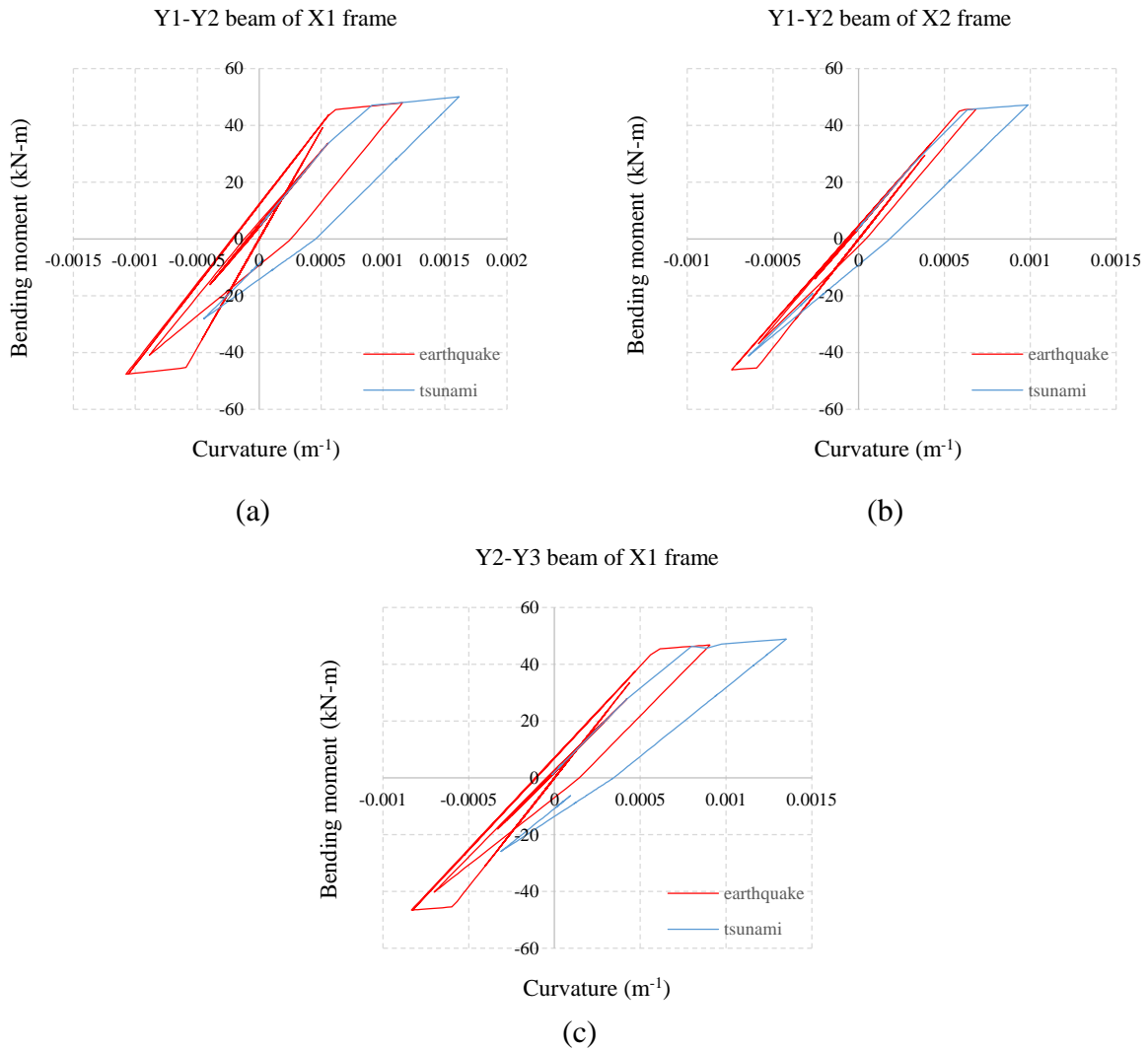


Fig. 2.32 The results of beams at 2<sup>nd</sup> floor

The results of beams at 2<sup>nd</sup> and 3<sup>rd</sup> floor are shown in Fig. 2.32 and Fig. 2.33 respectively. For all beams at 2<sup>nd</sup> floor shown in Fig. 2.32, bending behavior was in nonlinear range during earthquake response and then curvature increased during sequential tsunami response, in which it means that more structural damage in bending behavior occurred from sequential tsunami response. For beam between Y1-Y2 of X1 frame at 3<sup>rd</sup> floor in Fig. 2.33(a), more structural damage in bending behavior occurred from sequential tsunami response as well as all beams in Fig. 2.32. For beam between Y1-Y2 of X2 frame in Fig. 2.33(b), bending behavior was in linear range during earthquake and sequential

tsunami response, so that no damage occurred. For beam between Y2-Y3 of X1 frame in Fig. 2.33(c), bending behavior was in linear range during earthquake response and then curvature increased during sequential tsunami response, so that more structural damage in bending behavior occurred from sequential tsunami response. For bending strength of beams in Fig. 2.32 and Fig. 2.33, crack curvature was  $0.000592 \text{ m}^{-1}$ , yield curvature was  $0.00366 \text{ m}^{-1}$ , and ultimate curvature was  $0.0247 \text{ m}^{-1}$ . Since curvature of all beams at 2<sup>nd</sup> floor in Fig. 2.32 was less than yield curvature, these beams were still cracked as well as beam at 3<sup>rd</sup> floor in Fig. 2.33(a) and Fig. 2.33(c).

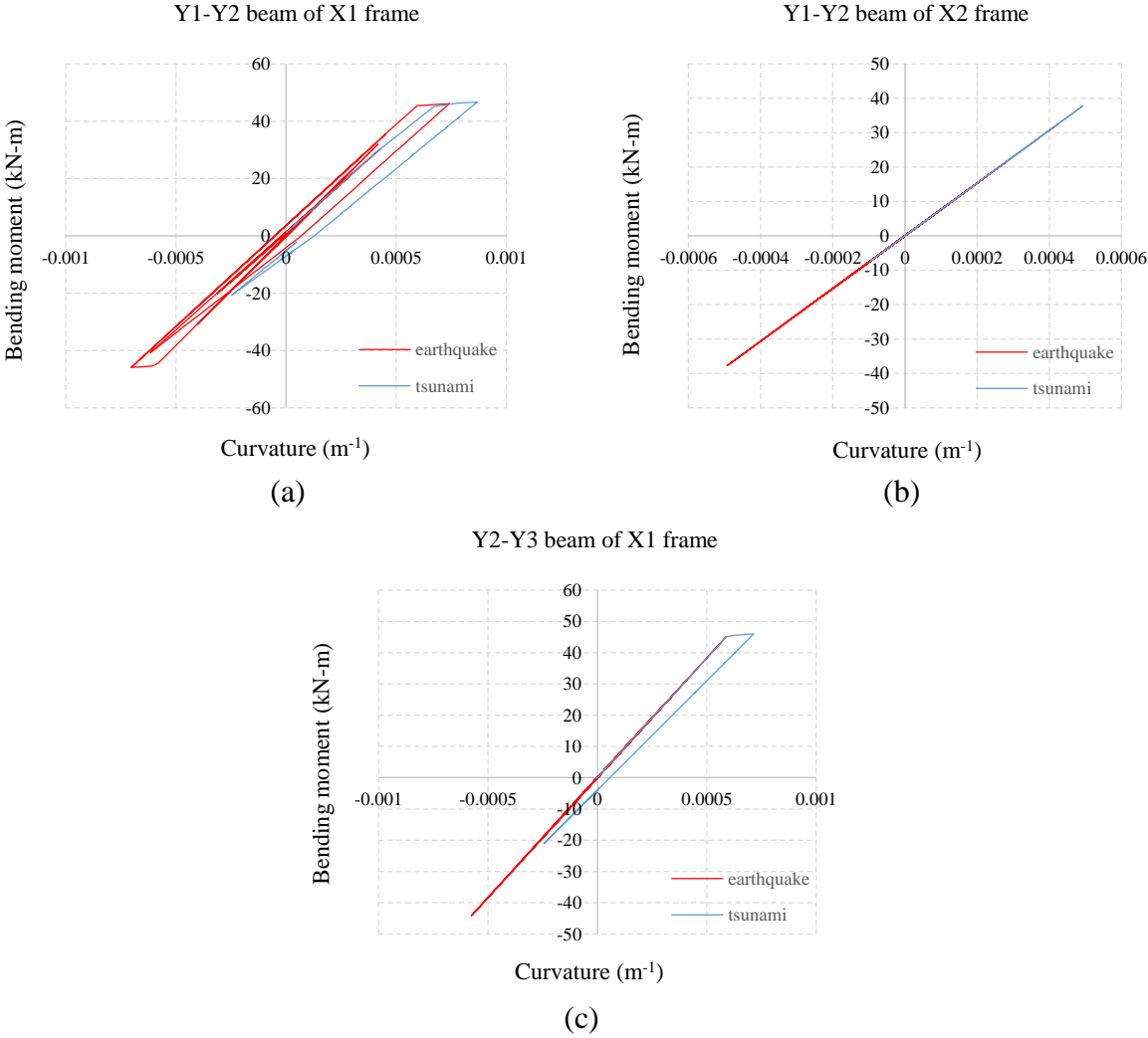


Fig. 2.33 The results of beams at 3<sup>rd</sup> floor

Table 2.3 shows failure mode of each structural member from earthquake response and sequential tsunami response. As can be seen in Table 2.3, the failure mode after earthquake response was cracking except for bending failure mode of column at 1<sup>st</sup> floor. This failure mode of all structural members had a significant effect to sequential damage from tsunami response. It was found that more damage from sequential tsunami response could occur with most of structural members except for in-plane bending failure mode of shear wall at 2<sup>nd</sup> and 3<sup>rd</sup> floor. Due to out-of-plane bending failure of wing wall at 1<sup>st</sup> floor, it was found that in-plane shear force was redistributed to concentrate on shear wall at 2<sup>nd</sup> wall. Comparing column at 1<sup>st</sup> floor with other floors, more serious damage from sequential tsunami response could occur significantly as same as the concept of earthquake response.

Table 2.3 Failure mode of each structural member from earthquake response and sequential tsunami response

Structural member	Failure mode	No. floor	Earthquake response	Sequential tsunami response
Shear wall	Bending	1 <sup>st</sup>	Cracking	Yielding
		2 <sup>nd</sup>	Cracking	Cracking
		3 <sup>rd</sup>	Cracking	Cracking
	Shear	1 <sup>st</sup>	Cracking	More cracking
		2 <sup>nd</sup>	Cracking	Reaching to ultimate
		3 <sup>rd</sup>	Cracking	More cracking
Column	Bending	1 <sup>st</sup>	Yielding	More yielding
		2 <sup>nd</sup>	Cracking	Yielding
		3 <sup>rd</sup>	Cracking	More cracking
Longitudinal beam	Bending	2 <sup>nd</sup>	Cracking	More cracking
		3 <sup>rd</sup>	Cracking	More cracking

## 2.7 CONCLUSIONS

Macro plate model was used to simulate in-plane and out-of-plane behavior of a wall member in a nonlinear analytical model of RC wall-frame buildings including tsunami load. Based on the verification results of the nonlinear analytical model with the test at E-Defense, the results show a good correlation for 25% and 50% of input ground motion

without considering post-peak response, although the input data of ground motion was slightly different. Based on the verification results of the analytical model with observed damage from tsunami in the 2011 Great East Japan earthquake and tsunami, the results of CASE-I, in which strength degradation was ignored in out-of-plane strength of transverse wall, seem to comply with observed damage for transverse wall and column. For CASE-II in which strength degradation was considered in out-of-plane strength of that, the results seem to underestimate comparing with observed damage. However, tsunami load in real situation might be larger than the calculated hydrostatic pressure. Focusing on the effect of strength degradation in CASE-II, it was found that macro plate model can simulate well out-of plane behavior of transverse wall.

The nonlinear structural model was proposed to investigate structural damage of RC wall-frame buildings subjected to earthquake and subsequent tsunami. Based on the same hysteresis model in the case of earthquake and tsunami, nonlinear structural analysis of a six-story RC wall-frame building was performed to study on sequential behavior of earthquake and tsunami response. From analysis results of the first three floors, it was found that more damage from sequential tsunami response could occur with most of structural members except for in-plane bending failure mode of shear wall. Due to out-of-plane bending failure of wing wall at 1<sup>st</sup> floor, it was found that out-of-plane shear force was redistributed to concentrate on wing wall at 2<sup>nd</sup> wall. Moreover, it was found that in-plane shear force was redistributed to concentrate on shear wall at 2<sup>nd</sup> wall. Comparing column at 1<sup>st</sup> floor with other floors, more serious damage from sequential tsunami response could occur significantly as same as the concept of earthquake response. After earthquake response, structural properties of RC wall-frame buildings can be changed to resist against the coming tsunami load which may be stronger or weaker. Therefore, it is necessary to consider the failure mechanism of sequential behavior in order to protect RC wall-frame buildings from earthquake and subsequent tsunami.

## **CHAPTER III**

### **DAMAGE PREDICTION IN A TARGET AREA**

#### **3.1 ABSTRACT**

For tsunami scenarios, evaluation of tsunami load acting each building depends on surrounding circumstance. Therefore, modeling of all buildings in a target area is important for damage prediction from earthquake and subsequent tsunami. In this chapter, sequential earthquake and tsunami simulation was developed to predict structural damage from earthquake and subsequent tsunami by means of the application in Integrated Earthquake Simulation (IES). Since IES can simulate only earthquake scenarios with beam-column frame models, IES was modified for input tsunami load acting on a proposed wall-frame model in order to simulate tsunami scenarios using predicted data of tsunami inundation depth. A target area in Kochi city was selected to simulate an earthquake and tsunami scenario because this area has many public buildings and is important for economic activities. A double-layer platform of high performance computing was proposed to simulate this earthquake and tsunami scenario with parallel processing on CPUs and GPUs. The results of sequential earthquake and tsunami simulation show that three-story RC buildings had a significant risk that maximum drift ratio could occur during sequential tsunami response. However, maximum drift ratio from sequential tsunami response was still less than 0.3% in which structural damage didn't occur obviously. For the worst case scenario that tsunami inundation depth was double, structural damage from sequential tsunami response was much more serious than that of the normal-case scenario in which maximum drift ratio was less than 5% for a four-story RC building. In addition, it was found that low-rise buildings (three- to seven-story) had a significant risk that maximum drift ratio was higher than 1% during sequential tsunami response. The results of sequential earthquake and tsunami simulation can be used to construct further prevention measures.

### 3.2 INTRODUCTION

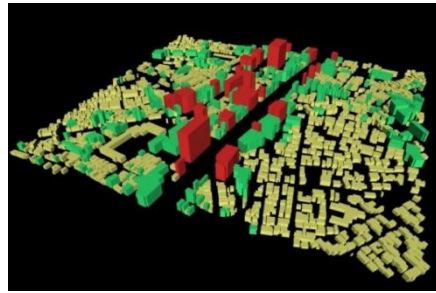
Based on past experience in the Great East Japan earthquake and tsunami, many buildings in Tohoku area were seriously damaged by earthquake and subsequent tsunami. In the future, severe damage as serious as the previous earthquake and tsunami may occur in other area of Japan, such as Tokai, Tonankai, Nankai area. In order to reduce the loss of human life in future earthquake and tsunami, damage prediction is a key role for constructing prevention measure and raising awareness of people. For damage prediction in a target area, computer technology has been applied to simulate earthquake scenarios, such as Integrated Earthquake Simulation (IES) [59]-[65]. Integrated Earthquake Simulation (IES) is an earthquake simulation tool for predicting and illustrating structural damage of all buildings in the target area simultaneously in selected earthquake scenarios. Based on Geographic Information System (GIS) data in Fig. 3.1(a), thousands of buildings in the target area are modeled to polygon shapes in Fig. 3.1(b) from building shape and height. Based on building design code, Common Modeling Data (CMD) is a modeling approach to convert a polygon shape in Fig. 3.2(a) as a structural model in Fig. 3.2(b), consisting of beam and column elements including section and material properties of each element. In Fig. 3.1(c), nonlinear structural analysis of all buildings in the target area is performed to predict structural damage and then illustrate structural damage of all buildings simultaneously as shown in Fig. 3.1(d).

For a target area, structural damage of each building is predicted from the results of nonlinear structural analysis. Object-Based Structural Analysis (OBASAN), a structural analysis program, which has been developed by our laboratory, is proposed to perform nonlinear structural analysis in IES. Therefore, there are two main parts in this study: the first part is IES for building modeling and the second part is OBASAN for nonlinear structural analysis. For thousands of buildings in the target area, IES can visualize structural damage to raise awareness of disaster prevention among people in that area. Since high performance computing (HPC) is a key role to carry out a large number of buildings in the target area, OpenMPI application has been applied to IES in order to enable

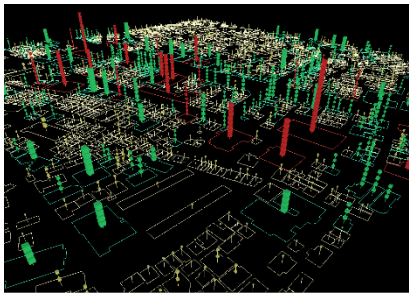
parallel processing on the Central Processing Units (CPUs).



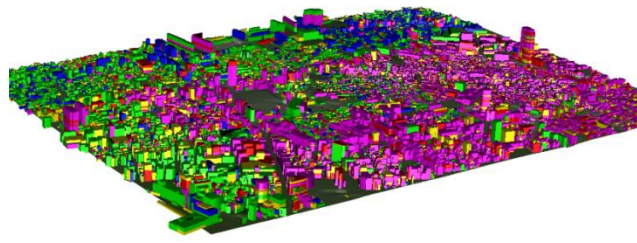
(a)



(b)

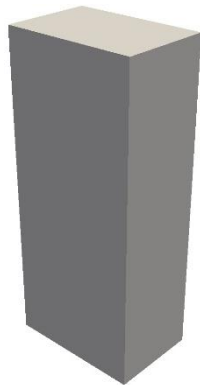


(c)

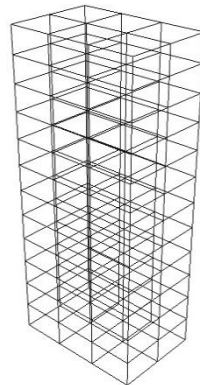


(d)

Fig. 3.1 Integrated Earthquake Simulation [62]



(a)



(b)

Fig. 3.2 Common Modeling Data (CMD) [68]

### 3.3 DAMAGE PREDICTION FROM EARTHQUAKE AND TSUNAMI

In this study, damage prediction of all RC buildings in a target area from earthquake and subsequent tsunami was proposed by means of the application in IES. Since IES can simulate only earthquake scenarios, IES was modified to input tsunami load acting on each building in order to simulate tsunami scenarios using data of tsunami inundation depth provided by Japan Cabinet Office (JCO). In IES, evaluation of tsunami load was included for all RC buildings as the same approach as earthquake scenarios and new building modeling was proposed to perform nonlinear structural analysis of each RC building subject to tsunami load.

#### 3.3.1 Evaluation of tsunami load

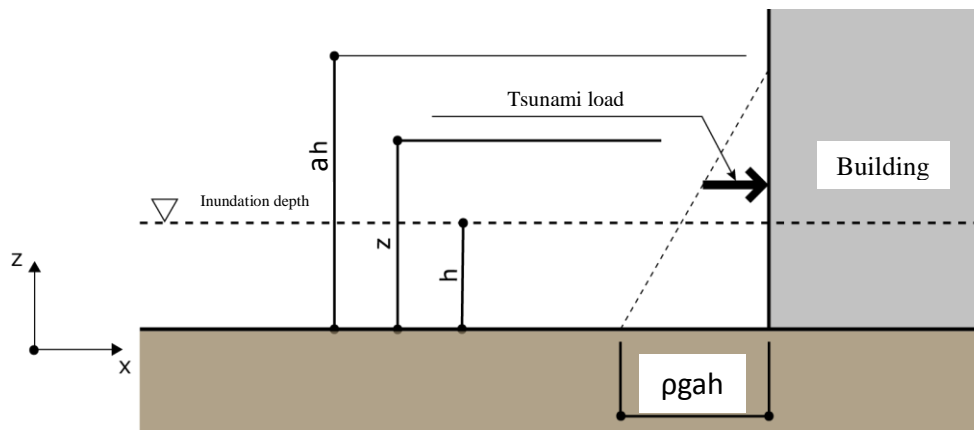


Fig. 3.3 Triangle distribution of hydrostatic pressure (JCO)

For earthquake scenarios, the wave data of strong ground motion was input to all RC buildings as same as previous in IES. For tsunami scenarios, the predicted data of tsunami inundation depth was input to all RC buildings in order to evaluate tsunami load, which also depends on surrounding circumstance in the target area. However, in this study, tsunami load was calculated by means of triangle distribution of hydrostatic pressure recommend by JCO as shown in Fig. 3.3. Due to considering effect of impact force,

tsunami load in Eq. (3.1) was magnified by  $a$  factor, which can vary from 1.0 to 3.0 depending on surrounding circumstance.

$$q_z = \rho_s g (ah - z) \quad (3.1)$$

in which  $q_z$  : hydrodynamic force,  $\rho_s$  : density of salt water = 1128 kg/m<sup>3</sup>,  $g$  : gravitational acceleration = 9.81 m/s<sup>2</sup>,  $h$  : inundation depth,  $z$  : height from ground level ( $0 \leq z \leq ah$ ),  $a$  : impact factor ( $1.0 \leq a \leq 3.0$ )

Fig. 3.4 shows the location of RC buildings (grey colour) and wooden houses (green colour) in a target area. Unless tsunami inundation depth and flow velocity, tsunami load acting on each building also depended on tsunami direction to this area, building location from coastal line, and building arrangement in this area. Focusing on one RC building in Fig. 3.4, tsunami load can be reduced by surrounding buildings and environment, whereas tsunami load can be increased by wooden debris from collapsed houses. As can be seen in Fig. 3.4, it shows that surrounding circumstance had a significant effect on evaluation of tsunami load for all RC buildings in the target area.



Fig. 3.4 Location of RC buildings and wooden houses in a target area

In Table 3.1, the  $a$  factor was investigated to evaluate tsunami load in Eq. (3.1) based on damage observation after the 2011 Great East Japan earthquake [54]. As shown in Table 3.1, the investigation of the  $a$  factor was separated to only two cases: area with structures to reduce tsunami load and area without structures to reduce tsunami load.

Table 3.1 The  $a$  factor based on damage observation after the 2011 Great East Japan earthquake [54]

Coefficient	Area with structures to reduce tsunami load	Area without structures to reduce tsunami load
a	1.0	$\geq 1.7$

The direction of tsunami load acting on each RC building in this study was assumed in both x- and y- directions as shown in Fig. 3.5.

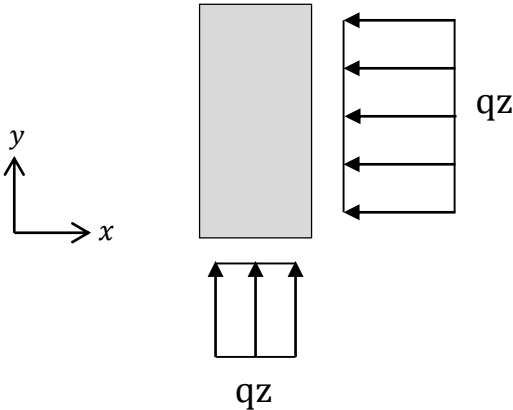


Fig. 3.5 The direction of tsunami load acting on each RC building in a target area

**3.3.2 Proposed building modeling**

In IES, Common Modeling Data (CMD) is a modeling approach to convert a polygon shape as a structural model, consisting of beam and column elements, based on building design code. As the first part of the simulation in this study, building modeling in CMD was modified to include wall elements to a structural model in order to perform nonlinear structural analysis of RC buildings subject to tsunami load. As shown in Fig. 3.6,

a polygon shape in Fig. 3.6(a) was converted to a structural model in Fig. 3.6(b), consisting of beam, column, wall elements.

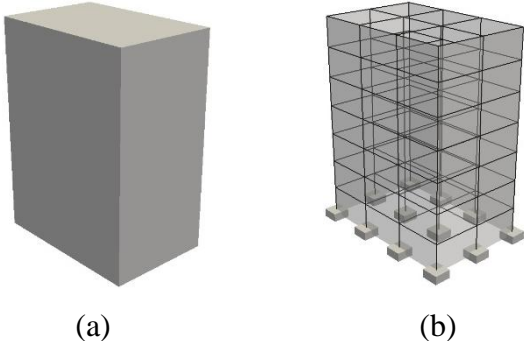


Fig. 3.6 Proposed building modeling

Since tsunami load was a distributed pressure acting on outside of RC buildings as shown in Fig. 3.3 and Fig. 3.5, wall elements were arranged to outside frames for resisting a distributed pressure of tsunami load. In order to apply this proposed building modeling of wall elements as the concept of CMD, wall elements were arranged to all outside frames of RC buildings covering building surface as wall cladding shown in Fig. 3.7. For this proposed building modeling, macro plate model was applied to represent wall elements in the structural model.

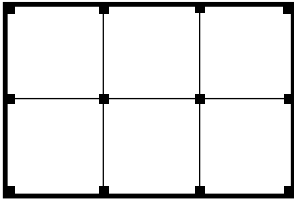


Fig. 3.7 Common Modeling Data for wall elements

In conclusion, all RC buildings in a target area were represented as a structural model, consisting of beam, column and wall elements, in order to perform nonlinear structural analysis of each RC building subject to earthquake and subsequent tsunami.

### 3.4 SEQUENTIAL ANALYSIS FROM EARTHQUAKE AND TSUNAMI

Object-Based Structural Analysis (OBASAN), a structural analysis program, which has been developed by our laboratory, was proposed to perform nonlinear structural analysis as the second part of the simulation. For earthquake and tsunami scenarios, strong ground motion shakes all buildings and causes some structural damage to all buildings in a target area. Subsequently, a tsunami reaches the target area and tsunami load causes more structural damage to buildings. In OBASAN, RC buildings were analyzed by inputting a sequential load of earthquake and tsunami as shown in Fig. 3.8. In the case of earthquake in Fig. 3.8(b), dynamic structural response analysis was performed to predict structural damage of each building, which was subject to strong ground motion. Sequentially, static pushover analysis was performed to predict more structural damage to each building, which was subject to tsunami load in Fig. 3.8(c).

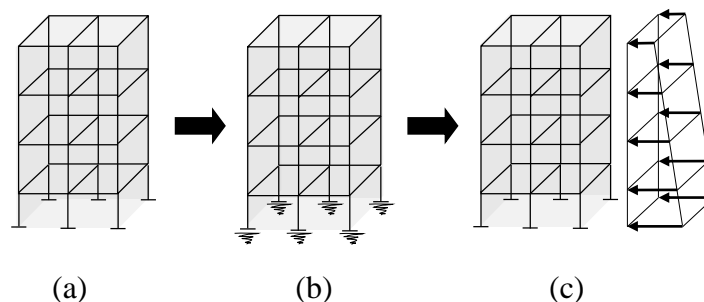


Fig. 3.8 Sequential analysis of earthquake and tsunami

In order to simulate sequential behavior of earthquake and tsunami response, nonlinear structural analysis was performed by means of the same hysteresis model shown in Fig. 3.9. The red line represents nonlinear structural analysis in earthquake scenario and the blue line represents nonlinear structural analysis in tsunami scenario. During an earthquake, nonlinear structural analysis starts from point A and moves along the red line of hysteresis loop. Then, nonlinear structural analysis stops at point B and some structural damage occurred from earthquake scenario. During tsunami scenario, nonlinear structural analysis starts from point B and moves along the blue line. Then nonlinear structural analysis stops at point C and more structural damage might occur from tsunami scenario.

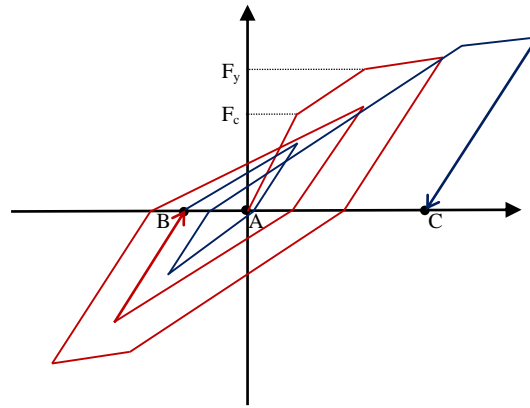


Fig. 3.9 Hysteretic loop for earthquake and subsequent tsunami

### 3.5 DOUBLE-LAYER PLATFORM OF HIGH PERFORMANCE COMPUTING

For damage prediction in a target area, thousands of buildings are modeled to perform nonlinear structural analysis. Since high performance computing (HPC) is a key role to carry out a large number of buildings in the target area, OpenMPI application has been applied to IES in order to enable parallel processing on the Central Processing Units (CPUs) for building modeling of all buildings [59]-[65]. In this study, a double-layer platform of HPC was proposed to simulate earthquake and tsunami scenarios in a reasonably short time. Since OBASAN has been developed by C++ programming language, CUDA application was applied to OBASAN in order to enable parallel processing on the Graphic Processing Units (GPUs) for nonlinear structural analysis of a building. Therefore, HPC was achieved by a double layer of parallel processing on CPUs and GPUs as shown in Fig. 3.10.

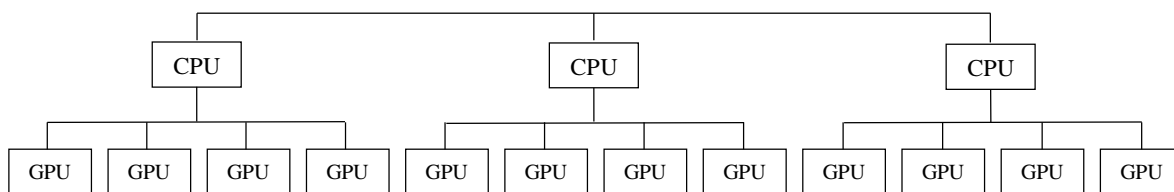
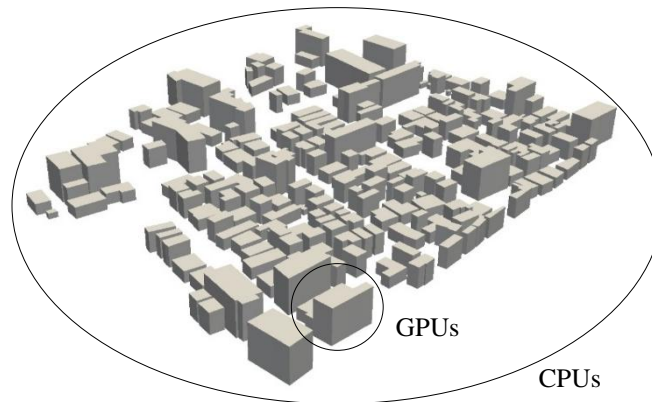


Fig. 3.10 A proposed double layer of parallel processing on CPUs and GPUs

CUDA application is one of General-Purpose computing on Graphic Processing Units (GPGPUs) which has high capability to carry out a large amount of data and a large number of simple calculation [69]-[70]. For nonlinear structural analysis in OBASAN, it was found that execution time was significantly occupied by matrix operation  $Ax = b$ , so CUDA application was firstly used to solve this matrix operation at every analysis steps on GPUs using CUBLAS and CUSPARSE library.

### 3.6 EARTHQUAKE AND TSUNAMI SCENARIO IN KOCHI CITY

In this study, a target area in Kochi city was selected to simulate an earthquake and tsunami scenario as shown in Fig. 3.11. This selected target area is in the center of Kochi city which has many public buildings and is important for economic activities. For damage prediction in this target area, an earthquake and tsunami scenario was simulated from input data, such as GIS data for building modeling, wave data of strong ground motion, and predicted data of tsunami inundation depth.



Fig. 3.11 A selected target area in Kochi city

### 3.6.1 GIS data for building modeling

Fig. 3.12 shows GIS data of this selected target area. In GIS data, building dimensions and number of floors were used to generate building shapes of all buildings as shown in Fig. 3.13 (a) in which each building can be classified to RC buildings, steel buildings, and wooden houses.



Fig. 3.12 GIS data of this target area

In Fig. 3.13(a), this selected target area had 480 RC buildings (grey color) and 1311 wooden houses (green color). Since damage prediction of all RC buildings in a target area from earthquake and subsequent tsunami was proposed in this study, 480 RC buildings in Fig. 3.13(b) were applied to simulate an earthquake and tsunami scenario.

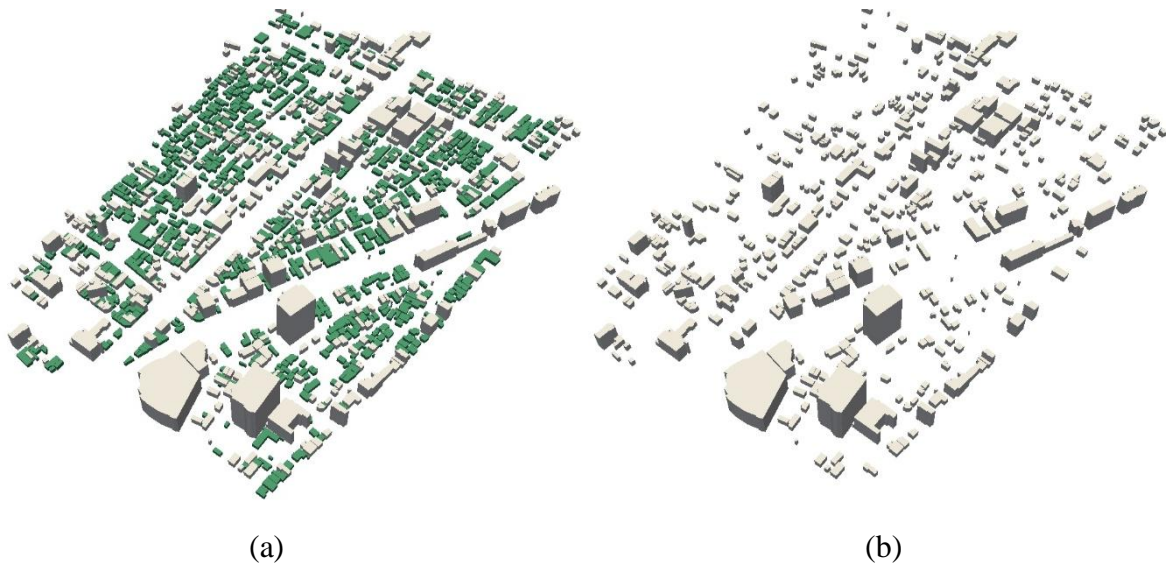


Fig. 3.13 Building shapes from GIS data

### 3.6.2 Wave data of strong ground motion

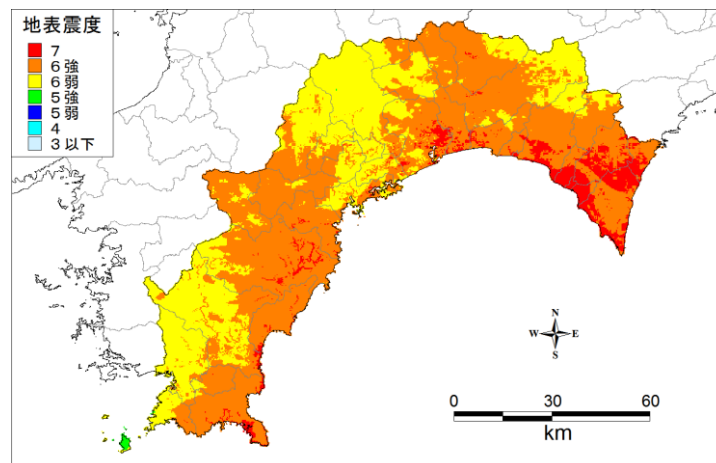


Fig. 3.14 Seismic hazard map for Nankai earthquake (JCO, 2012)

Japan Cabinet Office (JCO) has studied and predicted strong ground motion in future earthquake and tsunami for all risk area in Japan. For Nankai earthquake, seismic hazard map in Kochi city has been proposed by JCO as shown in Fig. 3.14.

The wave data of Kochi city has been developed by a study group of the Great Nankai earthquake model in 2012. This selected target area was separated to north zone and south zone according to two source data of earthquake model as shown in Fig. 3.15.



Fig. 3.15 Two separated zone for two source data of earthquake model

Fig. 3.16 shows the wave data of strong ground motion for this selected target area. The wave data in Fig. 3.16(a) was applied to all RC buildings in south zone and the wave data in Fig. 3.16(b) was applied to all RC buildings in north zone. As can be seen in Fig. 3.16(a) and 3.16(b), three motion components in the east-west, north-south, and up-down direction (EW, NS, and UD respectively) have been developed in a wave form of ground acceleration in which shear wave velocity ( $V_s$ ) is equal to 300 m/s. The peak ground acceleration of north zone in all EW, NS, and UD directions is higher than that of south zone.

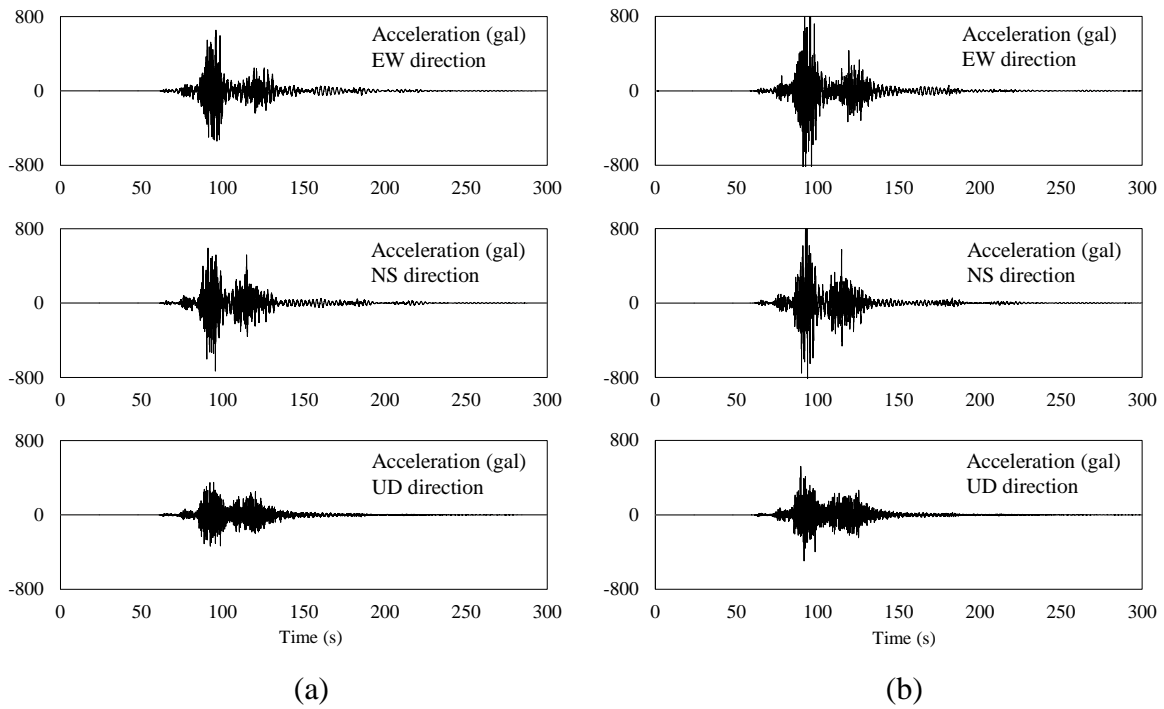


Fig. 3.16 The wave data of strong ground motion (JCO, 2012)

### 3.6.3 Predicted data of tsunami inundation depth

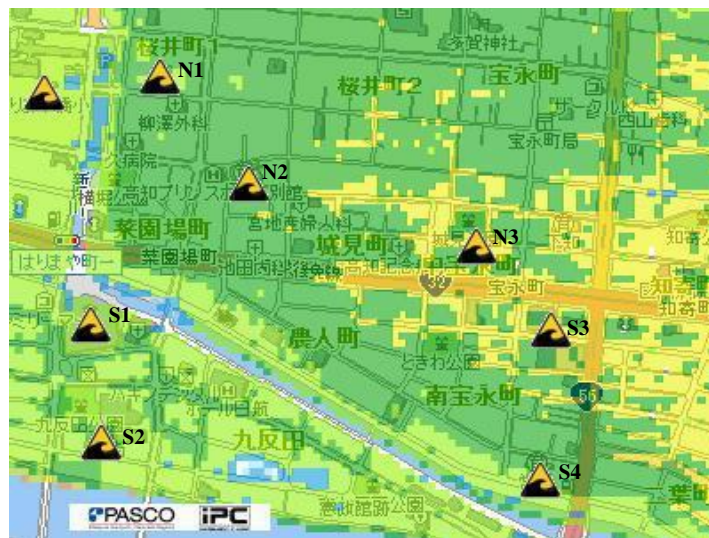


Fig. 3.17 Tsunami hazard map for Nankai earthquake (Kochi Prefecture Office)

Japan Cabinet Office (JCO) has studied and predicted tsunami inundation depth in future earthquake and tsunami for all risk area in Japan. For Nankai earthquake, tsunami hazard map in Kochi city has been proposed by JCO as shown in Fig. 3.17. Based on tsunami inundation model, the selected target area has three stations (N1, N2, and N3) in north zone and four stations (S1, S2, S3, and S4) in south zone for collecting tsunami inundation data in time history.

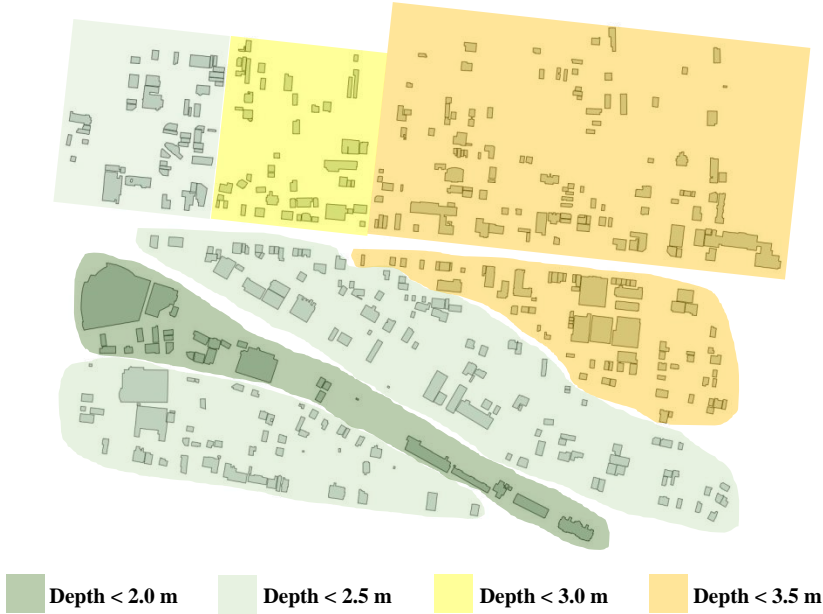


Fig. 3.18 Seven divided area for each station of tsunami inundation data

Based on tsunami hazard map in Fig. 3.17, this selected target area was divided to seven area according to seven stations of tsunami inundation data as shown in Fig. 3.18. In this target area, the maximum inundation depth was varied from 2.0 m to 3.5 m.

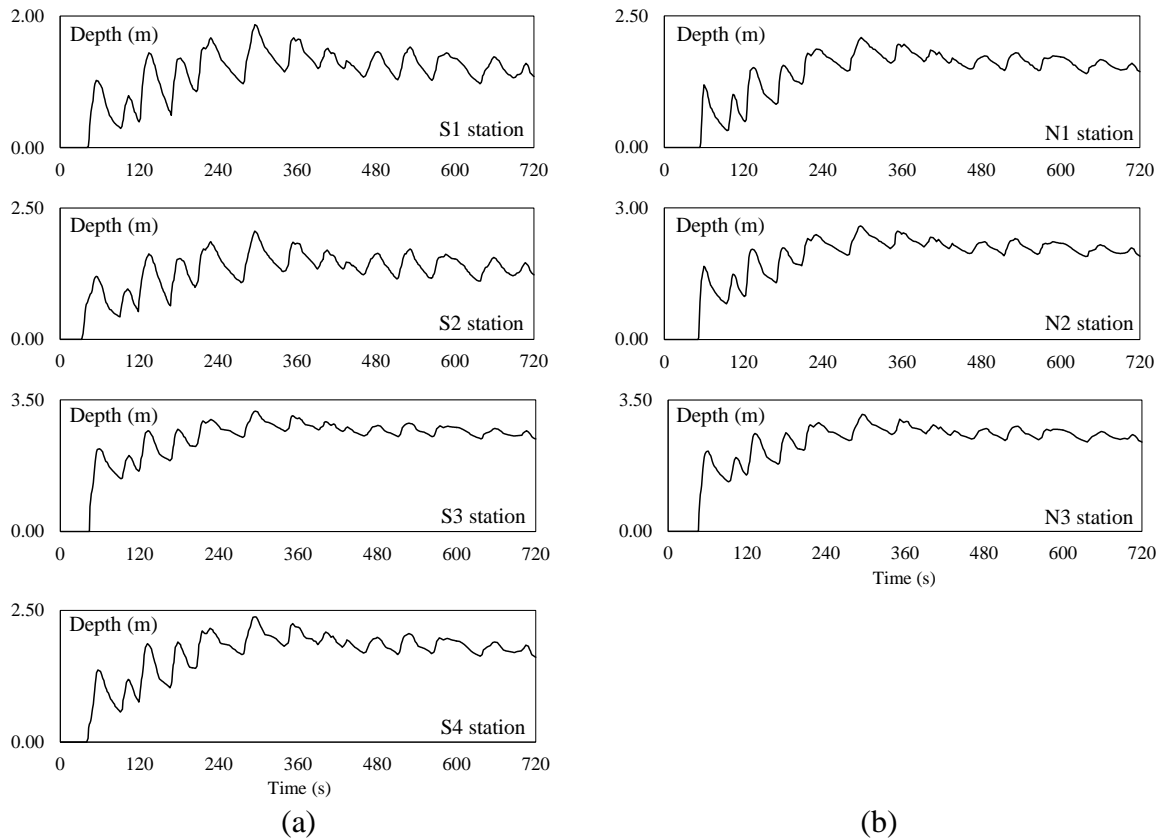


Fig. 3.19 Predicted inundation depth at each station (Kochi Prefecture Office)

Fig. 3.19 shows the predicted data of tsunami inundation depth for this selected target area. The inundation data in Fig. 3.19(a) was used to evaluate tsunami load for all RC buildings in south zone and the inundation data in Fig. 3.19(b) was used to evaluate tsunami load for all RC buildings in north zone.

### 3.7 RESULTS OF SEQUENTIAL EARTHQUAKE AND TSUNAMI SIMULATION

The results of sequential earthquake and tsunami simulation can be visualized as shown in Fig. 3.20. For each RC building, structural damage can be predicted by means of maximum story drift ratio.

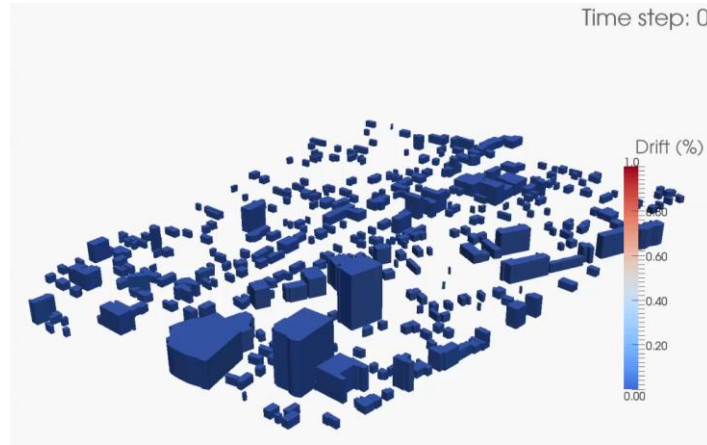


Fig. 3.20 Visualization of damage prediction

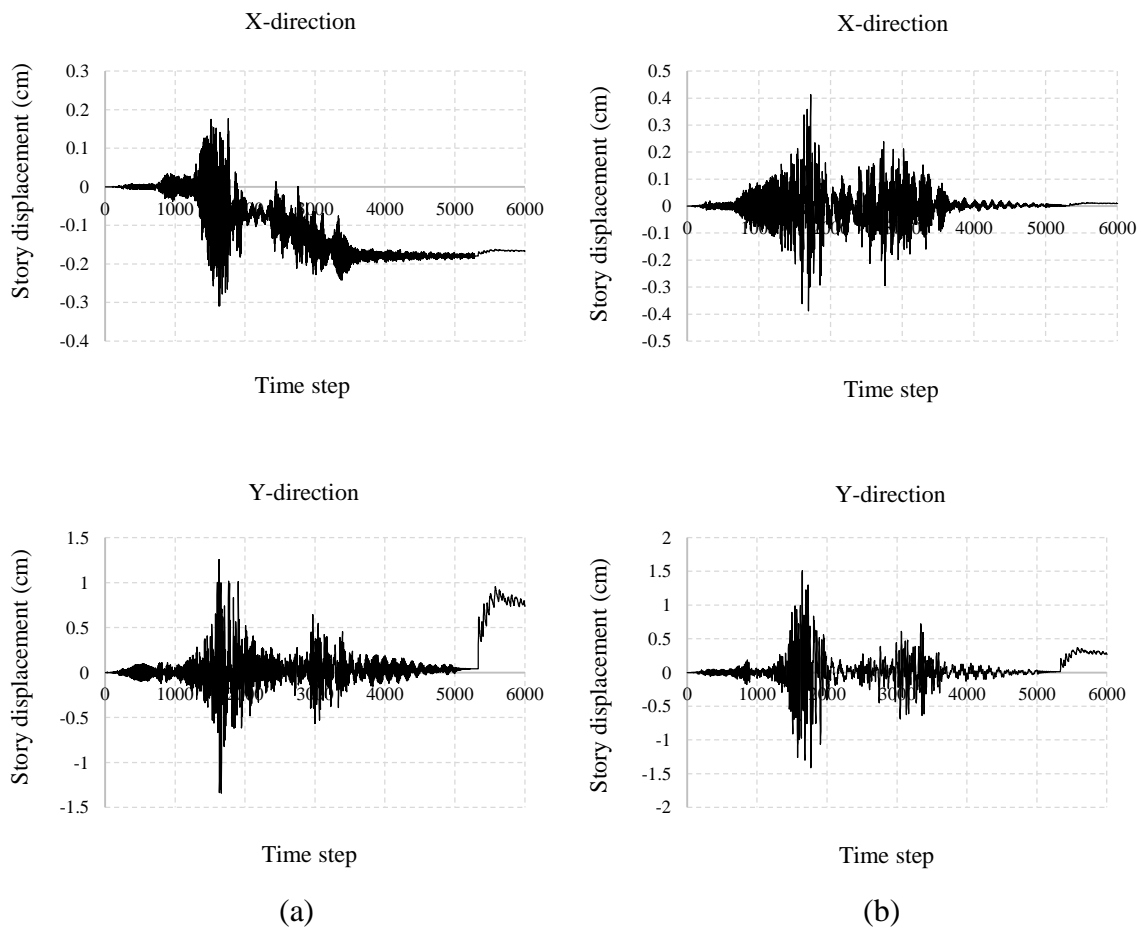


Fig. 3.21 Story displacement at 1<sup>st</sup> floor

For each RC building, the results of story displacement at 1<sup>st</sup> floor in x- and y-directions can be obtained as shown in Fig. 3.21. Fig. 3.21(a) shows the results of a three-story RC building and Fig. 3.21(b) shows the results of an eight-story RC building. As can be seen in Fig. 3.21, sequential tsunami response in y-direction had a significant effect on a three-story RC building. In addition, residual displacement occurred from earthquake response in x-direction. Therefore, the effect of sequential tsunami response depended on building height and also the direction of tsunami load.

Fig. 3.22 shows the results of maximum story drift ratio for each RC building in zone N1. For each RC building in Fig. 3.22, number of floors, maximum story drift ratio, occurrence during earthquake response or sequential tsunami response, and location of maximum story drift can be seen in Appendix I.

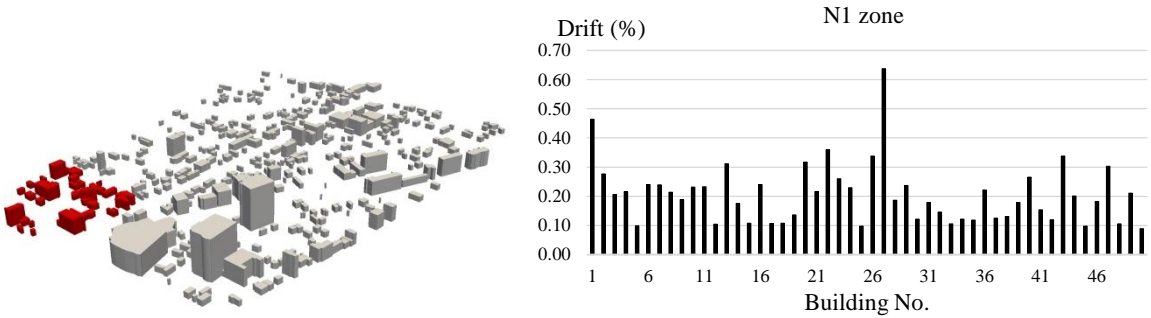


Fig. 3.22 Maximum story drift ratio for zone N1

Fig. 3.23 shows the results of maximum story drift ratio for each RC building in zone N2. For each RC building in Fig. 3.23, number of floors, maximum story drift ratio, occurrence during earthquake response or sequential tsunami response, and location of maximum story drift can be seen in Appendix II.

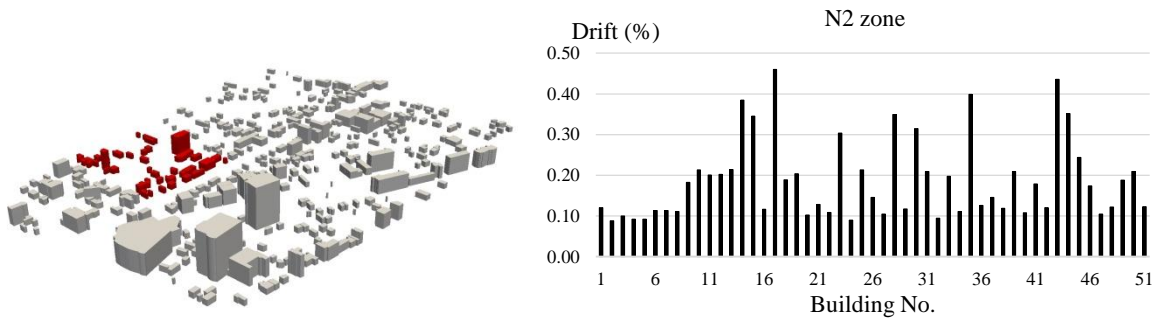


Fig. 3.23 Maximum story drift ratio for zone N2

Fig. 3.24 shows the results of maximum story drift ratio for each RC building in zone N3. For each RC building in Fig. 3.24, number of floors, maximum story drift ratio, occurrence during earthquake response or sequential tsunami response, and location of maximum story drift can be seen in Appendix III and Appendix IV.

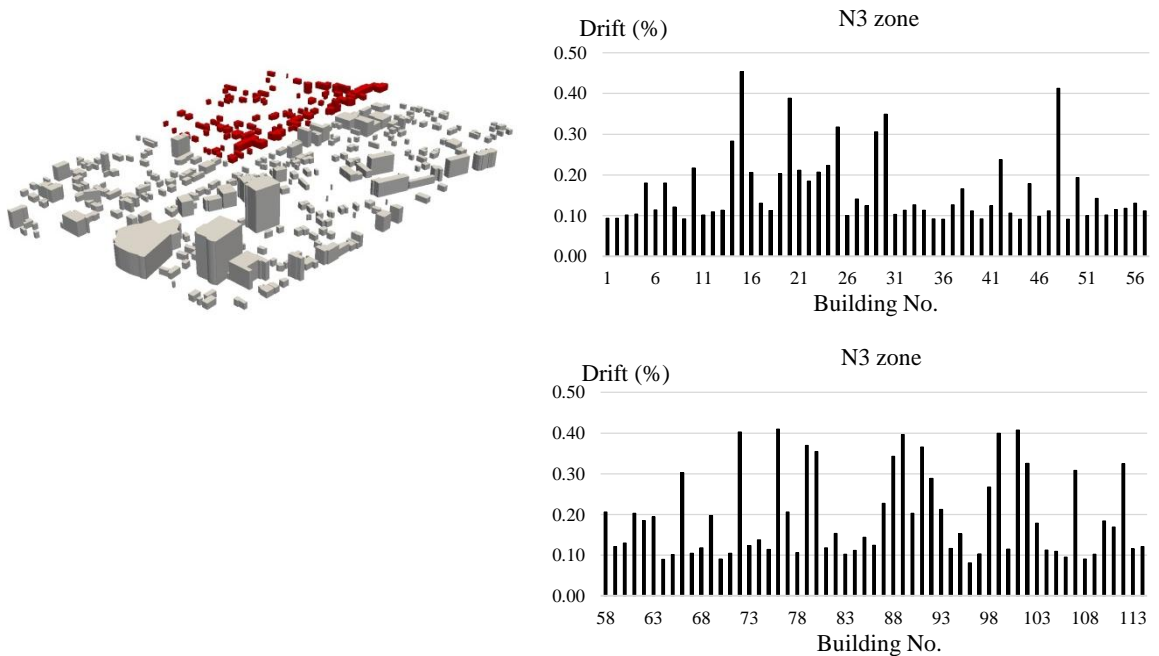


Fig. 3.24 Maximum story drift ratio for zone N3

Fig. 3.25 shows the results of maximum story drift ratio for each RC building in zone S1. For each RC building in Fig. 3.25, number of floors, maximum story drift ratio, occurrence during earthquake response or sequential tsunami response, and location of maximum story drift can be seen in Appendix III and Appendix IV.

occurrence during earthquake response or sequential tsunami response, and location of maximum story drift can be seen in Appendix V.

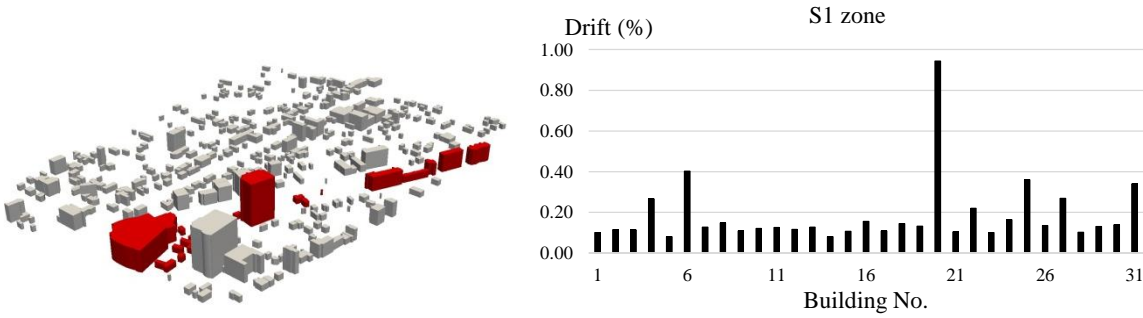


Fig. 3.25 Maximum story drift ratio for zone S1

Fig. 3.26 shows the results of maximum story drift ratio for each RC building in zone S2. For each RC building in Fig. 3.26, number of floors, maximum story drift ratio, occurrence during earthquake response or sequential tsunami response, and location of maximum story drift can be seen in Appendix VI.

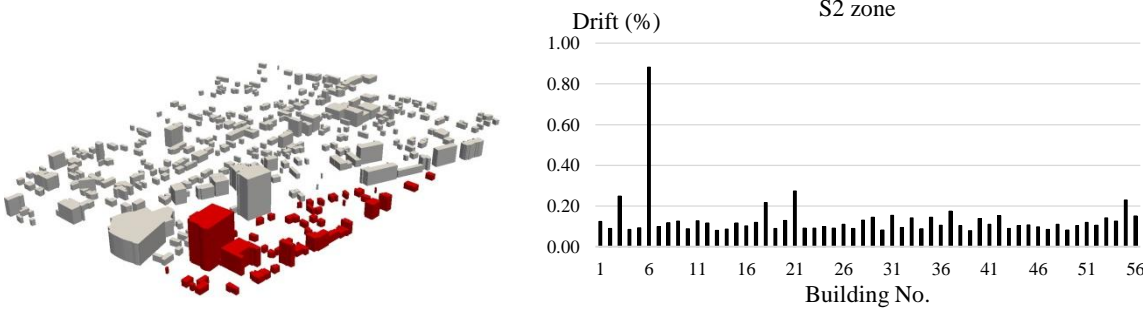


Fig. 3.26 Maximum story drift ratio for zone S2

Fig. 3.27 shows the results of maximum story drift ratio for each RC building in zone S3. For each RC building in Fig. 3.27, number of floors, maximum story drift ratio, occurrence during earthquake response or sequential tsunami response, and location of maximum story drift can be seen in Appendix VII.

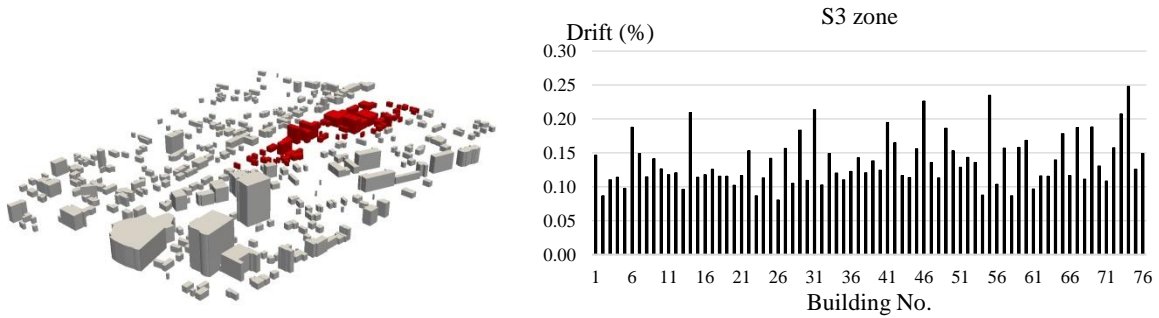


Fig. 3.27 Maximum story drift ratio for zone S3

Fig. 3.28 shows the results of maximum story drift ratio for each RC building in zone S4. For each RC building in Fig. 3.28, number of floors, maximum story drift ratio, occurrence during earthquake response or sequential tsunami response, and location of maximum story drift can be seen in Appendix VIII and Appendix IX.

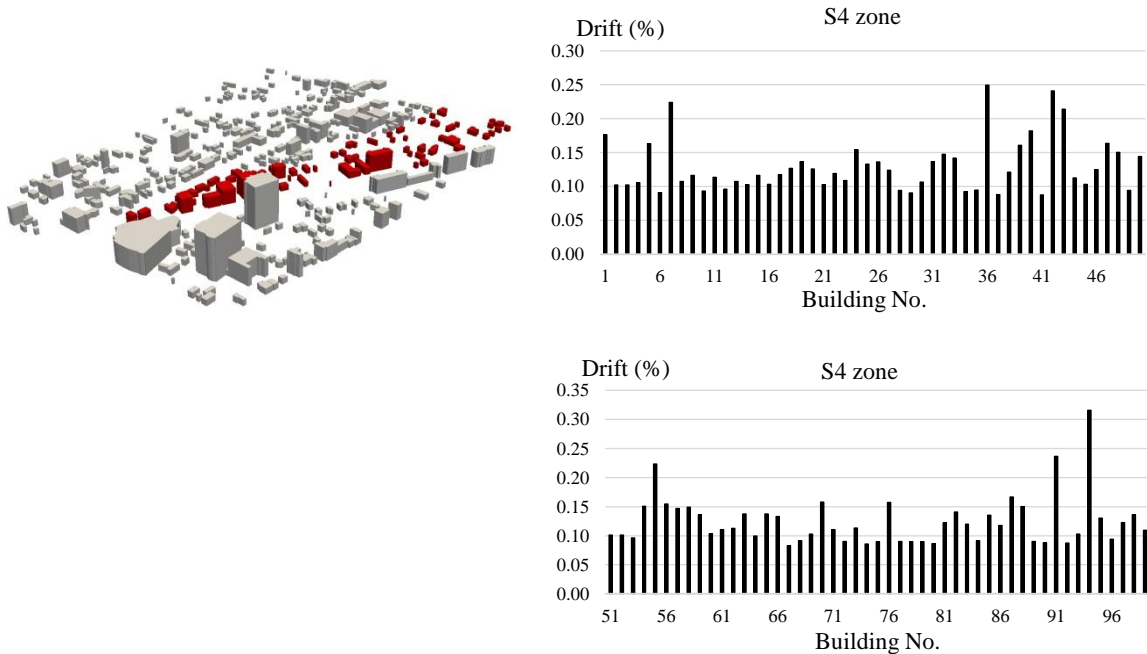


Fig. 3.28 Maximum story drift ratio for zone S4

Table 3.2 shows number of RC buildings in which maximum story drift ratio occurred during earthquake response and sequential tsunami response.

Table 3.2 Number of RC buildings for maximum story drift ratio

Zone	Number of RC buildings	Max drift during earthquake	Max drift during tsunami
N1	50	50	0
N2	51	50	1
N3	114	111	3
S1	31	24	7
S2	56	40	16
S3	76	45	31
S4	99	71	28
Total	477	391 (81.97%)	86 (18.03%)

### 3.8 THE WORST-CASE SCENARIO

Fig. 3.29 shows sequential earthquake and tsunami simulation assuming the worst-case scenario by increasing double of tsunami inundation depth. From the visualization of results in Fig. 3.29, maximum story drift ratio can occur less than 5% in which that of maximum story drift ratio in Fig. 3.20 can occur less than 1%.

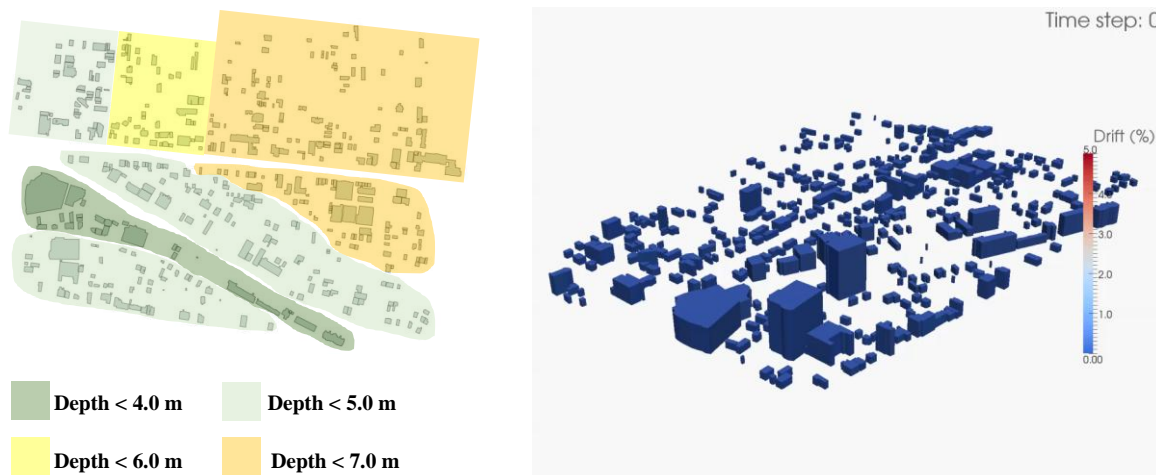


Fig. 3.29 The worst-case scenario by increasing double of tsunami inundation depth

Fig. 3.30 shows the results of the worst-case scenario for each RC building in zone N1. For each RC building in Fig. 3.30, number of floors, maximum story drift ratio,

occurrence during earthquake response or sequential tsunami response, and location of maximum story drift can be seen in Appendix X.

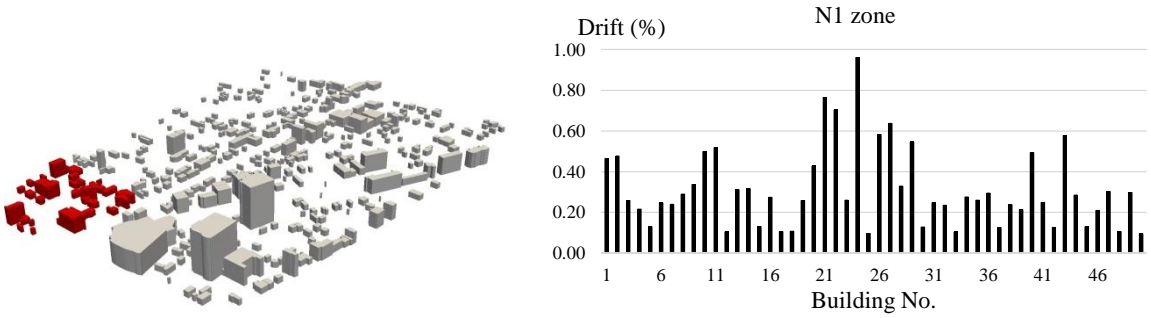


Fig. 3.30 Maximum story drift ratio for zone N1 (worst case)

Fig. 3.31 shows the results of the worst-case scenario for each RC building in zone N2. For each RC building in Fig. 3.31, number of floors, maximum story drift ratio, occurrence during earthquake response or sequential tsunami response, and location of maximum story drift can be seen in Appendix XI.

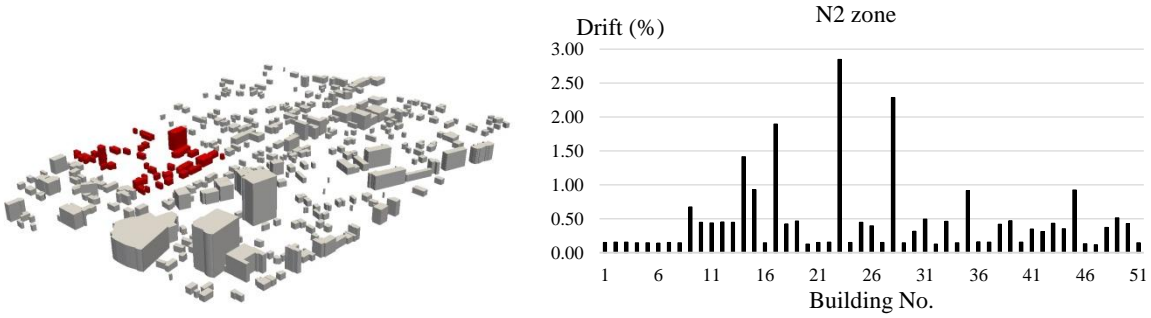


Fig. 3.31 Maximum story drift ratio for zone N2 (worst case)

Fig. 3.32 shows the results of the worst-case scenario for each RC building in zone N3. For each RC building in Fig. 3.32, number of floors, maximum story drift ratio, occurrence during earthquake response or sequential tsunami response, and location of maximum story drift can be seen in Appendix XII and Appendix XIII.

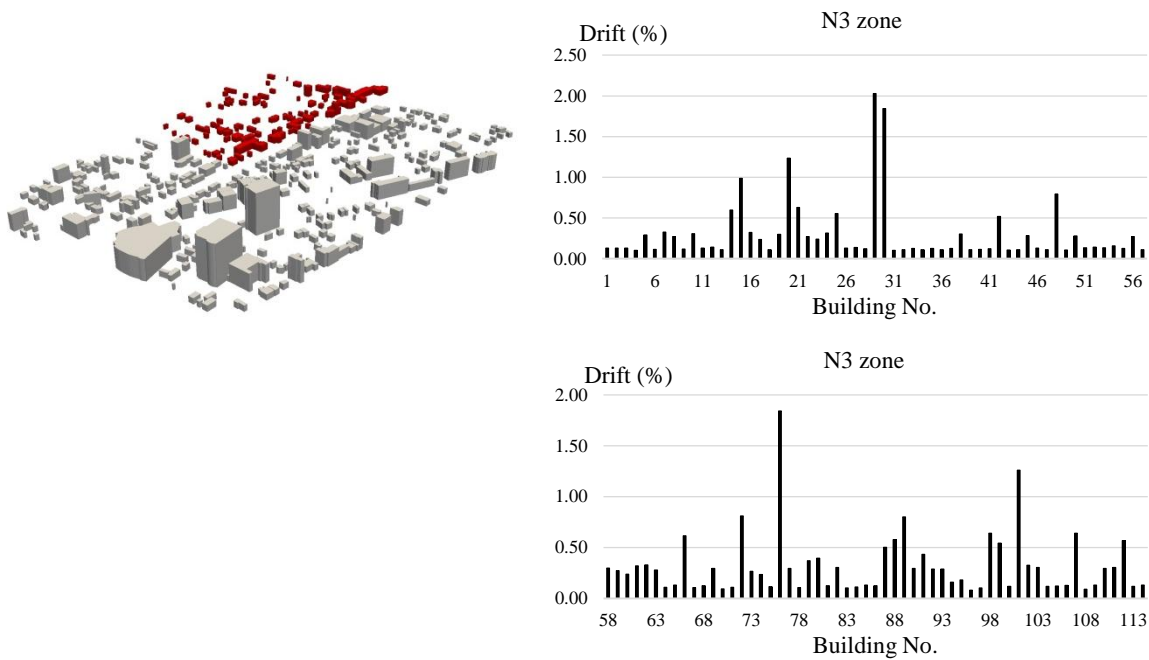


Fig. 3.32 Maximum story drift ratio for zone N3 (worst case)

Fig. 3.33 shows the results of the worst-case scenario for each RC building in zone S1. For each RC building in Fig. 3.33, number of floors, maximum story drift ratio, occurrence during earthquake response or sequential tsunami response, and location of maximum story drift can be seen in Appendix XIV.

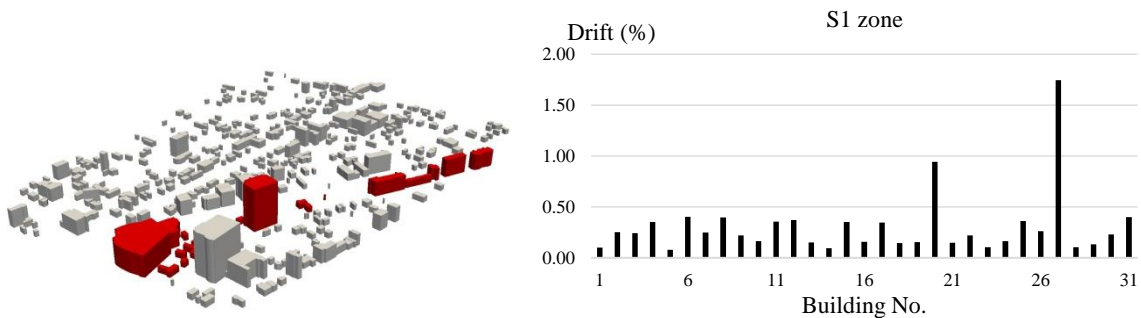


Fig. 3.33 Maximum story drift ratio for zone S1 (worst case)

Fig. 3.34 shows the results of the worst-case scenario for each RC building in zone S2. For each RC building in Fig. 3.34, number of floors, maximum story drift ratio, occurrence during earthquake response or sequential tsunami response, and location of maximum story drift can be seen in Appendix XIV.

occurrence during earthquake response or sequential tsunami response, and location of maximum story drift can be seen in Appendix XV.

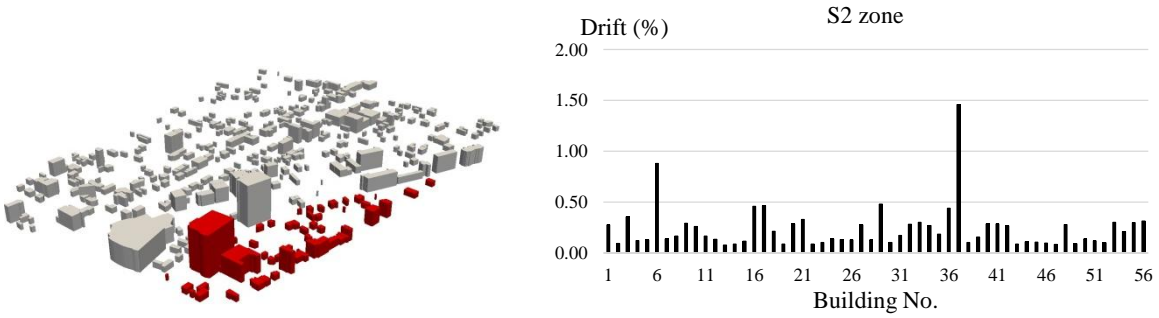


Fig. 3.34 Maximum story drift ratio for zone S2 (worst case)

Fig. 3.35 shows the results of the worst-case scenario for each RC building in zone S3. For each RC building in Fig. 3.35, number of floors, maximum story drift ratio, occurrence during earthquake response or sequential tsunami response, and location of maximum story drift can be seen in Appendix XVI.

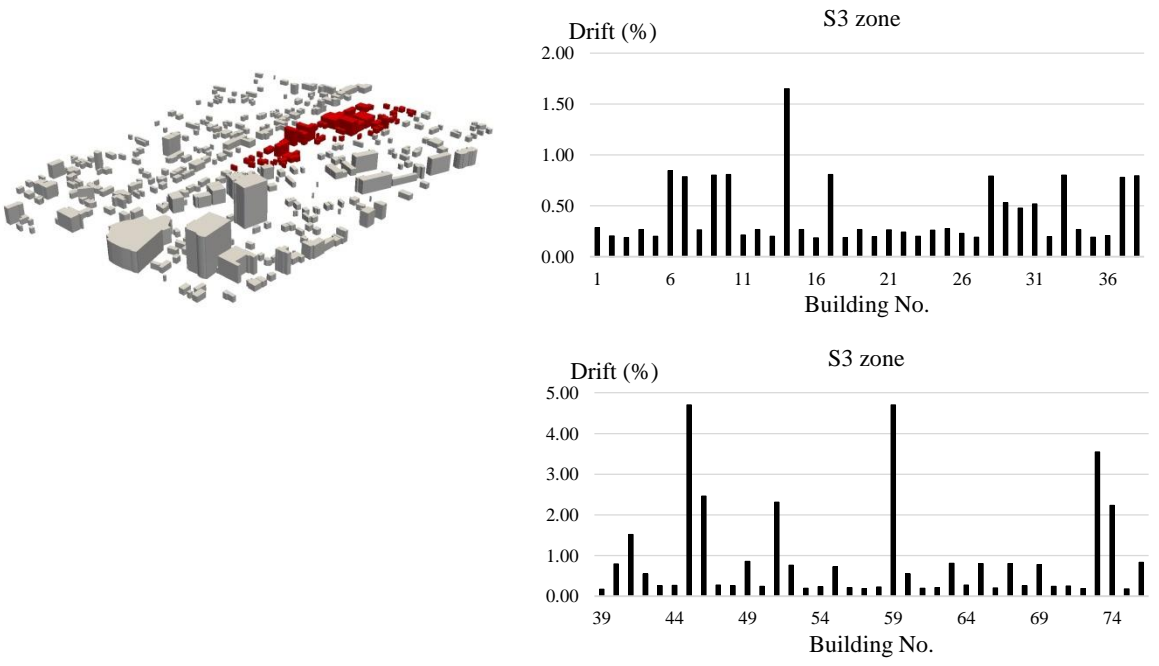


Fig. 3.35 Maximum story drift ratio for zone S3 (worst case)

Fig. 3.36 shows the results of the worst-case scenario for each RC building in zone S4. For each RC building in Fig. 3.36, number of floors, maximum story drift ratio, occurrence during earthquake response or sequential tsunami response, and location of maximum story drift can be seen in Appendix XVII and Appendix XVIII.

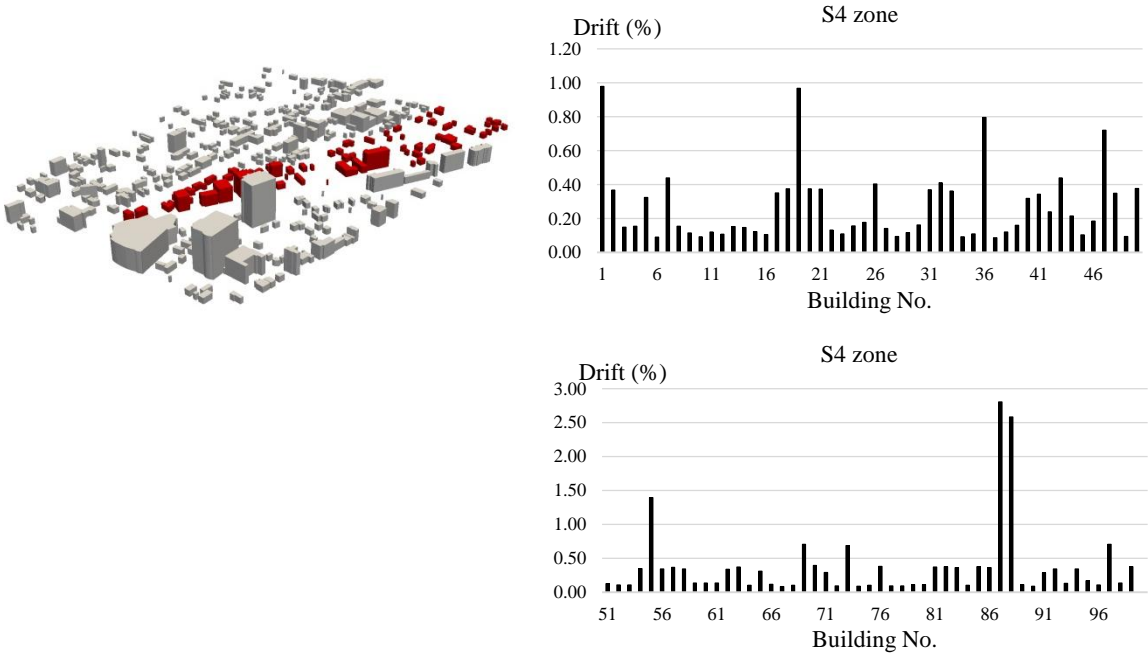


Fig. 3.36 Maximum story drift ratio for zone S4 (worst case)

Table 3.3 Number of RC buildings for maximum story drift ratio (worst case)

Zone	Number of RC buildings	Max drift during earthquake	Max drift during tsunami
N1	50	14	36
N2	51	3	48
N3	114	27	87
S1	31	13	18
S2	56	14	42
S3	76	0	76
S4	99	21	78
Total	477	92 (19.29%)	385 (80.71%)

Table 3.3 shows number of RC buildings for the worse-case scenario in which maximum story drift ratio occurred during earthquake response and sequential tsunami

response. Comparing Table 3.3 with Table 3.2 for most of RC buildings, maximum story drift ratio could occur during sequential tsunami response.

### 3.9 SINGLE AND SEQUENTIAL TSUNAMI RESPONSE

As can be seen in section 3.8, maximum story drift ratio occurred during sequential tsunami response for most of RC buildings. For these RC buildings, maximum story drift ratio from sequential tsunami response was compared with maximum story drift ratio from single tsunami response in Fig. 3.37 and Fig. 3.38. As can be seen in Fig. 3.37 and Fig. 3.38, maximum story drift ratio was different significantly between single and sequential tsunami response. This section aimed to show that sequential analysis from earthquake and tsunami is essential for damage prediction of RC buildings in earthquake and tsunami scenarios.

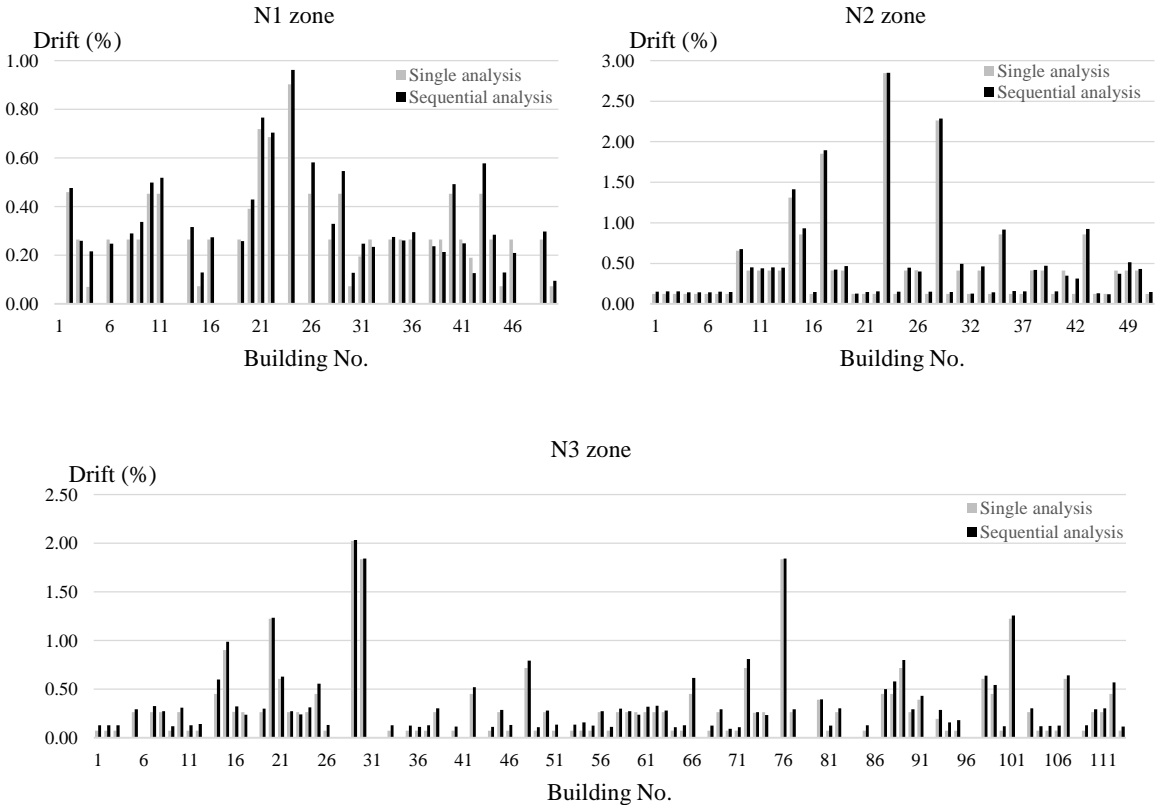


Fig. 3.37 Comparison between single and sequential tsunami response for north zone

The comparison of maximum story drift ratio between single and sequential tsunami response for RC buildings in north zone is shown in Fig. 3.37. For RC buildings in zone N1, maximum story drift ratio from sequential tsunami response was higher than maximum story drift ratio from single tsunami response except for building No. 3, 6, 19, 32, 35, 38, 39, 41, 42, and 46. Especially for building No. 4, 26, 29, and 43 in zone N1, maximum story drift ratio from sequential tsunami response was significantly higher than maximum story drift ratio from single tsunami response which means that the failure mode from earthquake response caused the weakness of these RC buildings to resist tsunami load. For building No. 39 and 46 in zone N1, maximum story drift ratio from sequential tsunami response was significantly lower than maximum story drift ratio from single tsunami response which means that the failure mode from earthquake response caused the strength of these RC buildings to resist tsunami load.

For RC buildings in zone N2, maximum story drift ratio from sequential tsunami response was higher than maximum story drift ratio from single tsunami response except for building No. 41 and 48. For RC buildings in zone N1, maximum story drift ratio from sequential tsunami response was higher than maximum story drift ratio from single tsunami response except for building No. 17, 23, 60, and 74.

The comparison of maximum story drift ratio between single and sequential tsunami response for RC buildings in south zone is shown in Fig. 3.38. For RC buildings in zone S1, maximum story drift ratio from sequential tsunami response was higher than maximum story drift ratio from single tsunami response except for building No. 10. For all RC buildings in zone S2, maximum story drift ratio from sequential tsunami response was higher than maximum story drift ratio from single tsunami response. For many RC buildings in zone S3, maximum story drift ratio from sequential tsunami response was lower than maximum story drift ratio from single tsunami response. For building No. 17 in zone S4, maximum story drift ratio from sequential tsunami response was significantly lower than maximum story drift ratio from single tsunami response.

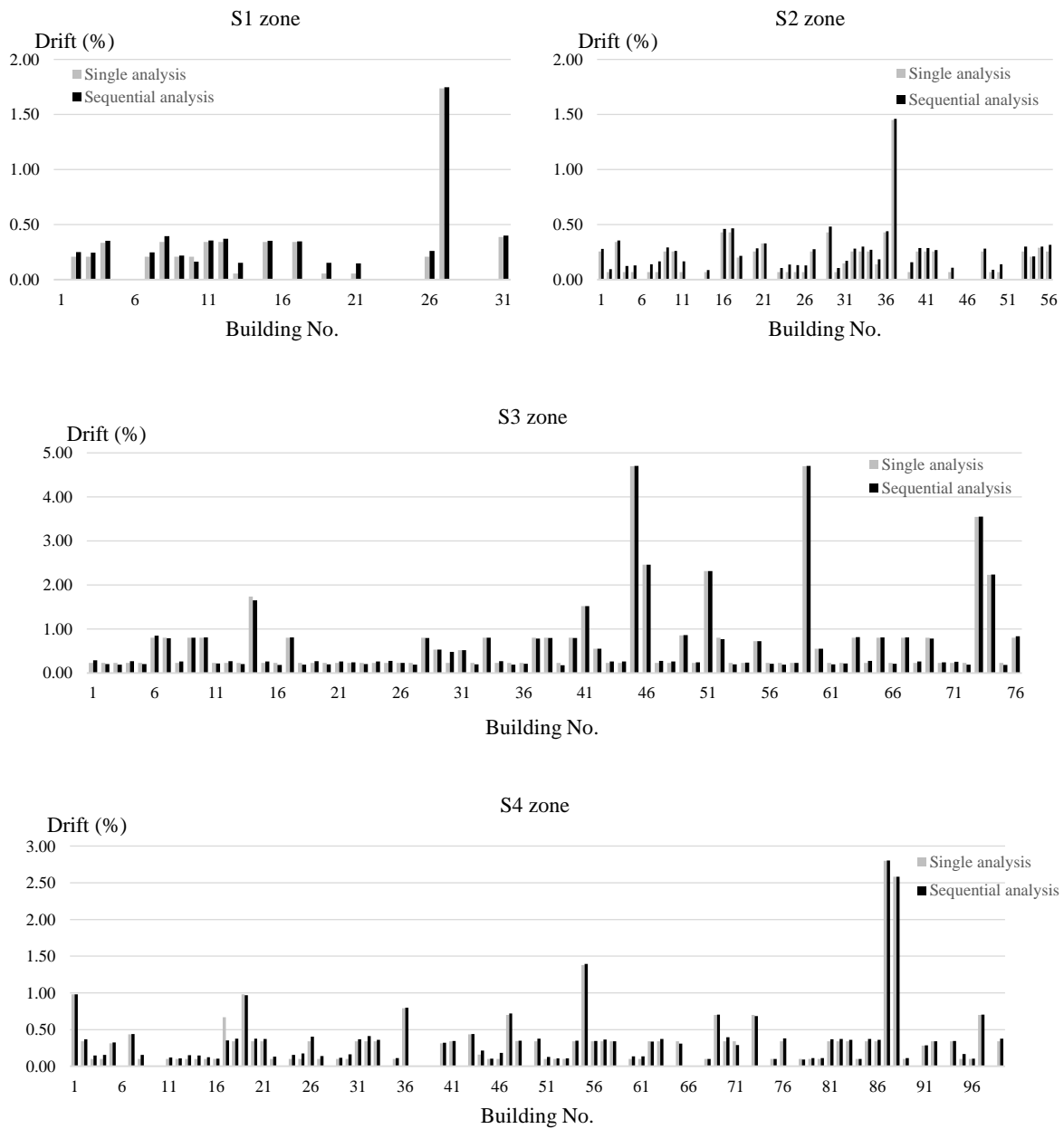


Fig. 3.38 Comparison between single and sequential tsunami response for south zone

### 3.10 CONCLUSIONS

For sequential earthquake and tsunami simulation in the target area of Kochi city, most of RC buildings had maximum drift ratio during earthquake response in which maximum drift ratio was 0.88% for a twenty-one story building in zone S2. In zone S3, many RC buildings had maximum drift ratio during sequential tsunami response in which tsunami inundation depth was a little higher than other zones. For all RC buildings, maximum drift ratio during sequential tsunami response was 0.22% occurred with a three-story building in zone S4 in which structural damage didn't occur obviously. For all zones, three-story buildings had a significant risk that maximum drift ratio could occur during tsunami response analysis.

For the worst-case scenario, most of RC buildings had maximum drift ratio during sequential tsunami response in which maximum drift ratio was 4.71% for a four-story building in zone S3. For all zone, low-rise buildings (three-story to seven-story) had a significant risk that maximum drift ratio was higher than 1% during sequential tsunami response. For the worst-case scenario, structural damage from sequential tsunami response was much more serious than that of the normal-case scenario in which tsunami inundation depth was double.

The comparison of maximum story drift ratio between single and sequential tsunami response shows that the failure mode from earthquake response can cause the strength or the weakness of a whole RC building to resist tsunami load. Therefore, sequential analysis from earthquake and tsunami is essential for damage prediction of RC buildings in earthquake and tsunami scenarios

The results of sequential earthquake and tsunami simulation can be used to designate tsunami evacuation buildings, which must be secured for people living in a surrounding area. These results can indicate a weak point of a city area and focus on this weak point. In addition, these results can be used to construct prevention measures in order control overall damage of a city area from earthquake and subsequent tsunami.

### 3.11 APPENDIX

Appendix I The results of damage prediction for zone N1

No.	Floors	Max drift (%)	During	Location	No.	Floors	Max drift (%)	During	Location
1	8	0.46	E	2	26	3	0.34	E	1
2	6	0.28	E	2	27	8	0.64	E	1
3	3	0.21	E	1	28	3	0.19	E	1
4	3	0.22	E	1	29	3	0.24	E	2
5	3	0.10	E	1	30	3	0.12	E	1
6	3	0.24	E	1	31	5	0.18	E	2
7	3	0.24	E	1	32	3	0.15	E	1
8	3	0.21	E	1	33	3	0.10	E	1
9	3	0.19	E	1	34	3	0.12	E	1
10	3	0.23	E	2	35	3	0.12	E	1
11	3	0.23	E	2	36	3	0.22	E	1
12	3	0.10	E	1	37	3	0.12	E	1
13	7	0.31	E	1	38	3	0.13	E	1
14	3	0.17	E	1	39	3	0.18	E	1
15	3	0.11	E	1	40	3	0.27	E	2
16	3	0.24	E	1	41	3	0.15	E	1
17	3	0.11	E	1	42	3	0.12	E	1
18	3	0.11	E	1	43	3	0.34	E	1
19	3	0.14	E	2	44	3	0.20	E	1
20	5	0.32	E	2	45	3	0.10	E	1
21	3	0.22	E	2	46	3	0.18	E	1
22	5	0.36	E	2	47	9	0.30	E	2
23	7	0.26	E	1	48	3	0.11	E	1
24	3	0.23	E	2	49	3	0.21	E	1
25	3	0.10	E	1	50	3	0.09	E	1

Appendix II The results of damage prediction for zone N2

No.	Floors	Max drift (%)	During	Location
1	3	0.12	E	1
2	3	0.09	E	1
3	3	0.10	T	1
4	3	0.09	E	1
5	3	0.09	E	1
6	3	0.11	E	1
7	3	0.11	E	1
8	3	0.11	E	1
9	5	0.18	E	2
10	3	0.21	E	1
11	3	0.20	E	1
12	3	0.20	E	1
13	3	0.21	E	1
14	3	0.39	E	1
15	3	0.35	E	1
16	3	0.12	E	1
17	3	0.46	E	2
18	3	0.19	E	1
19	3	0.20	E	1
20	3	0.10	E	1
21	3	0.13	E	1
22	3	0.11	E	1
23	4	0.30	E	2
24	3	0.09	E	1
25	3	0.21	E	1
26	3	0.15	E	1

No.	Floors	Max drift (%)	During	Location
27	3	0.11	E	1
28	3	0.35	E	2
29	3	0.12	E	1
30	11	0.32	E	1
31	3	0.21	E	1
32	3	0.09	E	1
33	3	0.20	E	1
34	3	0.11	E	1
35	3	0.40	E	1
36	3	0.13	E	1
37	3	0.15	E	2
38	3	0.12	E	1
39	3	0.21	E	1
40	3	0.11	E	1
41	3	0.18	E	1
42	3	0.12	E	1
43	11	0.44	E	1
44	11	0.35	E	1
45	3	0.24	E	2
46	3	0.17	E	2
47	3	0.10	E	1
48	3	0.12	E	1
49	3	0.19	E	1
50	3	0.21	E	1
51	3	0.12	E	1

### Appendix III The results of damage prediction for zone N3

No.	Floors	Max drift (%)	During	Location
1	3	0.09	E	1
2	3	0.09	E	1
3	3	0.10	E	1
4	3	0.10	E	1
5	3	0.18	E	1
6	3	0.11	E	1
7	3	0.18	E	1
8	3	0.12	E	1
9	3	0.09	E	1
10	3	0.22	E	1
11	3	0.10	E	1
12	3	0.11	E	1
13	3	0.11	E	1
14	3	0.28	E	2
15	3	0.45	E	2
16	3	0.21	E	1
17	3	0.13	E	1
18	3	0.11	E	1
19	3	0.20	E	1
20	4	0.39	E	2
21	4	0.21	E	2
22	3	0.19	E	1
23	3	0.21	E	1
24	3	0.22	E	1
25	3	0.32	E	2
26	3	0.10	E	1
27	3	0.14	E	1
28	3	0.12	E	1
29	4	0.31	E	2

No.	Floors	Max drift (%)	During	Location
30	4	0.35	E	2
31	3	0.10	E	1
32	3	0.11	E	1
33	3	0.13	E	1
34	3	0.11	E	1
35	3	0.09	T	1
36	3	0.09	E	1
37	3	0.13	E	1
38	3	0.17	E	1
39	3	0.11	E	1
40	3	0.09	E	1
41	3	0.12	E	1
42	3	0.24	E	2
43	3	0.11	E	1
44	3	0.09	E	1
45	3	0.18	E	1
46	3	0.10	E	1
47	3	0.11	E	1
48	3	0.41	E	2
49	3	0.09	E	1
50	3	0.19	E	1
51	3	0.10	E	1
52	3	0.14	E	1
53	3	0.10	E	1
54	3	0.11	T	1
55	3	0.12	E	1
56	3	0.13	E	1
57	3	0.11	E	1

Appendix IV The results of damage prediction for zone N3 (cont.)

No.	Floors	Max drift (%)	During	Location
58	3	0.21	E	1
59	3	0.12	E	1
60	3	0.13	E	1
61	3	0.20	E	1
62	3	0.18	E	1
63	3	0.19	E	1
64	3	0.09	E	1
65	3	0.10	E	1
66	3	0.30	E	2
67	3	0.10	E	1
68	3	0.12	E	1
69	3	0.20	E	1
70	3	0.09	E	1
71	3	0.10	E	1
72	3	0.40	E	2
73	4	0.12	E	2
74	3	0.14	E	1
75	3	0.11	E	1
76	4	0.41	E	2
77	3	0.21	E	1
78	3	0.11	E	1
79	3	0.37	E	1
80	5	0.35	E	2
81	3	0.12	E	1
82	3	0.15	E	1
83	3	0.10	E	1
84	3	0.11	E	1
85	3	0.14	E	2
86	3	0.12	E	1

No.	Floors	Max drift (%)	During	Location
87	3	0.23	E	1
88	3	0.34	E	2
89	3	0.40	E	1
90	3	0.20	E	1
91	5	0.37	E	2
92	7	0.29	E	2
93	5	0.21	E	2
94	3	0.12	T	1
95	3	0.15	E	1
96	3	0.08	E	1
97	3	0.10	E	1
98	4	0.27	E	2
99	3	0.40	E	1
100	3	0.11	E	1
101	4	0.41	E	2
102	8	0.33	E	2
103	3	0.18	E	1
104	3	0.11	E	1
105	3	0.11	E	1
106	3	0.10	E	1
107	4	0.31	E	2
108	3	0.09	E	1
109	3	0.10	E	1
110	3	0.18	E	1
111	3	0.17	E	2
112	3	0.33	E	2
113	3	0.12	E	1
114	3	0.12	E	1

Appendix V The results of damage prediction for zone S1

No.	Floors	Max drift (%)	During	Location
1	3	0.10	E	1
2	3	0.12	T	1
3	3	0.11	T	1
4	8	0.27	E	1
5	3	0.08	E	1
6	11	0.40	E	1
7	3	0.13	T	1
8	3	0.15	T	1
9	3	0.11	E	1
10	3	0.12	E	1
11	3	0.13	E	1
12	3	0.12	T	1
13	3	0.13	E	1
14	3	0.08	E	1
15	3	0.11	E	1
16	3	0.16	E	1
17	3	0.11	E	1
18	3	0.15	E	1
19	3	0.13	E	1
20	22	0.94	E	1
21	3	0.10	T	1
22	9	0.22	E	1
23	3	0.10	E	1
24	7	0.16	E	2
25	10	0.36	E	1
26	3	0.14	T	1
27	4	0.27	E	2
28	3	0.10	E	1
29	3	0.13	E	1
30	3	0.14	E	1
31	8	0.34	E	1

Appendix VI The results of damage prediction for zone S2

No.	Floors	Max drift (%)	During	Location
1	1	0.12	T	3
2	1	0.09	E	3
3	2	0.25	E	7
4	1	0.09	E	3
5	1	0.09	T	3
6	1	0.88	E	21
7	1	0.10	T	3
8	1	0.12	T	3
9	1	0.13	T	3
10	1	0.09	E	3
11	1	0.13	E	3
12	1	0.12	E	3
13	1	0.08	E	3
14	1	0.09	E	3
15	1	0.12	E	3
16	1	0.10	E	3
17	1	0.12	E	3
18	2	0.22	E	11
19	1	0.09	E	3
20	1	0.13	T	3
21	1	0.27	E	9
22	1	0.09	E	3
23	1	0.09	E	3
24	1	0.10	T	3
25	1	0.09	T	3
26	1	0.11	E	3
27	1	0.09	T	3
28	2	0.13	E	3

No.	Floors	Max drift (%)	During	Location
29	1	0.14	T	3
30	1	0.08	E	3
31	2	0.15	E	6
32	2	0.09	E	3
33	1	0.14	T	3
34	1	0.09	E	3
35	1	0.14	E	3
36	2	0.11	E	3
37	2	0.17	E	4
38	1	0.10	E	3
39	1	0.08	E	3
40	1	0.14	T	3
41	1	0.11	T	3
42	1	0.15	E	3
43	1	0.09	E	3
44	1	0.10	E	3
45	1	0.11	E	3
46	1	0.10	E	3
47	1	0.09	E	3
48	1	0.11	T	3
49	1	0.08	E	3
50	1	0.10	E	3
51	1	0.12	E	3
52	1	0.11	E	3
53	1	0.14	T	3
54	2	0.13	E	8
55	1	0.23	E	8
56	1	0.15	T	3

Appendix VII The results of damage prediction for zone S3

No.	Floors	Max drift (%)	During	Location
1	3	0.15	T	1
2	3	0.09	E	1
3	3	0.11	E	1
4	3	0.11	T	1
5	3	0.10	E	1
6	3	0.19	T	1
7	3	0.15	T	1
8	3	0.11	T	1
9	3	0.14	T	1
10	3	0.13	T	1
11	3	0.12	E	1
12	3	0.12	T	1
13	3	0.10	E	1
14	3	0.21	T	1
15	3	0.11	T	1
16	3	0.12	E	1
17	3	0.13	T	1
18	3	0.12	E	1
19	3	0.12	T	1
20	3	0.10	E	1
21	3	0.12	T	1
22	3	0.15	E	1
23	3	0.09	E	1
24	3	0.11	E	1
25	3	0.14	T	1
26	3	0.08	E	1
27	3	0.16	E	1
28	3	0.11	T	1
29	9	0.18	E	2
30	3	0.11	E	1
31	10	0.21	E	2
32	3	0.10	E	1
33	3	0.15	E	1
34	3	0.12	T	1
35	3	0.11	E	1
36	3	0.12	E	1
37	3	0.14	E	1
38	3	0.12	T	1

No.	Floors	Max drift (%)	During	Location
39	3	0.14	E	1
40	3	0.12	T	1
41	7	0.20	E	2
42	7	0.17	E	2
43	3	0.12	T	1
44	3	0.11	T	1
45	4	0.16	T	1
46	6	0.23	E	2
47	3	0.14	T	1
48	3	0.11	T	1
49	8	0.19	E	2
50	3	0.15	E	1
51	4	0.13	E	2
52	3	0.14	E	1
53	3	0.14	E	1
54	3	0.09	E	1
55	9	0.24	E	1
56	3	0.10	E	1
57	3	0.16	E	1
58	3	0.09	E	1
59	4	0.16	T	1
60	7	0.17	E	2
61	3	0.10	E	1
62	3	0.12	E	1
63	3	0.12	E	1
64	3	0.14	T	1
65	3	0.18	T	1
66	3	0.12	E	1
67	3	0.19	T	1
68	3	0.11	T	1
69	3	0.19	T	1
70	3	0.13	E	2
71	3	0.11	E	1
72	3	0.16	E	1
73	5	0.21	E	2
74	6	0.25	E	2
75	3	0.13	E	1
76	3	0.15	T	1

Appendix VIII The results of damage prediction for zone S4

No.	Floors	Max drift (%)	During	Location
1	5	0.18	E	2
2	3	0.10	T	1
3	3	0.10	T	1
4	3	0.11	T	1
5	7	0.16	E	2
6	3	0.09	E	1
7	8	0.22	E	2
8	3	0.11	T	1
9	3	0.12	E	1
10	3	0.09	E	1
11	3	0.11	E	1
12	3	0.10	E	1
13	3	0.11	T	1
14	3	0.10	T	1
15	3	0.12	E	1
16	3	0.10	E	1
17	3	0.12	E	1
18	3	0.13	T	1
19	3	0.14	E	2
20	3	0.13	T	1
21	3	0.10	E	1
22	3	0.12	E	1
23	3	0.11	E	1
24	3	0.15	E	1
25	3	0.13	E	1

No.	Floors	Max drift (%)	During	Location
26	3	0.14	T	1
27	3	0.12	T	1
28	3	0.09	E	1
29	3	0.09	E	1
30	3	0.11	T	1
31	3	0.14	T	1
32	3	0.15	T	1
33	3	0.14	T	1
34	3	0.09	E	1
35	3	0.09	E	1
36	6	0.25	E	2
37	3	0.09	E	1
38	3	0.12	E	1
39	3	0.16	E	1
40	7	0.18	E	2
41	3	0.09	E	1
42	8	0.24	E	2
43	8	0.21	E	2
44	3	0.11	E	1
45	3	0.10	E	1
46	3	0.13	T	1
47	3	0.16	T	1
48	3	0.15	E	1
49	3	0.09	E	1
50	3	0.14	T	1

Appendix IX The results of damage prediction for zone S4 (cont.)

No.	Floors	Max drift (%)	During	Location
51	3	0.10	E	1
52	3	0.10	E	1
53	3	0.10	E	1
54	3	0.15	E	1
55	3	0.22	T	1
56	3	0.15	E	1
57	3	0.15	T	1
58	3	0.15	E	1
59	3	0.14	E	1
60	3	0.10	E	1
61	3	0.11	E	1
62	3	0.11	E	1
63	3	0.14	E	1
64	3	0.10	E	1
65	3	0.14	E	1
66	3	0.13	T	1
67	3	0.08	E	1
68	3	0.09	E	1
69	3	0.10	E	1
70	3	0.16	T	1
71	3	0.11	E	1
72	3	0.09	E	1
73	3	0.11	T	1
74	3	0.09	E	1
75	3	0.09	E	1

No.	Floors	Max drift (%)	During	Location
76	3	0.16	T	1
77	3	0.09	E	1
78	3	0.09	E	1
79	3	0.09	E	1
80	3	0.09	E	1
81	3	0.12	T	1
82	3	0.14	E	1
83	3	0.12	E	1
84	3	0.09	E	1
85	3	0.14	T	1
86	3	0.12	T	1
87	4	0.17	E	2
88	4	0.15	E	2
89	3	0.09	E	1
90	3	0.09	E	1
91	11	0.24	E	2
92	3	0.09	E	1
93	3	0.10	E	2
94	10	0.32	E	1
95	3	0.13	E	1
96	3	0.09	E	1
97	3	0.12	T	1
98	3	0.14	E	1
99	3	0.11	T	1

Appendix X The results of damage prediction for zone N1 (worst case)

No.	Floors	Max drift (%)	During	Location
1	8	0.46	E	2
2	6	0.48	T	1
3	3	0.26	T	1
4	3	0.22	E	1
5	3	0.13	T	1
6	3	0.25	T	1
7	3	0.24	E	1
8	3	0.29	T	1
9	3	0.34	T	1
10	3	0.50	T	1
11	3	0.52	T	1
12	3	0.10	E	1
13	7	0.31	E	1
14	3	0.32	T	1
15	3	0.13	T	1
16	3	0.27	T	1
17	3	0.11	E	1
18	3	0.11	E	1
19	3	0.26	T	1
20	5	0.43	T	1
21	3	0.77	T	1
22	5	0.70	T	1
23	7	0.26	E	1
24	3	0.96	T	1
25	3	0.10	E	1

No.	Floors	Max drift (%)	During	Location
26	3	0.58	T	1
27	8	0.64	E	1
28	3	0.33	T	1
29	3	0.55	T	1
30	3	0.13	T	1
31	5	0.25	T	1
32	3	0.23	T	1
33	3	0.10	E	1
34	3	0.28	T	1
35	3	0.26	T	1
36	3	0.29	T	1
37	3	0.12	E	1
38	3	0.24	T	1
39	3	0.21	T	1
40	3	0.49	T	1
41	3	0.25	T	1
42	3	0.13	T	1
43	3	0.58	T	1
44	3	0.28	T	1
45	3	0.13	T	1
46	3	0.21	T	1
47	9	0.30	E	1
48	3	0.11	E	1
49	3	0.30	T	1
50	3	0.10	T	1

Appendix XI The results of damage prediction for zone N2 (worst case)

No.	Floors	Max drift (%)	During	Location
1	3	0.15	T	1
2	3	0.16	T	1
3	3	0.16	T	1
4	3	0.14	T	1
5	3	0.14	T	1
6	3	0.14	T	1
7	3	0.15	T	1
8	3	0.15	T	1
9	5	0.68	T	1
10	3	0.45	T	1
11	3	0.44	T	1
12	3	0.45	T	1
13	3	0.45	T	1
14	3	1.41	T	1
15	3	0.93	T	1
16	3	0.15	T	1
17	3	1.90	T	1
18	3	0.42	T	1
19	3	0.47	T	1
20	3	0.13	T	1
21	3	0.15	T	1
22	3	0.15	T	1
23	4	2.85	T	1
24	3	0.15	T	1
25	3	0.45	T	1
26	3	0.40	T	1

No.	Floors	Max drift (%)	During	Location
27	3	0.15	T	1
28	3	2.29	T	1
29	3	0.15	T	1
30	11	0.32	E	1
31	3	0.50	T	1
32	3	0.13	T	1
33	3	0.46	T	1
34	3	0.14	T	1
35	3	0.92	T	1
36	3	0.16	T	1
37	3	0.15	T	1
38	3	0.42	T	1
39	3	0.47	T	1
40	3	0.15	T	1
41	3	0.35	T	1
42	3	0.31	T	1
43	11	0.44	E	1
44	11	0.35	E	1
45	3	0.93	T	1
46	3	0.13	T	1
47	3	0.12	T	1
48	3	0.37	T	1
49	3	0.52	T	1
50	3	0.43	T	1
51	3	0.15	T	1

Appendix XII The results of damage prediction for zone N3 (worst case)

No.	Floors	Max drift (%)	During	Location
1	3	0.13	T	1
2	3	0.13	T	1
3	3	0.13	T	1
4	3	0.10	E	1
5	3	0.29	T	1
6	3	0.11	E	1
7	3	0.33	T	1
8	3	0.27	T	1
9	3	0.12	T	1
10	3	0.31	T	1
11	3	0.13	T	1
12	3	0.14	T	1
13	3	0.11	E	1
14	3	0.60	T	1
15	3	0.99	T	1
16	3	0.32	T	1
17	3	0.24	T	1
18	3	0.11	E	1
19	3	0.30	T	1
20	4	1.23	T	1
21	4	0.63	T	1
22	3	0.27	T	1
23	3	0.24	T	1
24	3	0.31	T	1
25	3	0.56	T	1
26	3	0.13	T	1
27	3	0.14	E	1
28	3	0.12	E	1
29	4	2.03	T	1

No.	Floors	Max drift (%)	During	Location
30	4	1.84	T	1
31	3	0.10	E	1
32	3	0.11	E	1
33	3	0.13	T	1
34	3	0.11	E	1
35	3	0.13	T	1
36	3	0.11	T	1
37	3	0.13	T	1
38	3	0.30	T	1
39	3	0.11	E	1
40	3	0.12	T	1
41	3	0.12	E	1
42	3	0.52	T	1
43	3	0.11	E	1
44	3	0.11	T	1
45	3	0.29	T	1
46	3	0.13	T	1
47	3	0.11	E	1
48	3	0.79	T	1
49	3	0.11	T	1
50	3	0.28	T	1
51	3	0.13	T	1
52	3	0.14	E	1
53	3	0.14	T	1
54	3	0.16	T	1
55	3	0.13	T	1
56	3	0.27	T	1
57	3	0.11	T	1

Appendix XIII The results of damage prediction for zone N3 (worst case) (con.t)

No.	Floors	Max drift (%)	During	Location
58	3	0.30	T	1
59	3	0.27	T	1
60	3	0.24	T	1
61	3	0.32	T	1
62	3	0.33	T	1
63	3	0.28	T	1
64	3	0.11	T	1
65	3	0.13	T	1
66	3	0.61	T	1
67	3	0.10	E	1
68	3	0.13	T	1
69	3	0.29	T	1
70	3	0.09	T	1
71	3	0.11	T	1
72	3	0.81	T	1
73	4	0.27	T	1
74	3	0.23	T	1
75	3	0.11	E	1
76	4	1.84	T	1
77	3	0.29	T	1
78	3	0.11	E	1
79	3	0.37	E	1
80	5	0.40	T	1
81	3	0.13	T	1
82	3	0.30	T	1
83	3	0.10	E	1
84	3	0.11	E	1
85	3	0.13	T	1
86	3	0.12	E	1

No.	Floors	Max drift (%)	During	Location
87	3	0.50	T	1
88	3	0.58	T	1
89	3	0.80	T	1
90	3	0.29	T	1
91	5	0.43	T	1
92	7	0.29	E	2
93	5	0.29	T	1
94	3	0.16	T	1
95	3	0.18	T	1
96	3	0.08	E	1
97	3	0.10	E	1
98	4	0.64	T	1
99	3	0.54	T	1
100	3	0.12	T	1
101	4	1.26	T	1
102	8	0.33	E	2
103	3	0.30	T	1
104	3	0.12	T	1
105	3	0.12	T	1
106	3	0.13	T	1
107	4	0.64	T	1
108	3	0.09	E	1
109	3	0.13	T	1
110	3	0.29	T	1
111	3	0.30	T	1
112	3	0.57	T	1
113	3	0.12	T	1
114	3	0.13	E	2

Appendix XIV The results of damage prediction for zone S1 (worst case)

No.	Floors	Max drift (%)	During	Location
1	3	0.10	E	1
2	3	0.25	T	1
3	3	0.24	T	1
4	8	0.35	T	1
5	3	0.08	E	1
6	11	0.40	E	1
7	3	0.25	T	1
8	3	0.40	T	1
9	3	0.22	T	1
10	3	0.16	T	1
11	3	0.36	T	1
12	3	0.37	T	1
13	3	0.15	T	1
14	3	0.10	E	1
15	3	0.35	T	1
16	3	0.16	E	1
17	3	0.35	T	1
18	3	0.15	E	1
19	3	0.15	T	1
20	22	0.94	E	1
21	3	0.15	T	1
22	9	0.22	E	1
23	3	0.10	E	1
24	7	0.16	E	2
25	10	0.36	E	1
26	3	0.26	T	1
27	4	1.75	T	1
28	3	0.10	E	1
29	3	0.13	E	1
30	3	0.23	T	1
31	8	0.40	T	1

Appendix XV The results of damage prediction for zone S2 (worst case)

No.	Floors	Max drift (%)	During	Location
1	3	0.28	T	1
2	3	0.10	T	1
3	7	0.36	T	1
4	3	0.12	T	1
5	3	0.13	T	1
6	21	0.88	E	1
7	3	0.14	T	1
8	3	0.17	T	1
9	3	0.29	T	1
10	3	0.26	T	1
11	3	0.17	T	1
12	3	0.14	E	1
13	3	0.08	E	1
14	3	0.09	T	1
15	3	0.12	E	1
16	3	0.46	T	1
17	3	0.47	T	1
18	11	0.22	T	1
19	3	0.09	E	1
20	3	0.29	T	1
21	9	0.33	T	1
22	3	0.09	E	1
23	3	0.11	T	1
24	3	0.14	T	1
25	3	0.13	T	1
26	3	0.13	T	1
27	3	0.28	T	1
28	3	0.13	E	2

No.	Floors	Max drift (%)	During	Location
29	3	0.48	T	1
30	3	0.11	T	1
31	6	0.17	T	1
32	3	0.28	T	1
33	3	0.30	T	1
34	3	0.27	T	1
35	3	0.19	T	1
36	3	0.44	T	1
37	4	1.46	T	1
38	3	0.10	E	1
39	3	0.16	T	1
40	3	0.29	T	1
41	3	0.29	T	1
42	3	0.27	T	1
43	3	0.09	E	1
44	3	0.11	T	1
45	3	0.11	E	1
46	3	0.10	E	1
47	3	0.09	E	1
48	3	0.28	T	1
49	3	0.09	T	1
50	3	0.14	T	1
51	3	0.12	E	1
52	3	0.10	E	1
53	3	0.30	T	1
54	8	0.21	T	1
55	8	0.30	T	1
56	3	0.32	T	1

Appendix XVI The results of damage prediction for zone S3 (worst case)

No.	Floors	Max drift (%)	During	Location
1	3	0.29	T	1
2	3	0.20	T	1
3	3	0.19	T	1
4	3	0.27	T	1
5	3	0.20	T	1
6	3	0.85	T	1
7	3	0.79	T	1
8	3	0.26	T	1
9	3	0.80	T	1
10	3	0.81	T	1
11	3	0.21	T	1
12	3	0.27	T	1
13	3	0.20	T	1
14	3	1.65	T	1
15	3	0.27	T	1
16	3	0.19	T	1
17	3	0.81	T	1
18	3	0.19	T	1
19	3	0.27	T	1
20	3	0.20	T	1
21	3	0.26	T	1
22	3	0.24	T	1
23	3	0.20	T	1
24	3	0.26	T	1
25	3	0.28	T	1
26	3	0.23	T	1
27	3	0.19	T	1
28	3	0.79	T	1
29	9	0.53	T	1
30	3	0.48	T	1
31	10	0.52	T	1
32	3	0.20	T	1
33	3	0.80	T	1
34	3	0.27	T	1
35	3	0.19	T	1
36	3	0.21	T	1
37	3	0.78	T	1
38	3	0.80	T	1
39	3	0.17	T	1
40	3	0.79	T	1
41	7	1.52	T	1
42	7	0.55	T	1
43	3	0.26	T	1
44	3	0.27	T	1
45	4	4.70	T	1
46	6	2.46	T	1
47	3	0.28	T	1
48	3	0.27	T	1
49	8	0.86	T	1
50	3	0.24	T	1
51	4	2.32	T	1
52	3	0.77	T	1
53	3	0.20	T	1
54	3	0.24	T	1
55	9	0.73	T	1
56	3	0.21	T	1
57	3	0.19	T	1
58	3	0.23	T	1
59	4	4.71	T	1
60	7	0.55	T	1
61	3	0.20	T	1
62	3	0.22	T	1
63	3	0.82	T	1
64	3	0.28	T	1
65	3	0.81	T	1
66	3	0.21	T	1
67	3	0.81	T	1
68	3	0.26	T	1
69	3	0.78	T	1
70	3	0.24	T	1
71	3	0.26	T	1
72	3	0.19	T	1
73	5	3.55	T	1
74	6	2.23	T	1
75	3	0.18	T	1
76	3	0.83	T	1

Appendix XVII The results of damage prediction for zone S4 (worst case)

No.	Floors	Max drift (%)	During	Location
1	5	0.98	T	1
2	3	0.37	T	1
3	3	0.15	T	1
4	3	0.15	T	1
5	7	0.33	T	1
6	3	0.09	E	1
7	8	0.44	T	1
8	3	0.16	T	1
9	3	0.12	E	1
10	3	0.09	E	1
11	3	0.12	T	1
12	3	0.11	T	1
13	3	0.15	T	1
14	3	0.15	T	1
15	3	0.12	T	1
16	3	0.11	T	1
17	3	0.35	T	1
18	3	0.38	T	1
19	3	0.97	T	1
20	3	0.38	T	1
21	3	0.37	T	1
22	3	0.13	T	1
23	3	0.11	E	1
24	3	0.16	T	1
25	3	0.18	T	1
26	3	0.40	T	1
27	3	0.14	T	1
28	3	0.09	E	1
29	3	0.12	T	1
30	3	0.16	T	1
31	3	0.37	T	1
32	3	0.41	T	1
33	3	0.36	T	1
34	3	0.09	E	1
35	3	0.11	T	1
36	6	0.80	T	1
37	3	0.09	E	1
38	3	0.12	E	1
39	3	0.16	E	1
40	7	0.32	T	1
41	3	0.34	T	1
42	8	0.24	E	2
43	8	0.44	T	1
44	3	0.22	T	1
45	3	0.10	T	1
46	3	0.18	T	1
47	3	0.72	T	1
48	3	0.35	T	1
49	3	0.09	E	1
50	3	0.38	T	1

Appendix XVIII The results of damage prediction for zone S4 (worst case) (con.t)

No.	Floors	Max drift (%)	During	Location
51	3	0.13	T	1
52	3	0.11	T	1
53	3	0.11	T	1
54	3	0.35	T	1
55	3	1.40	T	1
56	3	0.34	T	1
57	3	0.37	T	1
58	3	0.34	T	1
59	3	0.14	E	1
60	3	0.14	T	1
61	3	0.13	T	1
62	3	0.34	T	1
63	3	0.37	T	1
64	3	0.10	E	1
65	3	0.31	T	1
66	3	0.12	E	1
67	3	0.08	E	1
68	3	0.10	T	1
69	3	0.70	T	1
70	3	0.40	T	1
71	3	0.29	T	1
72	3	0.09	E	1
73	3	0.68	T	1
74	3	0.09	E	1
75	3	0.10	T	1

No.	Floors	Max drift (%)	During	Location
76	3	0.38	T	1
77	3	0.09	E	1
78	3	0.09	T	1
79	3	0.11	T	1
80	3	0.11	T	1
81	3	0.37	T	1
82	3	0.37	T	1
83	3	0.36	T	1
84	3	0.10	T	1
85	3	0.37	T	1
86	3	0.36	T	1
87	4	2.80	T	1
88	4	2.58	T	1
89	3	0.11	T	1
90	3	0.09	E	1
91	11	0.28	T	1
92	3	0.34	T	1
93	3	0.13	E	1
94	10	0.34	T	1
95	3	0.17	T	1
96	3	0.10	T	1
97	3	0.70	T	1
98	3	0.14	E	1
99	3	0.38	T	1

## CHAPTER IV

### RECOMMENDATIONS AND FUTURE RESEARCH

#### 4.1 RECOMMENDATIONS

##### 4.1.1 Sequential analysis from earthquake and tsunami for individual RC building

The example of a six-story RC wall-frame building was performed to study on sequential behavior of earthquake and tsunami response. The analysis results shows that more damage from sequential tsunami response could occur with most of structural members except for in-plane bending failure mode of shear wall. Due to out-of-plane bending failure of wing wall at 1<sup>st</sup> floor, it was found that out-of-plane shear force was redistributed to concentrate on wing wall at 2<sup>nd</sup> wall. Moreover, it was found that in-plane shear force was redistributed to concentrate on shear wall at 2<sup>nd</sup> wall.

Due to sequential analysis in the same hysteresis model, the occurrence of sequential tsunami response depended on the end of earthquake response in hysteresis rules in which more damage could occur or not. With this reason, sequential analysis from earthquake and tsunami had more accurate damage prediction than separated analysis from earthquake and tsunami. In practice, structural properties of a whole building can be changed after earthquake response to resist against the coming tsunami load which may be stronger or weaker. In addition, the failure of some structural components during tsunami flow can affect to other structural components and change structural properties of a whole building. Therefore, sequential analysis from earthquake and tsunami should be settled for a building design guideline of RC buildings in risk area instead of separated analysis from earthquake and tsunami.

### **4.1.2 Damage prediction of all RC building in a target area**

For a target area of Kochi city, sequential earthquake and tsunami simulation was performed to predict structural damage of all RC buildings using maximum story drift ratio. For damage prediction of all RC buildings in a target area, the results of sequential earthquake and tsunami simulation can express maximum story drift ratio, occurrence during earthquake response or sequential tsunami response, and location of maximum story drift. In addition, all analysis results of individual RC building can be recorded in data base in order to investigate structural damage of this RC building in micro scale.

The results of sequential earthquake and tsunami simulation can be used to designate tsunami evacuation buildings, which must be secured for people living in a surrounding area. These results can indicate a weak point of a city area and focus on this weak point. In addition, these results can be used to construct prevention measures in order control overall damage of a city area from earthquake and subsequent tsunami. Therefore, sequential earthquake and tsunami simulation should be used by government officer in order to make a policy on disaster management.

## **4.2 FUTURE RESEARCH**

### **4.2.1 Macro plate model**

Implementation of macro plate model, a practical model, into a computational platform will provide structural design engineers and researchers improved analytical capabilities to model and study nonlinear behavior of RC walls and their interaction with other structural members. The practical model can be used for nonlinear structural analysis of RC buildings represented by a wall-frame model. This practical model allows for possible further model improvements including applications to other structural members and joints. This research has already presented the verification of macro plate model with the test at E-Defense and observed damage. However, macro plate model should be verified

and calibrated with finite element analysis using a commercial numerical program in order to simulate a single wall member adequately for further application.

#### **4.2.2 Sequential analysis from earthquake and tsunami for individual RC building**

With many analysis cases of earthquake and tsunami scenarios, sequential analysis should be applied to many RC buildings in order to obtain more finding in sequential behavior from earthquake and tsunami. This sequential analysis should compare with a single analysis from earthquake or tsunami in order to investigate how much this sequential analysis can affect to structural damage of RC buildings and consider the significant contribution of sequential analysis to a building design guideline.

#### **4.2.3 Damage prediction of all RC building in a target area**

Since the main purpose of development of sequential earthquake and tsunami simulation is reliable damage prediction of a target area from future earthquake and tsunami, it is necessary to verify and modify this sequential earthquake and tsunami simulation with many cases in past earthquake and tsunami, such as the 2011 Great East Japan earthquake and tsunami. This research has already presented the verification of nonlinear structural analysis with the test at E-Defense and observed damage. However, there are two input data which are not reliable sufficiently for sequential earthquake and tsunami simulation, such as building modeling and evaluation of tsunami load. These two input data must be improved in order to obtain reliable damage prediction before applying this sequential earthquake and tsunami simulation in practice.

## REFERENCES

### BUILDING OVERTURNING

- [1] Architectural institute of Japan (2001). *Recommendations for design of building foundations*.
- [2] Adriano, B., Mas, E. and Koshimura, S. (2014). “Tsunami inundation features verification through numerical modeling and video analysis: case study of Onagawa town on the 2011 Tohoku earthquake.” *Proc., Asia Oceania Geosciences Society 11<sup>th</sup> Annual Meeting*.
- [3] Building Center of Japan (2007). *Technical standard manual for building (In Japanese)*.
- [4] Chock, G., Carden, L., Robertson, I., Olsen, M. and Guangren, Y. (2013). “Tohoku tsunami-induced building failure analysis with implications for U.S. tsunami and seismic design codes.” *Earthquake spectra*, Vol. 29, No. S1, S99-S126.
- [5] Fraser, S., Raby, A., Pomonis, A., Goda, K., Chian, S. C., Macabuag, J., Offord, M., Saito, K. and Sammonds, P. (2013). “Tsunami damage to coastal defences and buildings in the March 11<sup>th</sup> 2011 Mw9.0 Great East Japan earthquake and tsunami.” *Bulletin of Earthquake Engineering*, Springer, Vol. 11, 205-239.
- [6] Latcharote, P., Suppasri, A., Yamashita, A., Adriano, B., Koshimura, S., Kai, Y. and Imamura, F. (2014). “Mechanism and Stability Analysis of Overturned Building by the 2011 Great East Japan Earthquake and Tsunami in Onagawa Town.” *Proceeding of 14<sup>th</sup> Japan Earthquake Engineering Symposium (14JEES)*.
- [7] National institute for land and infrastructure management and building research institute in Japan (2012). “Report on field surveys and subsequent investigations of

building damage following the 2011 off the pacific coast of Tohoku earthquake.”  
*Building research data*, No.136, 6.2-32 – 6.2-40.

- [8] Suppasri, A., Shuto, N., Imamura, F., Koshimura, S., Mas E. and Yalciner, A. C. (2013). “Lesson learned from the 2011 Great East Japan tsunami: performance of tsunami countermeasures, coastal buildings, and tsunami evacuation in Japan.” *Pure and Applied Geophysics*, Vol. 170, 993-1018.
- [9] Suppasri, A., Koshimura, S., Imai, K., Mas, E., Gokon, H., Muhari, A. and Imamura F., (2012). “Damage Characteristic and Field Survey of the 2011 Great East Tsunami in Miyagi Prefecture.”, *Coastal Engineering Journal*, World Scientific Publishing Company and Japan Society of Civil Engineers, Vol.54, No.1, 125005.
- [10] Tokimatsu, K., Tamura, S., Suzuki, H. and Katsumata, K. (2012). “Building damage associated with geotechnical problems in the 2011 Tohoku Pacific Earthquake.” *Soils and Foundations*, Science direct, Vol. 52, No. 5, 956-974.

## **DEVELOPMENT OF WALL MODELS**

- [11] Azzato, F. and Vulcano, A. (1996). “Modeling of RC frame-wall structures for nonlinear seismic analysis.” *Proc., 11th World Conference on Earthquake Engineering*, No.1411.
- [12] Chen, S. and Kabeyasawa, T. (2000). “Modeling of reinforced concrete shear wall for nonlinear analysis.” *Proc., 12th World Conference on Earthquake Engineering*.
- [13] Chen, S., Matsumori T. and Kabeyasawa, T. (2006). “Analytical research of full-scale RC structure test on E-Defense.” *Proc., 8th U.S. National Conference on Earthquake Engineering*, No. 666.

- [14] Kabeyasawa, T., Shiohara, H., Otani, S. and Aoyama, H. (1983). "Analysis of the full-scale seven-story reinforced concrete test structure." *Journal (B)*, University of Tokyo, Vol.XXXVII, 432-478.
- [15] Kai, Y. (2001). "A study of RC space shear wall structure for nonlinear Analysis (in Japanese)." *Doctoral Dissertation*, University of Tokyo.
- [16] Kim, Y., Kabeyasawa, T. and Kabeyasawa, T. (2006). "Preliminary response analysis of a full-scale RC structure for 3-D shaking table test to collapse." *Proc., 8th U.S. National Conference on Earthquake Engineering*, No. 479.
- [17] Kim, Y., Kabeyasawa, T., Matsumori, T. and Kabeyasawa, T. (2007). "Dynamic collapse analysis of the six-story full-scale wall-frame tested at E-Defense." *Proc., 8th Pacific Conference on Earthquake Engineering*, No. 281.
- [18] Kim, Y., Kabeyasawa, T., Matsumori, T. and Kabeyasawa, T. (2007). "Dynamic collapse analysis of the six-story full-scale wall-frame building." *Journal of Structural Engineering Research Frontiers*.
- [19] Kim, Y., Kabeyasawa, T., Matsumori, T. and Kabeyasawa, T. (2008). "Analytical studies on a 6-story full-scale reinforced concrete wall-frame structure to collapse." *Proc., 14th World Conference on Earthquake Engineering*.
- [20] Kim, Y., Kabeyasawa, T., Matsumori, T. and Kabeyasawa, T. (2009). "Analytical study on collapse process of a full-scale 6-story reinforced concrete wall frame structure tested at E-Defense (in Japanese)." *Journal of Structural and Construction Engineering*, AIJ, Vol. 74, No. 641, 1327-1334.
- [21] Kim, Y., Kabeyasawa, T., Matsumori, T. and Kabeyasawa, T. (2012). "Numerical study of a full-scale six-story reinforced concrete wall-frame structure tested at E-Defense." *Journal of International Association for Earthquake Engineering, Earthquake Engineering and Structural Dynamics*, Wiley, No. 41, 1217-1239.

- [22] Kolozvari K. I. and Wallace J. W. (2012). "Modeling of cyclic shear–flexure interaction in reinforced concrete structural walls." *Proc., 15th World Conference on Earthquake Engineering*, No.2471.
- [23] Kolozvari K. I. and Wallace J. W. (2013). "Analytical modeling of cyclic shear–flexure interaction in reinforced concrete structural walls." *Doctoral Dissertation*, University of California, Los Angeles.
- [24] Matsui, T., Kabeyasawa, T., Koto, A., Kuramoto, H. and Nagashima, I. (2004) "Shaking table test and analysis of reinforced concrete walls." *Proc., 13th World Conference on Earthquake Engineering*, No.419.
- [25] Matsui, T., Kabeyasawa, T. and Kuramoto, H. (2006) "Response analysis of reinforced concrete wall-frame structure considering strength deterioration." *Proc., 8th U.S. National Conference on Earthquake Engineering*, No.1561.
- [26] Milev, J. I. (1996). "Two dimensional analytical model of reinforced concrete shear walls." *Proc., 11th World Conference on Earthquake Engineering*, No.320.
- [27] Okamura, H. and Maekawa, K. (1991). "Nonlinear analysis and constitutive models of reinforced concrete." *Gihodo-Shuppan Co.*
- [28] Orakcal, K. and Wallace, J. W. (2002) "Nonlinear modeling of RC and SRC structural walls." *Proc., 7th U.S. National Conference on Earthquake Engineering*.
- [29] Orakcal, K., Wallace, J. W. and Conte J. P. (2004) "Flexural modeling of reinforced concrete walls-model attributes." *ACI Structural Journal*, No. 101-S68, 688-698.
- [30] Orakcal, K., Massone, L. M. and Wallace, J. W. (2006) "Analytical modeling of reinforced concrete walls for predicting flexural and coupled-shear-flexural response." *PEER Report 2006/07*, Pacific Earthquake Engineering Research Center.

- [31] Saito, T., Teshigawara, M., Fukuyama, H., Kato, H., Kusunoki, K., Mukai, T. and Kabeyasawa, T. (2004) "Simulation of nonlinear behavior of reinforced concrete wall-frame structures under earthquake loads." *Proc., 13th World Conference on Earthquake Engineering*, No.1561.
- [32] Sanada, Y., Kabeyasawa, T. and Nakano, Y. (2004). "Analyses of reinforced concrete wall-frame structural systems considering shear softening of shear wall." *Proc., 13th World Conference on Earthquake Engineering*, No.3036.
- [33] Sanada, Y. and Kabeyasawa, T. (2007). "Test and analysis of RC shear walls focused on local forces." *Proc., 8th Pacific Conference on Earthquake Engineering*.
- [34] Steele, C. R. and Balch, C. D. "Introduction to the theory of plates." Dept. of Mechanical Engineering, Stanford University.
- [35] The 1<sup>st</sup>, 2<sup>nd</sup>, 3<sup>rd</sup>, 4<sup>th</sup>, and 5<sup>th</sup> U.S. - Japan workshop on performance-based earthquake engineering methodology for reinforced concrete building structures. (1999-2003). *PEER Report*, Pacific Earthquake Engineering Research Center.
- [36] The 1<sup>st</sup> and 2<sup>nd</sup> NEES/E-Defense workshop on collapse simulation of reinforced concrete building structures. (2005-2006). *PEER Report*, Pacific Earthquake Engineering Research Center.
- [37] Timoshenko, S. P. and Goodier N. (1970). *Theory of elasticity*, 3rd ed. New York, McGraw-Hill.
- [38] Tran T. A. and Wallace J. W. (2012). "Experimental and analytical studies of moderate aspect ratio reinforced concrete structural walls." *Doctoral Dissertation*, University of California, Los Angeles.
- [39] Vulcano, A. and Bertero, V. V. (1987). "Analytical modeling for predicting the lateral response of RC shear walls: evaluation of their reliability." *Report*

UCB/EERC-87/19, Earthquake Engineering Research Center, University of California, Berkeley.

- [40] Vulcano, A., Bertero, V. V. and Colotti, V. (1988). “Analytical modeling of R/C structural walls.” *Proc. of 9<sup>th</sup> World Conference on Earthquake Engineering*, Vol.VI, 41-46.
- [41] Vulcano, A. (1992). “Use of wall macroscopic models in the nonlinear analysis of RC frame-wall structures.” *Proc. of 10<sup>th</sup> World Conference on Earthquake Engineering*, 4309-4302.
- [42] Zienkiewicz, O. C. and Taylor R. L. (2005). *The finite element method for solid and structural mechanics*, 6th ed. Elsevier, Butterworth-Heinemann.
- [43] Zienkiewicz, O. C., Taylor R. L. and Zhu J. Z. (2005). *The finite element method: Its basis and fundamentals*, 6th ed. Elsevier, Butterworth-Heinemann.

## **EARTHQUAKE RESPONSE**

- [44] Chen, S., Matsui, T., Matsumori, T. and Kabeyasawa, T. (2005). “Collapse analysis of reinforced concrete structure under earthquakes.” *1<sup>st</sup> NEES/E-Defense workshop on collapse simulation of reinforced concrete building structures*, Berkeley 6-8 July 2005, 83-104.
- [45] Chen, S., Matsumori, T. and Kabeyasawa, T. (2006). “Analysis of the full-scale six-story reinforced concrete building tested at E-Defense.” *2<sup>nd</sup> NEES/E-Defense workshop on collapse simulation of reinforced concrete building structures*, Miki 30 October – 1 November 2006, 101-110.
- [46] Kabeyasawa, T., Matsumori, T., Katsumata, H. and Shirai, K. (2005). “Design of the full-scale six-story reinforced concrete wall-frame building for testing at E-Defense.” *1<sup>st</sup> NEES/E-Defense workshop on collapse simulation of reinforced concrete building structures*, Berkeley 6-8 July 2005, 23-46.

- [47] Kim, Y. and Kabeyasawa, T. (2005). "Dynamic analysis of reinforced concrete wall-frame to collapse." *1<sup>st</sup> NEES/E-Defense workshop on collapse simulation of reinforced concrete building structures*, Berkeley 6-8 July 2005, 189-204.
- [48] Kim, Y., Kabeyasawa, T., Matsumori, T. and Kabeyasawa, T. (2006). "Numerical simulation of the full-scale shake table test on a six-story reinforced concrete building." *2<sup>nd</sup> NEES/E-Defense workshop on collapse simulation of reinforced concrete building structures*, Miki 30 October - 1 November 2006, 119-128.
- [49] Kim, Y., Kabeyasawa, T., Matsumori, T. and Kabeyasawa, T. (2007). "Dynamic collapse analysis of the six-story full-scale wall-frame tested at E-Defense." *8<sup>th</sup> Pacific Conference on Earthquake Engineering*, Singapore 5-7 December 2007, 281.
- [50] Kim, Y., Kabeyasawa, T., Matsumori, T. and Kabeyasawa, T. (2009). "Analytical study on collapse process of a full-scale 6-story reinforced wall frame structure tested at E-Defense (in Japanese)." *Structural and Construction Engineering*, AIJ, 74 (641), 1327-1334.
- [51] Matsumori, T., Kazutaka, S. and Kabeyasawa, T. (2006). "Simulated earthquake test on a full-scale six-story reinforced concrete building at E-Defense, Part 1: outline of test program." *2<sup>nd</sup> NEES/E-Defense workshop on collapse simulation of reinforced concrete building structures*, Miki 30 October – 1 November 2006, 5-15.
- [52] Sanada, Y. and Kabeyasawa, T. (2005). "Preliminary analyses of full-scale reinforced concrete wall-frame specimen in DaiDaiToku project." *1<sup>st</sup> NEES/E-Defense workshop on collapse simulation of reinforced concrete building structures*, Berkeley 6-8 July 2005, 207-214.
- [53] Shirai, K., Matsumori, T. and Kabeyasawa, T. (2006). "Simulated earthquake test on a full-scale six-story reinforced concrete building at E-Defense, Part 2: study on distribution of seismic forces." *2<sup>nd</sup> NEES/E-Defense workshop on collapse*

*simulation of reinforced concrete building structures*, Miki 30 October – 1 November 2006, 17-28.

## **TSUNAMI RESPONSE**

- [54] Asai, T., Nakano, Y., Tateno, T., Fukuyama, H., Fujima, K., Haga, Y., Sugano, T. and Okada, T. (2012). “Tsunami load evaluation based on damage observation after the 2011 Great East Japan earthquake.” *Proceedings of the International Symposium on Engineering Lessons Learned from the 2011 Great East Japan Earthquake*, Tokyo, Japan.
- [55] Asai, T., Tateno, T., Fukuyama, H., Fujima, K., Sugano, T., Haga, Y. and Okada, T. (2012). “Tsunami load evaluation based on field investigations of the 2011 Great East Japan earthquake.” *15<sup>th</sup> World Conference in Earthquake Engineering*, Lisbon 24-28 September 2012.
- [56] Chock, G., Carden, L., Robertson, I., Olsen, M. and Guangren, Y. (2013). “Tohoku tsunami-induced building failure analysis with implications for U.S. tsunami and seismic design codes.” *Earthquake spectra*, 29(S1), S99-S126.
- [57] Kabeyasawa, T., Okuda, Y., Fukai, A., Fukuyama, H., Kato, H., Ishihara, T., Tajiri, S. and Tani, M. (2012). “Evaluation of lateral and buoyant forces on reinforced concrete buildings by the tsunami of the 2011 East Japan earthquake.” *15<sup>th</sup> World Conference in Earthquake Engineering*, Lisbon 24-28 September 2012.
- [58] Suppasri, A., Mas, E., Charvet, I., Gunasekera, R., Imai, K., Fukutani, Y., Abe, Y. and Imamura, F. (2013). “Building damage characteristics based on surveyed data and fragility curves of the Great East Japan earthquake and tsunami.” *Bulletin of Earthquake Engineering*, Springer, Vol. 66, 319-341.

## INTEGRATED EARTHQUAKE SIMULATION (IES)

- [59] Hori, M., Tanaka, S., Ichimura, T., Lalith, M., Miyamura, T., Ogino, M. and Okazawa, S. (2013). "Application of HPC to earthquake engineering - seismic structure response analysis and urban area earthquake simulation." *4<sup>th</sup> ECCOMAS Thematic Conference on Computational Methods in Structural Dynamics and Earthquake Engineering*, 1728.
- [60] Hori, M. (2011). "Introduction to computational earthquake engineering", 2nd Edition, Imperial College Press, London.
- [61] Hori, M. and Ichimura, T. (2008). "Current state of integrated earthquake simulation for earthquake hazard and disaster." *Journal of Seismology*, Springer science, 12, 307-321.
- [62] Hori, M., Ichimura, T. and Oguni, K. (2006). "Development of integrated earthquake simulation for estimation of strong ground motion, structural responses and human action in urban areas." *Asian Journal of Civil Engineering (Building and Housing)*, 7, 4, 381-392.
- [63] Ichimura, T., Hori, M., Terada, K. and Yamakawa, T. (2005). "On integrated earthquake simulator prototype: combination of numerical simulation and geographical information system." *Structural Eng./Earthquake Eng.*, JSCE, 22, 2, 233s-243s.
- [64] Ichimura, T. and Hori, M. (2004). "Development of prototype of integrated earthquake disaster simulator using digital city and strong ground motion simulator with high-resolution." *13th World Conference on Earthquake Engineering*, 1418.
- [65] Sobhaninejad, G., Hori, M. and Kabeyasawa, T. (2011). "Enhancing integrated earthquake simulation with high performance computing." Elsevier, *Advances in Engineering Software*, 42, 286-292.

- [66] Wijerathne, M.L.L., Hori, M., Kabeyasawa, T. and Ichimura, T. (2012). “Strengthening of parallel computation performance of integrated earthquake simulation.” ASCE, *Journal of Computing in Civil Engineering*.
- [67] Ichimura, T., Samo, T., Hori, M. and Itami, H. (2009). “Integrated earthquake simulator to generate advanced earthquake disaster information.” *Internet Journal for Society for Social Management Systems (SSMS)*.
- [68] Maddeggedara, L. and Hori, M. (2011). “Application of high performance computation for the prediction of urban area earthquake disaster.” *Internet Journal for Society for Social Management Systems (SSMS)*.

## **CUDA APPLICATION**

- [69] Kirk, D. B. and Hwu, W. W. (2013). “*Programming Massively Parallel Processors*.” 2nd Edition, Elsevier, Morgan Kaufmann.
- [70] NVIDIA Corporation, (2014). “*NVIDIA Developer Zone*.”

## **AIJ STANDARDS**

- [71] Architectural Institute of Japan (1990). “*Design Guidelines for Earthquake Resistant Reinforced Concrete Buildings based on Ultimate Strength Concept (in Japanese)*”
- [72] Architectural Institute of Japan (1997). “*Design Guidelines for Earthquake Resistant Reinforced Concrete Buildings based on Inelastic Displacement Concept (in Japanese)*”
- [73] Architectural Institute of Japan (1999). “*Design Guidelines for Earthquake Resistant Reinforced Concrete Buildings based on Allowable Stress Concept (in Japanese)*”

# LIST OF PUBLICATIONS

## JOURNAL PAPERS

Panon LATCHAROTE and Yoshiro KAI, Numerical derivations of a macroscopic model for reinforced concrete walls considering in-plane and out-of-plane behavior, *Journal of Japan Association for Earthquake Engineering*. (Accepted and Published on May, Vol.15, No.2)

Panon LATCHAROTE and Yoshiro KAI, Extension of nonlinear structural analysis from earthquake response to tsunami response in reinforced concrete wall-frame buildings, *Journal of Advanced Concrete Technology*. (Revised manuscript)

Panon LATCHAROTE, Anawat SUPPASRI, Akane YAMASHITA, Bruno ADRIANO, Shunichi KOSHIMURA, Yoshiro KAI and Fumihiko IMAMURA, Mechanism and stability analysis of overturned buildings by the 2011 great east Japan earthquake and tsunami in Onagawa town, *Journal of Earthquake and Tsunami, World Scientific*. (Resubmission required)

## PEER-REVIEW INTERNATIONAL CONFERENCES

Panon LATCHAROTE and Yoshiro KAI, Nonlinear Structural Analysis of Reinforced Concrete Buildings Suffering Damage from Earthquake and Subsequent Tsunami, *Proceeding of 10<sup>th</sup> U.S. National Conference on Earthquake Engineering (10NCEE)*, Earthquake Engineering Research Institute, DOI: 10.4231/D33J39197, July 2014.

Panon LATCHAROTE and Yoshiro KAI, High Performance Computing of Dynamic Structural Response Analysis for the Integrated Earthquake Simulation, *Proceeding of 13<sup>th</sup> East Asia-Pacific Conference on Structural Engineering and Construction (EASEC-13)*, H-1-1, September 2013.

Panon LATCHAROTE, Anawat SUPPASRI and Yoshiro KAI, Practical Applications of Earthquake and Tsunami Simulation Output for Disaster Management, *Internet Journal for Society for Social Management Systems (SSMS2013)*, Vol.3, SMS13-6767, December 2013.

Panon LATCHAROTE, Yoshiro KAI and Kiminori MATSUZAKI, Utilization of a Supercomputer in Earthquake and Tsunami Simulation, *Proceeding of 6<sup>th</sup> Thailand-Japan International Academic Conference (TJIA2013)*, 92-93, November 2013.

Panon LATCHAROTE and Yoshiro KAI, Object Oriented Modeling of Dynamic Structural Response Analysis, *Proceeding of 5<sup>th</sup> Thailand-Japan International Academic Conference (TJIA2012)*, 71-72, November 2012.

#### **PEER-REVIEW INTERNATIONAL CONFERENCES (UNDER PROCESS)**

Panon LATCHAROTE and Yoshiro KAI, Double-Layer Platform of High Performance Computing for Damage Prediction of RC Buildings subject to Earthquake and Subsequent Tsunami in a Target Area, *5<sup>th</sup> International Conference on Computational Methods in Structural Dynamics and Dynamics and Earthquake Engineering (COMPDYN2015)*, May 2015. (Paper accepted)

#### **DOMESTIC CONFERENCES**

Panon LATCHAROTE, Anawat SUPPASRI, Akane YAMASHITA, Bruno ADRIANO, Shunichi KOSHIMURA, Yoshiro KAI and Fumihiko IMAMURA, Mechanism and Stability Analysis of Overturned Building by the 2011 Great East Japan Earthquake and Tsunami in Onagawa Town, *Proceeding of 14<sup>th</sup> Japan Earthquake Engineering Symposium (14JEES)*, December 2014.

Panon LATCHAROTE and Yoshiro KAI, High Performance Computing of Dynamic Structural Response Analysis for the Integrated Earthquake Simulation, *Proceeding of AIJ Shikoku Chapter Architecture Research Meeting*, 57-58, May 2013

Erika NAKAGAWA, Keisuke ASADA, Panon LATCHAROTE and Yoshiro KAI, Study on the Method of Calculating Load Tsunami on Structures using the Survey Results of the Building Tsunami, *Proceeding of AIJ Shikoku Chapter Architecture Research Meeting*, 33-34, May 2013.

#### **BOOK CHAPTER**

Anawat SUPPRASRI, Ingrid CHARVET, Joshua MACABUAG, Tiziana ROSSETTO, Natt LEELAWAT, Panon LATCHAROTE and Fumihiko IMAMURA, Building Damage Assessment and Implications for Future Tsunami Fragility Estimations, *Coastal Disaster: Lessons Learnt for Engineers and Planners*, Elsevier Science and Technology Books, 2014.

#### **SPECIAL WORKS**

Panon LATCHAROTE, Earthquake and Tsunami Simulation and Disaster Prevention, *Lecture for Thai people in Japan*, Royal Thai Embassy, Tokyo, Japan

Panon LATCHAROTE, Erika NAKAGAWA, Akane YAMASHITA and Yoshiro KAI, Earthquake and Tsunami Simulation for a Target Area in Kochi City, *Broadcasting in Kochi Sun Sun TV*, Kochi, Japan